DE TTK

1949

Higher-order radiative corrections for jet production in QCD perturbation theory

PhD Thesis
Egyetemi Doktori (PhD) értekezés

Szőr Zoltán

Supervisor/Témavezető
Prof. Dr. Zoltán Trócsányi

University of Debrecen
Natural Sciences Doctoral Council
PhD School in Physics

Debreceni Egyetem
Természettudományi Doktori Tanács
Fizikai Tudományok Doktori Iskolája

Debrecen, 2017

Ezen értekezést a Debreceni Egyetem Természettudományi Doktori Tanács Fizikai Tudományok Doktori Iskolája Részecskefizika programja keretében készítettem a Debreceni Egyetem természettudományi doktori (PhD) fokozatának elnyerése céljából.
Nyilatkozom arról, hogy a tézisekben leírt eredmények nem képezik más PhD disszertáció részét.

Debrecen, 2017

Szőr Zoltán

Tanúsítom, hogy Szőr Zoltán doktorjelölt 2014-2017 között a fent megnevezett Doktori Iskola Részecskefizika programjának keretében irányításommal végezte munkáját. Az értekezésben foglalt eredményekhez a jelölt önálló alkotó tevékenységével meghatározóan hozzájárult. Nyilatkozom továbbá arról, hogy a tézisekben leírt eredmények nem képezik más PhD disszertáció részét.
Az értekezés elfogadását javaslom.

Debrecen, 2017

Prof. Dr. Trócsányi Zoltán
témavezető

Higher-order radiative corrections for jet production in QCD perturbation theory

Értekezés a doktori (PhD) fokozat megszerzése érdekében
a fizika tudományágban

Írta: Szőr Zoltán
okleveles fizikus
Készült a Debreceni Egyetem Fizikai Tudományok Doktori Iskolája
Részecskefizika programja keretében

Témavezető: Prof. Dr. Trócsányi Zoltán

A doktori szigorlati bizottság:

elnök: Dr. .....

tagok: Dr. .....

Dr. .....

A doktori szigorlat időpontja: .....

Az értekezés bírálói:

Dr. .....

Dr. .....

A bírálóbizottság:

elnök: Dr. .....

tagok: Dr. .....

Dr. .....

Dr. .....

Dr. .....

Az értekezés védésének időpontja: .....

"Atoms with curiosity that looks at itself
and wonders why it wonders" – Minilogue

Acknowledgements

I am really grateful to my supervisor Zoltán Trócsányi who led me through over the past seven years from my bachelor studies to the end of my PhD. I learned a lot from him and he provided excellent insights and viewpoints both in physics and outside of the field. He helped me to become a young researcher.

I would like to thank my colleagues and friends Ádám Kardos, István Nándori, Gábor Somogyi and Zoltán Tulipánt for their help and informal conversations over a cup of coffee about the final question of life, the universe and everything. They were always open to my questions and very keen to help me out.

I thank Bryan Webber and Pier Francesco Monni the discussions we had about resummation of jetrates which helped me to understand this topic in more details.

Finally I would like to thank my family, my beloved girlfriend and my friends for their support and warmest love, they provided over these three years.

I gratefully acknowledge the financial support provided by the Kavli Institute for Theoretical Physics and the New National Excellence Program of the Ministry of Human Capacities.

Contents

Part I

Preliminaries

Chapter 1

Introduction

The standard model of particle physics (SM) is one of the most successful and well tested theory of physics. It provides a precise description of phenomena observable at todays collision energy scales, with a few, but important exceptions (neutrino masses, dark matter and dark energy). The SM the quantum field theory of three fundamental interactions: the strong, the weak and the electromagnetic. Although all three interactions participate in collision processes, strongly interacting hadrons appear the most frequently in final states. The largest quantum corrections usually also come from the strong interaction due to its rather large coupling compared to the electroweak. The strong coupling α_S itself is one of the most important parameters of the standard model, therefore the more and more precise determination of its value is a constant challenge for the particle physics community. Thus quantum chromodynamics (QCD), the quantum field theory of the strong interaction in its own requires lot of research to provide precise theoretical predictions. In high energy physics theoretical calculations in QCD are computed with perturbative technique, where physical quantities are expanded as a series of α_S, and truncated at some given order. A different approach is the resummation of logarithmically enhanced terms at all order in α_S in kinematic regions, where soft-collinear radiation dominates. The current state-of-art of research is the calculation of next-to-next-to-leading order (NNLO) QCD corrections, and resummation of next-to-leading logarithms in general and next-to-next-to-leading logarithms for certain processes.

In this dissertation I discuss my results in QCD perturbation theory at next-to-next-to-leading order accuracy with resummation. After a brief introduction about QCD I review the features of jet production at electron-positron colliders, and present the theoretical background for making predictions in Chapter 2.

In the second part of the dissertation I present my results. In Chapter 3 I show

an automated method developed to compute master integrals numerically, which is required for the integrated subtraction terms. In Chapters 4 and 5 I make predictions for the three-jet rate in e^+e^- annihilation at next-to-next-to-leading order in perturbation theory matched with next-double logarithmic accurate resummation.

My personal contributions are summarized in the Summary and in the corresponding thesis booklet.

1.1 Basics of QCD

Quantum chromodynamics is the quantum field theory of the strong interaction. The theory has a local non-Abelian $SU(3)$ gauge symmetry, the symmetry of the color interaction. The interaction acts between colored spin-1/2 Dirac-fermions, named quarks and it is mediated by spin-1 bosons called gluons, the gauge fields of the theory. In contrast with electrons and photons, quarks and gluons, collectively called partons, cannot be observed directly in nature, they are always confined in composite particles called hadrons.

QCD involves quarks in 6 different flavors with masses m_f, summarized in Table 1.1. Each quark flavor comes in 3 different colors, they transform as a color triplet

Flavour	Q	m_f
u	2/3	2.3 MeV
d	-1/3	4.8 MeV
c	2/3	1.27 GeV
s	-1/3	95 MeV
t	2/3	173 GeV
b	-1/3	4.2 GeV

Table 1.1. The six quarks of QCD, with their electrical charges measured in e units and their approximate masses. The masses of the u and d quarks are based on chiral perturbation theory, while c, s and b quark masses are defined in the $\overline{\text{MS}}$ renormalization scheme. The top quark mass shown here is based on the pole mass definition.

under the fundamental representation of the $SU(3)$ group. The gluons transform as octets under the adjoint representation of the gauge group, hence in QCD there are 8 gluon fields with 8 different color charges. Due to the non-Abelian structure of the symmetry group, in contrast to Abelian QFTs like quantum electrodynamics, the gluon fields also carry the charge of the interaction and they interact with themselves. The Casimir-operators C_{F} in the fundamental and C_{A} in the adjoint representation of the gauge group (also named as color factors) has the following

values

$$C_{\mathrm{F}} = \frac{T_{\mathrm{R}}(N_{\mathrm{c}}^2 - 1)}{N_{\mathrm{c}}}\,, \quad C_{\mathrm{A}} = 2T_{\mathrm{R}}N_{\mathrm{c}}\,, \tag{1.1}$$

where T_{R} sets the normalization of the group generators and N_{c} denotes the number of colors. With three colors and choosing $T_{\mathrm{R}} = 1/2$ normalization the color factors are $C_{\mathrm{F}} = 4/3$ and $C_{\mathrm{A}} = 3$.

The QCD is perturbatively renormalizable. In the technical aspects this means that ultraviolet divergences emerging in quantum corrections can be removed systematically at every order in perturbation theory renormalizing only a finite number of parameters. Nevertheless, renormalization also has a physical meaning: the physical parameters of the theory such as the coupling and the quarks masses are dressed up with quantum corrections. The measure of this effect depends on the energy scale where we study the system. Thus the actual measurable value of the coupling and the quark masses changes with energy. In high energy collision, like at $Q = 91.2$ GeV Z-boson peak center-of-mass energy, the first five quarks masses become negligible, because their contributions are suppressed by m_f^2/Q^2 factors, and the production of top quarks is not kinematically possible (although they still have some off-shell effects). Practically in QCD perturbation theory all quarks are treated massless but the top quark. Thus below the top threshold the only renormalizable physical parameter of the theory is the strong coupling.

The scale dependence of the coupling is set by the renormalization group equation

$$\mu^2 \frac{\mathrm{d}}{\mathrm{d}\mu^2} \frac{\alpha_{\mathrm{S}}(\mu)}{4\pi} = \beta(\alpha_{\mathrm{S}}(\mu))\,, \tag{1.2}$$

where β is the QCD beta function, which sets the functional behavior of the running coupling. At one-loop accuracy in perturbation theory the solution of Eq. (1.2) is

$$\alpha_{\mathrm{S}}(\mu^2) = \frac{\alpha_{\mathrm{S}}(\mu_0^2)}{1 - \beta_0/(2\pi)\alpha_{\mathrm{S}}(\mu_0^2)\log(\mu^2/\mu_0^2)}\,, \tag{1.3}$$

where β_0 is the first coefficient of the beta function

$$\beta_0 = \frac{11C_{\mathrm{A}} - 4T_{\mathrm{R}}n_{\mathrm{f}}}{3}\,, \tag{1.4}$$

and n_{f} denotes the number of active quarks flavors at a given energy scale.

The value of $\alpha_{\mathrm{S}}(\mu_0^2)$ appearing Eq. (1.3) in is not given by theory, it has to be measured in experiments. The choice of μ_0^2 however is completely arbitrary, thus we introduced a new unphysical scale μ_0^2, what we call the renormalization scale. Physical observables must be independent of unphysical parameters, in perturbation theory it is satisfied in a perturbative sense: as we include more and more higher order corrections, the sensibility to the renormalization scale variation decreases.

Up to 16 quarks flavors β_0 has positive value, thus the running of α_S is monotonically decreasing with increasing energy scale. If we raise the energy scale, the coupling becomes smaller and smaller, the theory behaves asymptotically free at high energies. As a consequence in colliders at large center-of-mass energy, hadrons can be modeled as groups of weakly interacting free partons. Thus the application of QCD perturbation theory to calculate hadronic processes in high energy collisions is justified posteriori, although we will see that higher order corrections may have sizeable effects.

In QCD we can only make theoretical predictions for the so-called infrared safe observables. This is due to the Kinoshita-Lee-Nauenberg theorem which assures that measurable quantities in QCD are free of infrared singularities, provided we use infrared safe observables. The meaning of infrared safety is that the observable is insensitive to the inclusion of soft and collinear partons or in other words the observable does not depend on the long-distance physics. Typical infrared safe quantities are the total cross section, jet cross sections and event shape variables in e^+e^- collisions.

In the next chapter we are going to discuss features of jet physics and how to make predictions in QCD.

Chapter 2

Jet physics at e^+e^- colliders

The production of hadronic jets is a common feature of particle collisions. Jets are groups of energetic and collimated hadrons. Jets were and are still widely studied, they can be used to test the standard model and measure its parameters, they can signal new physics, and they provide important background for new physics searches. In electron-positron colliders jets provide a clean signal to test hadron physics and the QCD part of SM, since all hadrons emerge from the final state only. Thus jet production in e^+e^- collisions is the most popular choice to measure the value of the strong coupling.

Jets can be characterized by the event shape variables, such as the thrust [1, 2], jet broadening [3], and the C-parameter [4], etc. Besides event shapes, jets are often described by the so called jet rate observable, the relative production rate of n-jets compared to all hadronic events. The number of jets is determined using jet clustering algorithms. These algorithms define a distance measure (not necessarily in x-space) and combine final state particles in some certain way into jets.

The n-jet rate at a given Q^2 center-of-mass energy is defined as the ratio of the n-jet cross section and the total hadronic cross section

$$R_n(\vec{a}) = \frac{\sigma_{\mathrm{n-jet}}(\vec{a})}{\sigma_{\mathrm{tot}}}\,, \tag{2.1}$$

where $\vec{a}$ denotes the set of jet resolution parameters characteristic to a given jet algorithm. The jet algorithms can be divided into two groups: the iterative cone algorithms and the sequential jet finding algorithms. Iterative cone algorithms are usually preferred by experiments because the clustered jets have cone like shapes. However most of the formulated cone algorithms are not infrared safe (except the SISCOne algorithm [5]), therefore no theoretical predictions can be made for these

quantities. On the other hand sequential clustering algorithms, like JADE [6, 7] , $k_\perp$ [8], Cambridge [9], anti-$k_\perp$ [10], etc. all satisfy infrared safety and has been used extensively both in experimental and in theoretical research.

At leading order in perturbation theory jets are usually modeled by partons in the first approximation, we associate one parton for each jet, as in hard scattering process only the partons take part. Further corrections can be included with parton showers where we dress up each hard scattered parton with additional multiple emissions of soft and collinear partons. Finally empirical models for hadronization can be applied to connect the parton and the hadron level physics.

In the followings we discuss how we can make theoretical predictions using QCD perturbation theory. We start with a general overview, then we briefly go through the main aspects of computing NNLO cross sections with the CoLoRFulNNLO method.

2.1 Jet cross sections in perturbation theory

In quantum field theory the cross section is defined as

$$\sigma(J) = \frac{1}{2Q^2} \int \mathrm{d}\Phi_m(p_1, \ldots, p_m; \sqrt{Q^2}) \frac{1}{S} \sum_{\text{spin}} \langle \mathcal{M}_m | \mathcal{M}_m \rangle J_m \,, \tag{2.2}$$

where $\sqrt{Q^2}$ is the center-of-mass energy, J is an infrared safe observable and $|\mathcal{M}_m\rangle$ is the renormalized matrix element, while S is a symmetry factor.

In massless QCD the renormalized amplitudes are expressed in terms of the unrenormalized amplitudes $|\mathcal{A}_m\rangle$. The $|\mathcal{A}_m\rangle$ amplitudes containing loops have ultraviolet (UV) singularities coming from the upper ∞ limit of the loop integral. First the divergences require regularization, to make them explicit. In QCD the usual regularization method is dimensional regularization, which provides a Lorentz- and gauge invariant way to handle both ultraviolet and infrared (see later) singularities simultaneously. We generalize the expressions into an arbitrary d spacetime dimension via analytic continuation. Then we set $d = 4 - 2\epsilon$, with $|\epsilon| << 1$ being a small complex number in general. As a result the integrands are no longer divergent and singularities appear as poles in ϵ after loop integration.

UV divergences in loop amplitudes can be removed systematically at every order of perturbation theory with renormalization. Up to two loops the renormalized matrix elements in the $\overline{\text{MS}}$ scheme are given as follows

$$|\mathcal{M}_m^{(0)}\rangle = \left(4\pi\alpha_{\text{S}}(\mu)\right)^{q/2} \left(S_\epsilon^{\overline{\text{MS}}}\right)^{-q/2} |\mathcal{A}_m^{(0)}\rangle \,, \tag{2.3}$$

$$|\mathcal{M}_m^{(1)}\rangle = \left(4\pi\alpha_{\text{S}}(\mu)\right)^{q/2} \left(S_\epsilon^{\overline{\text{MS}}}\right)^{-q/2} \frac{\alpha_{\text{S}}(\mu)}{4\pi} \left[\left(S_\epsilon^{\overline{\text{MS}}}\right)^{-1} |\mathcal{A}_m^{(1)}\rangle - \frac{q}{2} \frac{\beta_0}{\epsilon} |\mathcal{A}_m^{(0)}\rangle \right], \tag{2.4}$$

and

$$|\mathcal{M}_m^{(2)}\rangle = \Big(4\pi\alpha_{\mathrm{S}}(\mu)\Big)^{q/2}\Big(S_\epsilon^{\overline{\mathrm{MS}}}\Big)^{-q/2}\left(\frac{\alpha_{\mathrm{S}}(\mu)}{4\pi}\right)^2\Bigg[\Big(S_\epsilon^{\overline{\mathrm{MS}}}\Big)^{-2}|\mathcal{A}_m^{(2)}\rangle - \frac{q+2}{2}\frac{\beta_0}{\epsilon}\Big(S_\epsilon^{\overline{\mathrm{MS}}}\Big)^{-1}|\mathcal{A}_m^{(1)}\rangle + \frac{q}{2}\left(\frac{q+2}{4}\frac{\beta_0^2}{\epsilon^2} - \frac{\beta_1}{\epsilon}\right)|\mathcal{A}_m^{(0)}\rangle\Bigg], \tag{2.5}$$

where β_0 was already defined in Eq. (1.4) and β_1 is the second coefficient of the QCD β function

$$\beta_1 = \frac{34}{3}C_{\mathrm{A}}^2 - \frac{20}{3}C_{\mathrm{A}}T_{\mathrm{R}}n_{\mathrm{f}} - 4C_{\mathrm{F}}T_{\mathrm{R}}n_{\mathrm{f}}\,. \tag{2.6}$$

Besides overall factors in Eqs. (2.4) and (2.5), there are counterterms containing unrenormalized amplitudes with less loops, which remove the ultraviolet divergences from the renormalized amplitudes. The factor $S_\epsilon^{\overline{\mathrm{MS}}} = (4\pi)^\epsilon \exp(-\epsilon\gamma_{\mathrm{E}})$ corresponds to the $\overline{\mathrm{MS}}$ scheme and often denoted in the literature as S_ϵ, but we reserve the latter for the factor

$$S_\epsilon = \frac{(4\pi)^\epsilon}{\Gamma(1-\epsilon)}\,. \tag{2.7}$$

The m particle phase space appearing in Eq. (2.2) is defined as

$$\mathrm{d}\Phi_m(p_1,\ldots,p_m;Q) = \left[\prod_{i=1}^m \frac{\mathrm{d}^d p_i}{(2\pi)^{d-1}}\delta_+(p_i^2-m_i^2)\right](2\pi)^d\delta^{(d)}(p_1^\mu+\cdots+p_m^\mu-Q^\mu)\,. \tag{2.8}$$

In perturbation theory the cross section is formally an expansion in the strong coupling α_{S} where up to NNLO accuracy it is sum of three terms

$$\sigma_m = \sigma_m^{\mathrm{LO}} + \sigma_m^{\mathrm{NLO}} + \sigma_m^{\mathrm{NNLO}} + \ldots\,. \tag{2.9}$$

The leading order cross section is the integral of the m particle differential Born cross section

$$\sigma_m^{\mathrm{LO}} = \int_m \mathrm{d}\sigma_m^{\mathrm{B}} J_m\,, \tag{2.10}$$

where

$$\mathrm{d}\sigma_m^{\mathrm{B}} = \mathrm{d}\Phi_m \langle\mathcal{M}_m^{(0)}|\mathcal{M}_m^{(0)}\rangle\,, \tag{2.11}$$

and $|\mathcal{M}_m^{(0)}\rangle$ is the m partonic Born matrix element. The NLO correction is composed from two different contributions, the $m+1$ partonic real correction and the m partonic virtual correction.

$$\sigma_m^{\mathrm{NLO}} = \int_{m+1}\mathrm{d}\sigma_{m+1}^{\mathrm{R}} J_{m+1} + \int_m \mathrm{d}\sigma_m^{\mathrm{V}} J_m\,. \tag{2.12}$$

The real contribution is simply the square of the $m+1$ tree-level matrix element

$$\mathrm{d}\sigma^{\mathrm{R}}_{m+1} = \mathrm{d}\Phi_{m+1}\langle\mathcal{M}^{(0)}_{m+1}|\mathcal{M}^{(0)}_{m+1}\rangle\,, \tag{2.13}$$

while the virtual correction is the interference of the tree-level and one-loop matrix elements for m external partons

$$\mathrm{d}\sigma^{\mathrm{V}}_{m} = \mathrm{d}\Phi_{m}2\mathrm{Re}\langle\mathcal{M}^{(0)}_{m}|\mathcal{M}^{(1)}_{m}\rangle\,. \tag{2.14}$$

Finally the NNLO correction is the sum of double real, the real-virtual, and the double virtual terms

$$\sigma^{\mathrm{NNLO}}_{m} = \int_{m+2}\mathrm{d}\sigma^{\mathrm{RR}}_{m+2}J_{m+2} + \int_{m+1}\mathrm{d}\sigma^{\mathrm{RV}}_{m+1}J_{m+1} + \int_{m}\mathrm{d}\sigma^{\mathrm{VV}}_{m}J_{m}\,, \tag{2.15}$$

The first two terms defined in the same way as in Eqs. (2.13) and (2.14) but with an extra particle

$$\mathrm{d}\sigma^{\mathrm{RR}}_{m+2} = \mathrm{d}\Phi_{m+2}\langle\mathcal{M}^{(0)}_{m+2}|\mathcal{M}^{(0)}_{m+2}\rangle\,,\quad \mathrm{d}\sigma^{\mathrm{RV}}_{m+1} = \mathrm{d}\Phi_{m+1}2\mathrm{Re}\langle\mathcal{M}^{(0)}_{m+1}|\mathcal{M}^{(1)}_{m+1}\rangle\,, \tag{2.16}$$

The double virtual contribution is the sum of the interference of the two-loop and the tree level matrix element, and the one-loop squared matrix element

$$\mathrm{d}\sigma^{\mathrm{VV}}_{m} = \mathrm{d}\Phi_{m}\Big(2\mathrm{Re}\langle\mathcal{M}^{(0)}_{m+2}|\mathcal{M}^{(2)}_{m}\rangle + \langle\mathcal{M}^{(1)}_{m}|\mathcal{M}^{(1)}_{m}\rangle\Big)\,. \tag{2.17}$$

2.2 The rise of singularities

Naively trying to calculate the first radiative correction we quickly encounter two serious problems. First, the loop integral in the one-loop matrix element is still divergent in the infrared (IR) limits. Secondly the phase space integral of the real contribution has non-integrable singularities. There are phase space configurations when one parton becomes collinear to another or a gluon turns soft and the $m+1$ matrix element diverges in these limits. These divergences have to be regularized and made explicit. This problem also can be handled using dimensional regularization. The KLN-theorem ensures that the cross section, such as σ^{NLO} is free of infrared divergences if the observable J is infrared safe. If we take the sum

$$\sigma^{\mathrm{NLO}} = \left[\int_{m+1}\mathrm{d}\sigma^{\mathrm{R}}_{m+1}J_{m+1} + \int_{m}\mathrm{d}\sigma^{\mathrm{V}}_{m}J_{m}\right]_{d=4}\,, \tag{2.18}$$

the infrared poles coming from loop integral cancel the poles coming from the phase space integral of the real contribution and we can set $\epsilon = 0$, removing the

regularization. The problem is that usually the d-dimensional phase space integral cannot be done analytically for the real contribution, because the integrand expression is too complicated (the double real even more). Numerical methods, such as Monte Carlo integration are ill-defined in $d = 4 - 2\epsilon$ dimensions. There are methods to deal with d-dimensional phase space integrals, like sector decomposition [11] and Mellin-Barnes integrals [12]. Both ways resolve the ϵ poles before integration, and pole coefficients are turned into four dimensional integrals, that can be computed with numerical methods.

In sector-decomposition we cut the n-dimensional integration range into sectors such that in one sector only one integration variable can have singularity, then we remap these sectors back to the original integration range (practically the n-dimensional unit hypercube). In addition we also has to regularize the integrals (with a + distribution for example), if it is necessary. Using these rules iteratively the original expression can be written as a sum of integrals, in which the integrand can be expanded in ϵ before integration, and the pole coefficients are finite integrals.

Using Merlin-Barnes (MB) integrals, we can turn sums in denominators into products introducing an extra complex contour integration. Then we can exploit the Barnes lemmas for MB integrals and use the apparatus of complex calculus, such as the residue theorem and contour shifting to manipulate the integrals into forms which can be computed analytically or numerically.

The drawback of these methods is that they often generate even bigger expressions and/or require non-trivial algebraic manipulations and integral transformations of the integrand prior to the application. Therefore their direct use to calculate complicated amplitudes is not practical, but they are really powerful on simpler integrals as we will see in Chapter 3.

One possible solution to the problem is to introduce subtraction terms that match the infrared limits of the integrand, and render the real matrix element integrable in $d = 4$ dimensions

$$\sigma^{\mathrm{NLO}} = \int_{m+1} \left[\mathrm{d}\sigma^{\mathrm{R}}_{m+1} J^{(m)}_{m+1} - \mathrm{d}\sigma^{\mathrm{R,A_1}}_{m+1} J_m \right]_{d=4} + \int_m \left[\mathrm{d}\sigma^{\mathrm{V}}_m + \int_1 \mathrm{d}\sigma^{\mathrm{R,A_1}}_{m+1} \right]_{d=4} J^{(m)}_m \,, \tag{2.19}$$

where $\mathrm{d}\sigma^{\mathrm{R,A_1}}_{m+1}$ is the $m+1$ particle approximate cross section. The approximate cross section is usually defined based on the universal factorization properties of QCD matrix elements. For example if particle i becomes collinear with particle r the $m+1$ particle tree-level matrix element factorizes as

$$\langle \mathcal{M}^{(0)}_{m+1} | \mathcal{M}^{(0)}_{m+1} \rangle \simeq 8\pi\alpha_{\mathrm{S}}\mu^{2\epsilon} \frac{1}{s_{ir}} \langle \mathcal{M}^{(0)}_m | \hat{P}^{(0)}_{f_i f_r} | \mathcal{M}^{(0)}_m \rangle \,, \tag{2.20}$$

where $s_{ir} = (p_i + p_r)^2$ and $\hat{P}^{(0)}_{f_i f_r}$ is the tree-level Altarelli-Parisi splitting kernel defined later explicitly in Eq. (6.10). Similarly, the squared matrix element factorizes

when a gluon r becomes soft

$$\langle \mathcal{M}^{(0)}_{m+1} | \mathcal{M}^{(0)}_{m+1} \rangle \simeq -8\pi\alpha_{\mathrm{S}}\mu^{2\epsilon} \sum_{i,j\neq i} \frac{1}{2} \mathcal{S}_{ij}(r) \langle \mathcal{M}^{(0)}_{m} | \mathbf{T}_i \mathbf{T}_j | \mathcal{M}^{(0)}_{m} \rangle \,, \tag{2.21}$$

where we sum over all external particles except r and the eikonal factor is defined as $\mathcal{S}_{ij}(r) = \frac{2s_{ij}}{s_{ir}s_{jr}}$. $\mathbf{T}_i$ is the color charge operator in the fundamental representation of the $SU(3)$ group if parton i is an (anti-)quark, or in the adjoint representation if parton i is a gluon.

Subtraction terms are defined based on infrared limits, but extended over the whole phase space using phase space mappings, such that they match the original squared matrix element in each phase space points in d-dimensions.

The $\int_1 \mathrm{d}\sigma^{\mathrm{R,A_1}}_{m+1}$ term is the subtraction term integrated over the one-particle unresolved phase space, which is added back to the virtual contribution to keep the original expression unchanged. The definition of the $\mathrm{d}\sigma^{\mathrm{R,A_1}}_{m+1}$ subtraction term is not unique. At NLO accuracy there are various solutions like the dipole method [13], the Frixione-Kunszt-Signer subtraction scheme [14, 15], the Nagy-Soper subtraction [16] or the Nagy-Trócsanyi subtraction scheme [17]. There are standard automated computer programs which with [18, 19, 20, 21, 22, 23, 24, 25, 26, 27] one can calculate a wide range of processes up to NLO accuracy.

Going one order higher in the perturbative series the complexity of the problem grows rapidly. The state-of-the-art research is the calculation of differential cross sections at NNLO accuracy. There are multiple subtraction methods such as the antenna subtraction [28], the sector-improved residue subtraction [29], the $q_\perp$ subtraction [30] and the CoLoRFulNNLO subtraction method. The n-jettiness slicing method [31], based on the soft-collinear effective field theory [32] also provides a possible way to calculate NNLO accurate cross sections. Recently none of these methods provides a standard, fully automated way yet to compute processes at NNLO accuracy, similarly to NLO automated programs.

2.3 Jet production in CoLoRFulNNLO

In the rest of the dissertation we will focus on the CoLoRFulNNLO (Completely Local subtRactions for Fully differential predictions at NNLO accuracy) subtraction method, summarize its philosophy and shortly discuss how we can compute jet cross sections at NNLO accuracy. We do not wish to go into the details, hence we only provide a sketchy summary. If the reader is interested in the detailed description and the precise definition of the expressions, they can be found in the following series of publications [33, 34, 35, 36, 37, 38, 39, 40, 41, 42, 43, 44].

In the CoLoRFulNNLO subtraction scheme, regularization of matrix elements is based on local subtractions. The subtraction terms are, like $\mathrm{d}\sigma^{\mathrm{R,A_1}}_{m+1}$, constructed

from the known factorization formulae of the QCD matrix elements in the infrared limits, like Eqs. (2.20) and (2.21). The singular matrix elements are rendered finite locally in each point in phase space. To fulfill this requirement, the subtraction candidates are extended over the whole phase space using phase space mappings in d-dimensions. The phase space mappings of the different subtraction terms in the CoLoRFulNNLO scheme lead to exact phase space factorizations, namely

$$\mathrm{d}\Phi_{m+1}(\{p\}) = \mathrm{d}\Phi_m(\{\hat{p}\})[\mathrm{d}p_r^{(1)}]\,, \tag{2.22}$$

where $[\mathrm{d}p_r^{(1)}]$ is the single unresolved phase space. Using this property, the subtraction term can be integrated independently of the rest of the m partonic phase space.

$$\int_1 \mathrm{d}\sigma_{m+1}^{\mathrm{R,A_1}} \equiv \int_1 [\mathrm{d}p_r^{(1)}]\mathrm{d}\sigma_{m+1}^{\mathrm{R,A_1}} = \mathrm{d}\sigma_m^{\mathrm{B}} \otimes \mathbf{I}_1^{(0)}(\{p\}_m;\epsilon)\,. \tag{2.23}$$

$\mathbf{I}_1^{(0)}$ is called the color insertion operator and it has the following structure in color space

$$\mathbf{I}_1^{(0)}(\{p\}_m;\epsilon) = \mathcal{C}_\epsilon \sum_i \left[\mathrm{C}_{1,i}^{(0)}(y_{iQ};\epsilon)\mathbf{T}_i^2 + \sum_{k\neq i} \mathrm{S}_1^{(0),(i,k)}(Y_{ik,Q};\epsilon)\mathbf{T}_i\mathbf{T}_k \right], \tag{2.24}$$

where summation indices i,k run over all external colored particles and the prefactor is

$$\mathcal{C}_\epsilon = \left[\frac{\alpha_\mathrm{S}}{2\pi} \frac{S_\epsilon}{S_\epsilon^{\overline{\mathrm{MS}}}} \left(\frac{\mu^2}{Q^2} \right)^\epsilon \right]. \tag{2.25}$$

The insertion operator acts on the squared matrix element with inserting color matrices

$$\langle \mathcal{M}_m | \mathcal{M}_m \rangle \otimes \mathbf{T}_i\mathbf{T}_j = \langle \mathcal{M}_m | \mathbf{T}_i\mathbf{T}_j | \mathcal{M}_m \rangle \equiv |\mathcal{M}_{m,(i,j)}|^2\,. \tag{2.26}$$

The kinematic variables y_{iQ}, $Y_{ik,Q}$ appearing in the operator are defined as

$$y_{iQ} = \frac{2p_iQ}{Q^2}\,, \quad y_{ik} = \frac{2p_ip_k}{Q^2}\,, \quad Y_{ik,Q} = \frac{y_{ik}}{y_{iQ}y_{kQ}}\,. \tag{2.27}$$

The kinematic functions $\mathrm{C}_{1,i}^{(0)}$ and $\mathrm{S}_1^{(0),(i,k)}$ were computed in Ref. [34] and their functional forms are universal and independent of the final state kinematics.

At NNLO accuracy the problem becomes more involved, since there are more possible unresolved limits with overlappings, hence the number of subtraction terms is largely increased. We start with rewriting Eq. (2.15) into an equivalent form

$$\sigma^{\mathrm{NNLO}} = \int_{m+2} \mathrm{d}\sigma_{m+2}^{\mathrm{NNLO}} + \int_{m+1} \mathrm{d}\sigma_{m+1}^{\mathrm{NNLO}} + \int_m \mathrm{d}\sigma_{m+2}^{\mathrm{NNLO}}\,, \tag{2.28}$$

where the three different terms are defined as

$$\mathrm{d}\sigma^{\mathrm{NNLO}}_{m+2} = \left\{ \mathrm{d}\sigma^{\mathrm{RR}}_{m+2} J^{(m)}_{m+2} - \mathrm{d}\sigma^{\mathrm{RR,A_2}}_{m+2} J^{(m)}_{m} - \left[\mathrm{d}\sigma^{\mathrm{RR,A_1}}_{m+2} J^{(m)}_{m+1} - \mathrm{d}\sigma^{\mathrm{RR,A_{12}}}_{m+2} J^{(m)}_{m} \right] \right\}_{d=4}, \tag{2.29}$$

$$\mathrm{d}\sigma^{\mathrm{NNLO}}_{m+1} = \left\{ \left[\mathrm{d}\sigma^{\mathrm{RV}}_{m+1} + \int_1 \mathrm{d}\sigma^{\mathrm{RR,A_1}}_{m+2} \right] J^{(m)}_{m+1} - \left[\mathrm{d}\sigma^{\mathrm{RV,A_1}}_{m+1} + \left(\int_1 \mathrm{d}\sigma^{\mathrm{RR,A_1}}_{m+2} \right)^{A_1} \right] J^{(m)}_{m} \right\}_{d=4}, \tag{2.30}$$

$$\begin{aligned} \mathrm{d}\sigma^{\mathrm{NNLO}}_{m} = \Bigg\{ & \mathrm{d}\sigma^{\mathrm{VV}}_{m} + \int_2 \left[\mathrm{d}\sigma^{\mathrm{RR,A_2}}_{m+2} - \mathrm{d}\sigma^{\mathrm{RR,A_{12}}}_{m+2} \right] \\ & + \int_1 \left[\mathrm{d}\sigma^{\mathrm{RV,A_1}}_{m+1} + \left(\int_1 \mathrm{d}\sigma^{\mathrm{RR,A_1}}_{m+2} \right)^{A_1} \right] \Bigg\}_{d=4} J^{(m)}_{m} \,. \end{aligned} \tag{2.31}$$

The double-real squared matrix element is singular both in the double-unresolved and in the single-unresolved limits. The subtraction term $\mathrm{d}\sigma^{\mathrm{RR,A_2}}_{m+2}$ regularizes the double-unresolved limits (e.g. triple collinear, double soft) of the $m+2$ particle squared matrix element, while $\mathrm{d}\sigma^{\mathrm{RR,A_1}}_{m+2}$ matches the single-unresolved limits. Since the double- and the single-unresolved limits overlap, the overlapping region is subtracted twice. In order to avoid double counting, $\mathrm{d}\sigma^{\mathrm{RR,A_{12}}}_{m+2}$ is present to remove the overlap of double- and single-unresolved subtraction terms. Hence the double-real contribution is completely regularized and can be computed in $d=4$ dimensions, removing the regularization.

The integral of $\mathrm{d}\sigma^{\mathrm{RR,A_1}}_{m+2}$ subtraction terms is added back to the real-virtual contribution, and it cancels the ϵ poles of $\mathrm{d}\sigma^{\mathrm{RV}}_{m+1}$, secured by the KNL theorem. However the real-virtual squared matrix element $\mathrm{d}\sigma^{\mathrm{RV}}_{m+1}$ also has infrared singularities in the single-unresolved limits. It is regularized by the $\mathrm{d}\sigma^{\mathrm{RV,A_1}}_{m+1}$ counterterm. The integrated subtraction term $\int_1 \mathrm{d}\sigma^{\mathrm{RR,A_1}}_{m+2}$ has also infrared divergences that are subtracted by $\left(\int_1 \mathrm{d}\sigma^{\mathrm{RR,A_1}}_{m+2} \right)^{\mathrm{A_1}}$ counterterm. We note that while the factorization of squared matrix elements in the infrared limits is guaranteed by QCD, the $\int_1 \mathrm{d}\sigma^{\mathrm{RR,A_1}}_{m+2}$ subtraction term does not necessarily has this property, it has to be ensured by its definition.

Finally the integrated double-unresolved, the one-loop single unresolved and the iterated single-unresolved counterterms are added back to the two-loop contribution. The poles of the double-virtual matrix element cancel against the poles of the integrated subtraction terms according to the KNL-theorem.

Similarly to the NLO case, the integrated counterterms can be written as

$$\int_2 \mathrm{d}\sigma^{\mathrm{RR,A_2}}_{m+2} = \mathrm{d}\sigma^{\mathrm{B}}_{m} \otimes \mathbf{I}^{(0)}_2(\{p\}_m;\epsilon)\,, \tag{2.32}$$

$$\int_1 \mathrm{d}\sigma_{m+2}^{\mathrm{RR,A_1}} = \mathrm{d}\sigma_{m+1}^{\mathrm{R}} \otimes \mathbf{I}_1^{(0)}(\{p\}_{m+1};\epsilon)\,, \tag{2.33}$$

$$\int_2 \mathrm{d}\sigma_{m+2}^{\mathrm{RR,A_{12}}} = \mathrm{d}\sigma_{m}^{\mathrm{B}} \otimes \mathbf{I}_{12}^{(0)}(\{p\}_{m};\epsilon)\,, \tag{2.34}$$

$$\int_1 \mathrm{d}\sigma_{m+1}^{\mathrm{RV,A_1}} = \mathrm{d}\sigma_{m}^{\mathrm{V}} \otimes \mathbf{I}_1^{(0)}(\{p\}_{m};\epsilon) + \mathrm{d}\sigma_{m}^{\mathrm{B}} \otimes \mathbf{I}_1^{(1)}(\{p\}_{m};\epsilon)\,, \tag{2.35}$$

$$\int_1 \left(\int_1 \mathrm{d}\sigma_{m+2}^{\mathrm{RR,A_1}} \right)^{\mathrm{A_1}} = \mathrm{d}\sigma_{m}^{\mathrm{B}} \otimes \left[\frac{1}{2} \left\{ \mathbf{I}_1^{(0)}(\{p\}_{m};\epsilon), \mathbf{I}_1^{(0)}(\{p\}_{m};\epsilon) \right\} + \mathbf{I}_{1,1}^{(0,0)}(\{p\}_{m};\epsilon) \right], \tag{2.36}$$

where the anti-commutator is

$$\left\{ \mathbf{I}_1^{(0)}(\{p\}_{m};\epsilon), \mathbf{I}_1^{(0)}(\{p\}_{m};\epsilon) \right\} = \mathbf{I}_1^{(0)}(\{p\}_{m};\epsilon)\mathbf{I}_1^{(0)}(\{p\}_{m};\epsilon) + \mathbf{I}_1^{(0)}(\{p\}_{m};\epsilon)\mathbf{I}_1^{(0)}(\{p\}_{m};\epsilon)\,, \tag{2.37}$$

and the form of color insertion operators $\mathbf{I}_2^{(0)}$, $\mathbf{I}_{12}^{(0)}$, $\mathbf{I}_1^{(1)}$ and $\mathbf{I}_{1,1}^{(0,0)}$ will be later defined in Chapter 3.

The pole structure of the integrated counterterms were calculated analytically and they cancel the poles of the two-loop squared matrix element.[1] As a result Eqs. (2.29), (2.30) and (2.31) are all free of ϵ poles at the integrand level and regularization can be removed setting $\epsilon = 0$. Thus the integrals can be performed in $d = 4$ dimensions with usual Monte Carlo techniques.

The CoLoRFulNNLO scheme for e^+e^- collisions is implemented in the `MCCSM` (Monte Carlo for the ColorfulNNLO Subtraction Method) partonic numerical Monte Carlo program. The program has been used to calculate the $H \to b\bar{b}$ decay rate at NNLO accuracy [45], and event shapes for three-jet production in e^+e^- collisions [46, 44, 47]. Recently we calculated the three-jet rate at NNLO accuracy in e^+e^- annihilation matched with next-to-double logarithmic resummation (see definition in the next chapter) using the $k_\perp$ and the anti-$k_\perp$ jet clustering algorithms [48, 47], which results will be later discussed in details in Chapter 4 and 5.

2.4 Resummation of logarithmic terms

Fixed-order calculations provide good description for many observables. However there are regions in phase space where multiple soft-collinear emissions dominates and the fixed-order prediction fails due to the presence of logarithmically enhanced

[1] Which is highly not trivial. In three-jet production 200000 lines of analytic expression cancels exactly into 0.

contributions. In these regions the small value of α_S gets compensated by a logarithmic term L, and the effective expansion parameter $\alpha_S L \approx 1$ becomes non-perturbative. Thus all-order resummation of these contributions is needed. For event shape variables f the resummed logarithmic terms exponentiate completely

$$f(L) \sim \exp(Lg_1(\alpha_S L) + g_2(\alpha_S L) + \alpha_S g_3(\alpha_S L) + \dots)\,, \tag{2.38}$$

where g_1, g_2, g_3 and so on are functions which resums the different logarithmic terms. The g_1 function includes the leading logarithmic (LL) terms $\alpha_S^n L^{n+1}$, g_2 includes the next-to-leading logarithmic (NLL) terms in the exponent and so forth. However not all kind of observables, for example jet rates, exponentiate therefore the more general definition is [49] for the observable O

$$O(L) \sim \exp(Lg_1(\alpha_S L) + g_2(\alpha_S L) + \alpha_S g_3(\alpha_S L) + \dots)\mathcal{F}(L)\,. \tag{2.39}$$

The accuracy of resummation is determined by the type of logarithms included, thus the knowledge of the g_1, g_2, ... and the $\mathcal{F}(L)$ functions.

In the literature we can find another type of definition for the accuracy of resummation based on the α_S expansion of the resummed formula. Thus LL accuracy means resummation of all $\alpha_S^n L^{2n}$ type logarithmic terms, NLL accuracy means resummation of all $aS^n L^{2n-1}$ kind of logarithmic terms and so on. In order to avoid confusion whether the (N)LL accuracy is meant for the resummed or the expanded version, we introduce the definition of double logarithmic (DL) and next-to-double logarithmic (NDL) accuracy, as the $\alpha_S^n L^{2n}$ and $\alpha_S^n L^{2n-1}$ terms of the fixed-order expansion are often called double and next-to-double logarithms. By NDL accuracy we mean that the observable O can be written as a function with α_S expansion in the form

$$O(L) = \sum_{n=1}^{\infty} \alpha_S^n \Big(G_{n,2n} L^{2n} + G_{n,2n-1} L^{2n-1} + \mathcal{O}(L^{2n-2}) \Big)\,, \tag{2.40}$$

where all $G_{n,2n}$ and $G_{n,2n-1}$ coefficients are known. This is a looser condition compared to Eq. (2.39), NLL always includes NDL accuracy, but the inverse is not necessarily true.

Analytic NLL accurate resummation has been achieved for many observables [50, 51, 52, 53, 54, 3, 55, 56, 57, 58] in e^+e^- collisions. The resummation of jet rates are available at NDL accuracy for the $k_\perp$ and the general inclusive $k_\perp$ algorithm [8, 59]. Some event shapes have been also resummed beyond NLL accuracy [60, 61, 62, 63, 64, 65]. The drawback of these analytic computations however is that their derivation is based on observable dependent factorization properties, hence the calculations have to be carried out independently for every single quantity. This problem can be solved by using numerical approaches, which provide general methods for resummation up to NLL [49] for general observables fulfilling

the requirement of the method and recently NNLL accuracy for event shapes variables [66].

The fixed-order and resummed calculations can be matched together to provide an enhanced theoretical prediction that describes a wider range of data for a given observable. There are two different matching schemes which are usually used: the R-matching and the $\log R$-matching schemes [50].

In the R-matching scheme we add together the predictions of the resummed and the fixed-order calculations and subtract the overlapping contributions:

$$O^{\text{matched}}(L) = O^{\text{resummed}}(L) - O^{\text{resummed}}_{exp}(L) + O^{\text{FO}}(L)\,, \tag{2.41}$$

where $O^{\text{resummed}}_{exp}(L)$ is the fixed-order α_{S} expansion of the resummed calculation.

In the $\log R$-matching however we perform the matching for the logarithm of the observable $O(L)$:

$$\log O^{\text{matched}}(L) = \log O^{\text{resummed}}(L) - \Big(\log O^{\text{resummed}}(L)\Big)_{exp} + \tilde{O}^{\text{FO}}(L)\,. \tag{2.42}$$

$\Big(\log O^{\text{resummed}}(L)\Big)_{exp}$ is the α_{S} expansion of the logarithm of the resummed prediction, while $\tilde{O}^{\text{FO}}(L)$ is the exponentiated form of the fixed-order calculation such that it fulfills the following requirement

$$\exp\Big(\tilde{O}^{\text{FO}}(L)\Big) \xrightarrow{\alpha_{\text{S}}\,\text{exp}} \frac{\alpha_{\text{S}}}{2\pi}A(L) + \left(\frac{\alpha_{\text{S}}}{2\pi}\right)^2 B(L) + \left(\frac{\alpha_{\text{S}}}{2\pi}\right)^3 C(L) + \mathcal{O}(\alpha_{\text{S}}^4)\,. \tag{2.43}$$

The preferred matching scheme is $\log R$-matching, because it is less sensitive for missing subleading logarithms. Due to these missing logarithms the difference $O^{\text{FO}}(L) - O^{\text{resummed}}_{exp}(L)$ can diverge which ends in unphysical behavior in the asymptotic region. However in the $\log R$-matching not the difference but the ratio of the fixed-order like contributions is used which approaches 1 in the asymptotic region, even if the difference does not converge to 0.

For event shape observables both matching schemes are feasible but as mentioned usually the $\log R$-matching scheme is preferred. For jet rates presently only the R-matching scheme was used, but in principle one could work out the relevant formulae for $\log R$-matching following the general idea presented in Eq. (2.42). We started research in this topic, however it is not completely worked out yet hence we do not include $\log R$-matching in this dissertation, but will be published in [47].

2.5 The importance of three-jet production

As we mentioned in the introduction the precise determination of the strong coupling α_{S} is a constantly revisited problem in high energy physics. With the de-

velopment of experimental accuracy and new analysis methods, and availability of improved theoretical predictions the measurement of α_S becomes more precise.

Electron-positron colliders provide an ideal environment to test the strong coupling of QCD with the study of the production of two or more hadronic jets. A favorable choice is the production of three jets, because the production rate is proportional to α_S at already leading order of perturbation theory.

In the past twenty years the measurement of α_S has been performed many times using LEP and LEP2 data at various center-of-mass energies [67, 68, 69, 70, 71, 72, 73, 74, 75, 76, 77]. Some of these measurements were based on the study of the three-jet rate using jet clustering algorithms [68, 70, 72, 75, 77].

The key of accuracy is to provide precise theoretical predictions, which are available at NNLO accuracy for the $k_\perp$ algorithm [78, 79, 80, 81], and for the general inclusive $k_\perp$ and the SISCOne algorithm [81].

Although the work of Schieck et al. [77] used NNLO accurate predictions matched with NDL accurate resummation for the three-jet rate using the $k_\perp$ at various energy scales in the analysis, the $\sqrt{Q^2} = 91.2$ GeV center-of-mass energy was not included, and no matched predictions has been published yet for the three-jet rate at $\sqrt{Q^2} = 91.2$ GeV.

Besides this there are also three different varieties [8, 82, 83] for the three-jet rate resummation with the $k_\perp$ algorithm, which were not compared before. Also the resummation for general inclusive $k_\perp$ algorithm at NDL accuracy is available [59].

In my dissertation I explore these uncharted territories and I make matched predictions at NNLO+NDL accuracy for the three-jet rate including both the $k_\perp$ and the general inclusive $k_\perp$ algorithm. Before the discussion of the jet rates I present my work in the development of the CoLoRFulNNLO subtraction scheme, where I calculated the integrated subtraction terms numerically. After I presented my results in e^+e^- collisions, I discuss some intermediate work done in the extension of the CoLoRFulNNLO subtraction scheme to hadron-hadron collisions.

Part II

Results

Chapter 3

Numerical integration of subtraction terms

We have seen that the double- and single-unresolved integrated subtraction terms must be added back to the real-virtual and the double-virtual contribution in order to keep the whole expression unchanged. These integrated subtraction terms are known analytically up to the $\mathcal{O}(\epsilon^{-1})$ pole. However the finite part is not exactly known yet in full analytic form, since it is the most complicated to compute. In this chapter we discuss the numerical calculation of the finite part of the integrated counterterms in the three-jet kinematics. We start with the introduction of the problem, namely the necessity of computing large number of integrals, then we review the automated method developed to solve this problem. Finally we discuss our results.

3.1 Statement of the problem

The integrated subtraction terms in Eq. (2.31), similarly to $\int_1 \mathrm{d}\sigma_{m+1}^{R,A_1}$ can be decomposed into an universal color insertion operator acting on the Born amplitude. Let us start with the integrated double-unresolved counterterm that can be written as

$$\int_2 \mathrm{d}\sigma_{m+2}^{\mathrm{RR,A_2}} = \mathrm{d}\sigma_m^{\mathrm{B}} \otimes \mathbf{I}_2^{(0)}(\{p\}_m;\epsilon)\,. \tag{3.1}$$

The insertion operator $\mathbf{I}_2^{(0)}$ has the following color structure

$$\begin{aligned}\mathbf{I}_2^{(0)}(\{p\}_m;\epsilon) = \mathcal{C}_\epsilon^2\Bigg\{ &\sum_i \left[\mathrm{C}_{2,i}^{(0)}(y_{iQ};\epsilon)\mathbf{T}_i^2 + \sum_{j\neq i}\mathrm{C}_{2,ij}^{(0)}(y_{iQ},y_{jQ},Y_{ij,Q};\epsilon)\mathbf{T}_j^2\right]\mathbf{T}_i^2 \\ &+ \sum_{j,l\neq j}\left[\mathrm{S}_2^{(0),(j,l)}(Y_{jl,Q};\epsilon)C_\mathrm{A} + \sum_i \mathrm{CS}_{2,i}^{(0),(j,l)}(y_{iQ},Y_{ij,Q},Y_{il,Q},Y_{jl,Q};\epsilon)\mathbf{T}_i^2\right]\mathbf{T}_j\mathbf{T}_l \\ &+ \sum_{i,k\neq i}\sum_{j,l\neq j}\mathrm{S}_2^{(0),(i,k)(j,l)}(Y_{ik,Q},Y_{ij,Q},Y_{il,Q},Y_{jk,Q},Y_{kl,Q},Y_{jl,Q};\epsilon)\{\mathbf{T}_i\mathbf{T}_k,\mathbf{T}_j\mathbf{T}_l\}\Bigg\},\end{aligned} \tag{3.2}$$

where $\mathrm{C}_{2,i}^{(0)}$, $\mathrm{C}_{2,ij}^{(0)}$, ... are kinematic functions similarly the functions turning up in $\mathbf{I}_1^{(0)}$ and the summation indices run over all external colored particles.

The integral of the $\mathrm{d}\sigma_{m+2}^{\mathrm{RR,A_{12}}}$ counterterm, which removes the overlap of the single- and double-unresolved regions of the double-real contribution is

$$\int_2 \mathrm{d}\sigma_{m+2}^{\mathrm{RR,A_{12}}} = \mathrm{d}\sigma_m^\mathrm{B}\otimes\mathbf{I}_{12}^{(0)}(\{p\}_m;\epsilon)\,, \tag{3.3}$$

where, $\mathbf{I}_{12}^{(0)}$ insertion operator has the same color structure as $\mathbf{I}_2^{(0)}$, but with different kinematic functions, labeled with 12 subscript.

The integrated subtraction term of the real-virtual cross section is sum of two terms

$$\int_1 \mathrm{d}\sigma_{m+1}^{\mathrm{RV,A_1}} = \mathrm{d}\sigma_m^\mathrm{V}\otimes\mathbf{I}_1^{(0)}(\{p\}_m;\epsilon) + \mathrm{d}\sigma_m^\mathrm{B}\otimes\mathbf{I}_1^{(1)}(\{p\}_m;\epsilon)\,, \tag{3.4}$$

where the insertion operator is

$$\begin{aligned}\mathbf{I}_1^{(1)}(\{p\}_m;\epsilon) = \mathcal{C}_\epsilon^2\sum_i\Bigg[&\mathrm{C}_{1,i}^{(1)}(y_{iQ};\epsilon)C_\mathrm{A}\mathbf{T}_i^2 + \sum_{k\neq i}\mathrm{S}_1^{(1),(i,k)}(Y_{ik,Q};\epsilon)C_\mathrm{A}\mathbf{T}_i\mathbf{T}_k \\ &+ \sum_{k\neq i}\sum_{l\neq i,k}\mathrm{S}_1^{(1),(i,k,l)}(Y_{ik,Q},Y_{il,Q},Y_{kl,Q};\epsilon)\sum_{a,b,c}f_{abc}\mathbf{T}_i^a\mathbf{T}_k^b\mathbf{T}_l^c\Bigg],\end{aligned} \tag{3.5}$$

and $\mathbf{I}_1^{(0)}$ was earlier defined in Eq. (2.24).

Finally the integral of the subtraction defined for the integrated single-unresolved $m+2$ particle subtraction term is

$$\int_1\left(\int_1 \mathrm{d}\sigma_{m+2}^{\mathrm{RR,A_1}}\right)^{\mathrm{A_1}} = \mathrm{d}\sigma_m^\mathrm{B}\otimes\left[\frac{1}{2}\Big\{\mathbf{I}_1^{(0)}(\{p\}_m;\epsilon),\mathbf{I}_1^{(0)}(\{p\}_m;\epsilon)\Big\} + \mathbf{I}_{1,1}^{(0,0)}(\{p\}_m;\epsilon)\right], \tag{3.6}$$

with

$$\mathbf{I}_{1,1}^{(0,0)}(\{p\}_m;\epsilon) = \mathcal{C}_\epsilon^2 \sum_i \left[\mathrm{C}_{1,1,i}^{(0,0)}(y_{iQ};\epsilon) C_\mathrm{A} \mathbf{T}_i^2 + \sum_{k\neq i} \mathrm{S}_{1,1}^{(0,0),(i,k)}(Y_{ik,Q};\epsilon) C_\mathrm{A} \mathbf{T}_i \mathbf{T}_k \right]. \tag{3.7}$$

Similarly to $\mathbf{I}_1^{(0)}$, the kinematic functions present in the $\mathbf{I}_2^{(0)}$, $\mathbf{I}_{12}^{(0)}$, $\mathbf{I}_1^{(1)}$ and $\mathbf{I}_{1,1}^{(0,0)}$ operators can be computed independently of the kinematics. Presently their functional form is known fully analytically for the poles up to $\mathcal{O}(\epsilon^{-1})$ and in the asymptotic region for the finite part. Some functions may not show up in every process, for example the $\mathrm{S}_1^{(1),(i,k,l)}(Y_{ik,Q}, Y_{il,Q}, Y_{kl,Q};\epsilon)$ term only contributes in processes with more than three hard partons.

The kinematic functions can be written as a linear combination of so-called master integrals. Thus the computation of the insertion operators is reduced to the calculation of the master integrals. These integrals come in high numbers, the CoLoRFulNNLO scheme consist of around 250 different integrals, the exact numbers are summarized in Table 3.1. The master integrals originate from the

Insertion operator	No. of integrals
$\mathbf{I}_1^{(0)}, \mathbf{I}_1^{(1)}, \mathbf{I}_{1,1}^{(0,0)}$	67
$\mathbf{I}_{12}^{(0)}$	109
$\mathbf{I}_2^{(0)}$	104

Table 3.1. The number of integrals appearing in the insertion operators. Since there are some relations between certain integrals, the exact number is a bit less but still around 250.

Altarelli-Parisi splitting kernels and the eikonal factors integrated over the unresolved phase space in d-dimensions. They are functions of kinematic variables defined in Eq. (2.27).

Now let us consider an example: the master integrals $\mathcal{I}_{2\mathcal{C},1}^{(j,k,l,m)}$ of the $\mathbf{I}_2^{(0)}$ insertion operator originating from triple-collinear limits depends on the kinematic variable y_{iQ} defined in Eq. (2.27). The nomenclature is the following: the first number in the subscription refers to the insertion operator in which the master integral turns up, the label $\mathcal{C}$, $\mathcal{S}$ or $\mathcal{CS}$ shows which kinematic function the integral belongs to. Finally there is a simple numbering of the integrals of similar kind.

The $\mathcal{I}^{(j,k,l,m)}_{2\mathcal{C},1}$ integral has a rather complicated expression

$$\begin{aligned}\mathcal{I}^{(j,k,l,m)}_{2\mathcal{C},1}(y_{iQ},\epsilon;\alpha_0,d_0) &= 2^{-4\epsilon}\frac{\Gamma^2(1-\epsilon)}{\pi\Gamma(1-2\epsilon)}y_{iQ}\int_0^{\alpha_0}\mathrm{d}\alpha\int_0^1\mathrm{d}t\,\mathrm{d}\tau\,\mathrm{d}v\,\mathrm{d}w \\ &\times\alpha^{-1-2\epsilon}(1-\alpha)^{2d_0-3+2\epsilon}(\alpha+(1-\alpha)y_{iQ})^{-1-2\epsilon}(2\alpha+(1-\alpha)y_{iQ})^{-m} \\ &\times t^{k+l+1-2\epsilon}(1-t)^{j+l+m+1-2\epsilon}\tau^{l-\epsilon}(1-\tau)^{j-\epsilon}v^{-\epsilon}(1-v)^{-\epsilon} \\ &\times w^{-1/2-\epsilon}(1-w)^{-1/2-\epsilon}(1-\tau+\tau t)^{-j-l-2+2\epsilon}(\alpha+(1-\alpha)y_{iQ}v)^m\,,\end{aligned} \tag{3.8}$$

where depending on the choice of j,k,l,m $(=-1,0,1,2)$ parameters of the integral we could have 256 different integrals, however the actual number related to the triple-collinear kernels is only 13.

The integral has singularities on the integration borders and singularities can overlap in general. These singularities can be resolved either using the sector decomposition method or the Mellin-Barnes integral representations as we mentioned earlier. After resolving the divergences, the integrand can be expanded in ϵ up to desired order and the series coefficients become finite integrals in $d=4$ dimension. However these coefficient integrals typically have large integrands resulting from the pole-resolving procedure, and their complexity increases as we consider higher order terms in the ϵ expansion. Some of the 250 integrals are known fully analytically, like all the integrals appearing in $\mathbf{I}^{(0)}_1$, but in general only the pole coefficients are known. Thus the finite part must be computed numerically.

Since the master integrals are functions of the kinematic variables, they would have to be evaluated in every phase space point when we perform the Monte Carlo integration of the differential cross section. The large number of such complicated integrals portrayed in Eq. (3.8) and the fact that the numerical calculation of the finite parts takes minutes per integral[1] make the direct use of the master integrals in a partonic Monte Carlo code hopeless.

One possible solution is to calculate the master integrals numerically on a sufficiently fine grid of kinematic variables, then fit the results with a simpler analytic function. In the case of one or two kinematic variables we showed that the master integrals can be fitted with sum of a logarithmic and a polynomial function [84], as shown in Figs. A.1 and A.2 in Appendix A. However master integrals depending on 3 or more kinematic variables would require a robust grid with too many points to evaluate and the functional form of the fit becomes also complicated.

In practical applications of the CoLoRFulNNLO scheme, like $e^+e^-\to 2\,\text{or}\,3$ jets we can take advantage from the special final state kinematics. In the two jet case for example the jets are back-to-back and the insertion operators depend

[1] Usually the decomposition part takes couple of seconds, but numerical integration is rather expensive.

only on the y_{12} kinematic variable. Due to the kinematic constraints of two-jet production the insertion operators and the master integrals must be evaluated in only one point. In three-jet production the insertion operators depend on only two independent kinematic variables: y_{13} and y_{23}, therefore the operators can be fitted on a plane without any further complications.

We distributed 175 points in the $y_{13} - y_{23}$ plane to cover the whole phase space. We know that the insertion operators have a logarithmic dependence on y_{ij}, therefore points in the asymptotic regions are distributed uniformly on logarithmic scale.

The master integrals depend directly on the $y_{iQ} = 1 - y_{kl}$ and $Y_{ij,Q}$ variables defined in Eq. (2.27) with $i, j = 1, 2, 3$ in the three-jet kinematics. When we choose one point from the $y_{13} - y_{23}$ plane, we have to evaluate the master integrals in all possible y_{iQ} and $Y_{ij,Q}$ combinations. For example $\mathcal{I}^{(j,k,l,m)}_{2\mathcal{C},1}$ is a function of y_{iQ}, therefore we have to perform the numerical integration three times using y_{1Q}, y_{2Q} and y_{3Q} respectively. The master integral $\mathcal{I}_{2\mathcal{S},2}$ of the $\mathbf{I}^{(0)}_2$ operator related to integrated double-soft limit depends on $Y_{ij,Q}$, $Y_{ik,Q}$ and $Y_{jk,Q}$, thus six different possible combinations belong to one specific $y_{13} - y_{23}$ pair. To obtain all the insertion operators on the grid consisting 175 point pairs, we have to calculate $\mathcal{O}(10^4)$ numerical integrals. Considering the large number of integrations and the required time, the procedure must be automated as much as possible and one can run the whole calculation on large computers without any further intervention.

3.2 Automated numerical calculation of integrals

The numerical integrations can be performed with already existing tools. Sector decomposition was implemented in various programs, like `SecDec` [85, 86, 87, 88, 89], `FIESTA` [90, 91, 92, 93] and a program provided by Bogner et al [94], all three approaches focusing mainly on multi-loop integrals. For master integrals that we calculated via sector decomposition we chose the program `SecDec`, because it provides sector decomposition for generic phase space integrals from its first release. `SecDec` can take multipoint lists as an input from which it calculates the integrals sequentially in those point. The program uses the `CUBA` [95] library for integration[2]. Although in principle the integration can run on multiple threads, our observation is that only one thread is used effectively by `CUBA`, even if there are other forked threads. Multiple points cannot be calculated simultaneously for the same integral, because some intermediate files could mix up during calculation providing wrong results in the end. Also if we would like to calculate a different type of integral, we have to set up and run the process manually again and again. Clearly `SecDec` was not designed to calculate phase space integrals in industrial

[2]We found the `Cuhre` algorithm the most suitable

manner, but it can perfectly serve as a basis for our purpose, without any serious modifications.[3]

The double soft integrals of $\mathbf{I}_2^{(0)}$ were calculated using Mellin-Barnes technique. This technology is implemented in several `Mathematica` packages collectively called `MBTools` [96, 97] and allows to perform numerical integration for integrals in the Mellin-Barnes representation. In these cases the integrals are calculated by running `Mathematica` package files which takes similar multipoint input lists and produces result files in the same fashion as `SecDec` does. Thus the automation of the MB type calculations works in the same spirit as it will be described below for `SecDec`, therefore we will not distinct between these two different type of approaches.

We built up an automated framework around `SecDec` which manages the distribution, and the calculation of the integrals and finally collects the results. The basic idea is the following: since basically one integration uses only one core effectively, regardless of the corresponding settings, we use a one core per integration principle. Based on this we automate the whole calculation process from the beginning up to the end in the following way:

- we set up `SecDec` N-times, where $N \leq n_{\text{cores}}$, in order to avoid any crosstalk between intermediate files.
- We take the set of integrals wished to be calculated and distribute them uniformly between the present `SecDec` setups.
- We use the advantage that `SecDec` can compute these integrals in multiple points sequentially, provided the list of points.
- We write launching scripts for each `SecDec` used, ensuring that simultaneously only one integral is calculated in one thread.
- We launch N threads of `SecDec` calculations parallel on N CPU cores.
- If all the integrations are ready, we collect the results in two steps: first we collect all the individual result files produced by `SecDec` for each point into simple data tables for each integral separately, then we transform these data into the desired final format.

The first point of the previous list is basically the installation process. The master integrals have to be implemented in `SecDec` input format only once, the multipoint input files are generated automatically for every integral from the $y_{13} - y_{23}$ gridpoints with a computer program. After this has been set up we only start the process and then wait until it is finished.

[3] However some minor patching was necessary.

3.2.1 ICalc

The algorithm portrayed above is realized in a computer program called `ICalc`.[4] `ICalc` is written in `python 2.7` language, which provides an easy way of scripting with very powerful tools. `ICalc` is built around `SecDec-2.1` [86, 87], the most up-to-date version during the time of development. Since then `SecDec-3.0` [88] was released with a completely rewritten loop part, however the general part, which we use for our calculations was not changed, thus we did not upgrade it. Borowka et al. also released `pySecDec` [89] a brand new reincarnation of the original program, but our calculation was already done with the original `ICalc` setup.

During its installation process `ICalc` creates N identical copies of `SecDec` folders and installs them. The user only needs to provide the integrand inputs in the proper `SecDec` format and the multipoint list, and a simple input card for `ICalc` in a predefined directory structure. Depending on the users desire, `ICalc` can launch two `C++` programs to collect the results. The `CollectRes` program scans the result files generated by `SecDec` and takes out the pole coefficient values with the corresponding integration error. The results are collected into data tables for each integral separately. Once the data files are ready, `ICalc` executes the `MakeMath` program. The insertion operators are coded in `Mathematica`, and due to this reason we need to define the master integrals in each calculated kinematic point as function in this format. The `MakeMath` program does this job, and transform the data sheets into `SeriesData` objects as a function of the kinematic variables. For example let we have some function which is denoted by $\mathcal{T}^{-1}_{1\mathcal{C},0}(\alpha_0, y_{1Q})$ depending on two variables and having labels $1\mathcal{C}, 0, -1$. After numerical calculation in the $\alpha_0 = 1.0i\,, y_{1Q} = 0.2$ point we get the following data table

α_0	y_{1Q}	ϵ^{-2}	ϵ^{-1}	ϵ^{0}
1.0	0.2	0.5	-6.078	-21.239

which is then transformed into `Mathematica` format in the following way

```
T1C[0,1.0,0.2,-1]:=SeriesData[e,0,0.5,-6.078,-21.239,-2,1,1];
```

3.3 Results and application

Using the `ICalc` framework, we calculated the $\mathbf{I}^{(0)}_{2}$, $\mathbf{I}^{(0)}_{12}$, $\mathbf{I}^{(1)}_{1}$ and $\mathbf{I}^{(0,0)}_{1,1}$ operators over the grid in 175 pointpairs (partially the $\mathbf{I}^{(0)}_{12}$ operator was obtained using a different computation method). We tested our numerical accuracy on the poles, we compared the numerical results against the analytical ones in each point and they showed agreement as visible in Fig 3.1.

[4] `ICalc` stands for IntegralCalculator.

In Fig. 3.1 we show the relative accuracy of ϵ^{-1} pole of the following combination of insertion operators

$$\mathbf{I}_{\text{sum}} \equiv \mathbf{I}_2^{(0)} - \mathbf{I}_{12}^{(0)} + \mathbf{I}_1^{(1)} + \mathbf{I}_{1,1}^{(0,0)} \,. \tag{3.9}$$

The $\mathbf{I}_{\text{sum}}$ combination is computed numerically from the master integrals, and is compared to analytic result of the same quantity. Half of the phase space point

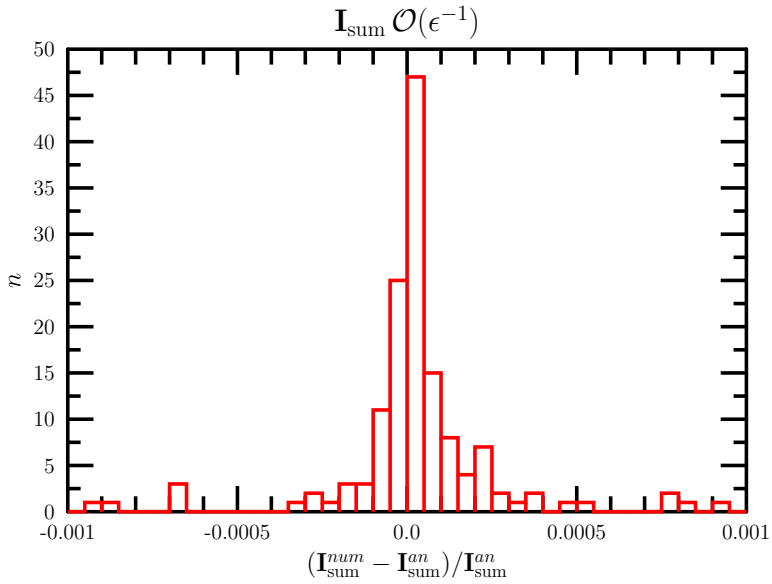

Figure 3.1. Histogram showing the distribution of the relative accuracy of the numerically calculated insertion operators in all 175 points.

has 10^{-4} or better relative accuracy, and most of the points are below in the $[-5 \cdot 10^{-3}, 5 \cdot 10^{-4}]$ region.

Following our original intention, we fitted the insertion operators with a logarithmic function which had a good agreement with the numerically calculated results. Although the main contribution comes from logarithmic behavior, we know that the insertion operator also contain rational functions which are finite in the borders. Therefore we added extra polynomial terms to the logarithmic fit function to estimate the robustness of the fit. However when we varied the functional form, the fitted values of the logarithmic coefficients changed as well. Physical predictions were found to be sensitive to such changes in the end regions,

where indeed the logarithms are the dominant contributions. In order to avoid large and overestimated systematical uncertainties, we computed the asymptotic behavior of the master integrals analytically.

We found that the

$$\mathbf{J}_2 \equiv \mathbf{I}_2^{(0)} - \mathbf{I}_{12}^{(0)} + \mathbf{I}_1^{(1)} + \mathbf{I}_{1,1}^{(0,0)} + \frac{1}{4}\Big\{\mathbf{I}_1^{(0)}, \mathbf{I}_1^{(0)}\Big\} \tag{3.10}$$

combination of insertion operators forms a relatively simple expression. Using this definition Eq. (2.31) in the three-jet kinematics can be written as

$$\mathrm{d}\sigma_3^{\mathrm{NNLO}} = \Big[\mathrm{d}\sigma_3^{\mathrm{VV}} + \mathrm{d}\sigma_3^{\mathrm{B}} \otimes \Big(\mathbf{J}_2 + \frac{1}{4}\Big\{\mathbf{I}_1^{(0)}, \mathbf{I}_1^{(0)}\Big\}\Big) + \mathrm{d}\sigma_3^{\mathrm{V}} \otimes \mathbf{I}_1^{(0)}\Big] J_3\,, \tag{3.11}$$

where only the $\mathbf{J}_2$ operator contains numerical pieces. The finite part of $\mathbf{J}_2$ can be decomposed into an asymptotic part which contains logarithmic terms and diverges at the edges of the phase space, and a regular part that is finite over the whole phase space

$$Fin\Big(\mathbf{J}_2\Big) = Fin\Big(\mathbf{J}_2^{\mathrm{asy}}\Big) + Fin\Big(\mathbf{J}_2^{\mathrm{reg}}\Big)\,, \tag{3.12}$$

where the explicit expression of $Fin\Big(\mathbf{J}_2^{\mathrm{asy}}\Big)$ can be found in Ref. [44]. We obtained $Fin\Big(\mathbf{J}_2^{\mathrm{reg}}\Big)$ by subtracting the analytic asymptotic formula from the numerical finite part of $\mathbf{J}_2$. We found that the regular part can be approximated well by a constant in the whole phase space (within uncertainties), and its value is

$$Fin\Big(\mathbf{J}_2^{\mathrm{reg}}\Big) = \mathcal{C}_\epsilon^2(-650)\,. \tag{3.13}$$

We implemented Eq. 3.11 as the double-virtual contribution in the `MCCSM` partonic Monte Carlo code, that we used to calculate physical observables in $e^+e^- \to 3\,$jets production at NNLO accuracy [46, 44, 48, 47].

Chapter 4

The three-jet rate using the $k_\perp$ algorithm

At the LEP collider the most common jet clustering algorithm was the $k_\perp$ algorithm [8]. The algorithm only depends on a single jet resolution parameter $y_{\rm cut}$. The $k_\perp$ algorithm was developed in 1991 to replace the original JADE clustering algorithm [6, 7] which was the primarly used algorithm before the $k_\perp$. Although the JADE satisfies infrared safety, the algorithm prevents all order resummation of large logarithmic contributions of $\log 1/y_{\rm cut}$ for small values of $y_{\rm cut}$, even at the leading-logarithmic accuracy. This lead to the introduction of the $k_\perp$ algorithm, which replaces the jet invariant mass with transverse momentum as a distance measure. As a result resummation of double- and next-to-double logarithms becomes possible.

4.1 The $k_\perp$ algorithm

The $k_\perp$ algorithm has an iterative clustering procedure, and depends on a single $y_{\rm cut}$ jet resolution parameter. The clustering steps of the algorithm are the following:

1. Calculate the distance measure y_{ij} defined as

$$y_{ij} = \frac{2\min(E_i^2, E_j^2)(1-\cos\theta_{ij})}{Q^2} \tag{4.1}$$

   for every final state particle pair i, j and find the minimal one.

2. If the smallest y_{kl} is smaller than $y_{\rm cut}$, combine particle k and l according to the prescripted recombination scheme and go to Step 1.

3. If the smallest y_{kl} is bigger than y_{cut}, stop clusterization.

The resulting objects after clusterization are considered jets. The different recombination schemes tell how to combine momenta of two particles into one. In this work we use the so-called E-scheme for recombination where the resulting momenta is simply the sum of the-four momenta of the combined particles

$$p^\mu_{(ij)} = p^\mu_i + p^\mu_j \,. \tag{4.2}$$

In contrast for example, in the P-scheme the energy component of the combined momenta is rescaled to have zero invariant mass.

For the $k_\perp$ algorithm one can uniquely define transition values. Transition values $y_{i-1\leftarrow i}$ are certain values of y_{cut}, where the number of jets change from i into $i-1$ for a given final-state configuration. The distribution of the transition value behaves as an event shape observable. Using the $k_\perp$ algorithm every transition value $y_{i-1\leftarrow i}$ can be computed running the clusterization only once for a given configuration of momenta independently of y_{cut}, such that in every clusterization step the smallest y_{kl} value will be the corresponding $y_{i-1\leftarrow i}$ transition value, and we repeat the steps until all partons are clustered into two jets. Number of jets is a monotonically decreasing function of y_{cut} for every possible phase space configuration.

These two properties described above connect the $\frac{\mathrm{d}\sigma}{\mathrm{d}y_{i-1\leftarrow i}}$ differential distributions and the $\sigma_{\mathrm{n-jet}}(y_{\mathrm{cut}})$ cross section. Using this relation the three-jet cross section can be computed as

$$\sigma_{3-jet}(y_{\mathrm{cut}}) = \int_{y_{\mathrm{cut}}}^1 \mathrm{d}y_{2\leftarrow 3} \frac{\mathrm{d}\sigma}{\mathrm{d}y_{2\leftarrow 3}} - \int_{y_{\mathrm{cut}}}^1 \mathrm{d}y_{3\leftarrow 4} \frac{\mathrm{d}\sigma}{\mathrm{d}y_{3\leftarrow 4}} \,. \tag{4.3}$$

The three-jet cross section for a chosen y_{cut} gets contributions from the $\frac{\mathrm{d}\sigma}{\mathrm{d}y_{2\leftarrow 3}}$ differential cross section for every $y_{2\leftarrow 3}$ value which is greater than y_{cut}. However the resulting quantity in itself would include all events with $y_{3\leftarrow 4} \in [0,1]$. Events with $y_{3\leftarrow 4} \in [0, y_{\mathrm{cut}}]$ indeed are four-jet events which cluster into three-jets, but events with $y_{3\leftarrow 4} \in [y_{\mathrm{cut}}, 1]$ do not cluster into three-jets. Thus we need to subtract the integrated $\int_{y_{\mathrm{cut}}}^1 \mathrm{d}y_{3\leftarrow 4} \frac{\mathrm{d}\sigma}{\mathrm{d}y_{3\leftarrow 4}}$ distribution to get the correct three-jet cross section. Eq. (4.3) provides a very useful relation to speed up numerical calculations since one can calculate the differential cross sections, then do a simple integration with the desired y_{cut} according to the formula above.

4.2 Perturbative expansion

The three-jet rate is known in perturbation theory up to NNLO accuracy as series expansion in the strong coupling α_S at an arbitrary μ renormalization scale

$$R_3^{\mathrm{FO}}(\mu) = \frac{\sigma_{3-\mathrm{jet}}}{\sigma_{\mathrm{tot}}} = \frac{\alpha_S(\mu)}{2\pi} A_3(\mu) + \left(\frac{\alpha_S(\mu)}{2\pi}\right)^2 B_3(\mu) + \left(\frac{\alpha_S(\mu)}{2\pi}\right)^3 C_3(\mu) + \mathcal{O}(\alpha_S^4)\,, \tag{4.4}$$

where the dependence on the jet algorithm parameter is implicit, but neglected in the notation. In experiments the natural normalization is to the total hadronic cross section σ_{tot}. In perturbation theory up to NNLO accuracy this reads as [98, 99]

$$\sigma_{\mathrm{tot}} = \sigma_0 \left[1 + \frac{\alpha_S}{2\pi} A_{\mathrm{tot}} + \left(\frac{\alpha_S}{2\pi}\right)^2 B_{\mathrm{tot}} + \left(\frac{\alpha_S}{2\pi}\right)^3 C_{\mathrm{tot}} + \mathcal{O}(\alpha_S^4)\right]. \tag{4.5}$$

In theory (as in our case), cross sections are often normalized to the leading-order hadronic cross section σ_0, which is the leading-order cross section for two jet production in e^+e^- collisions

$$\frac{\sigma_{3-\mathrm{jet}}}{\sigma_0} = \frac{\alpha_S}{2\pi} \bar{A}_3 + \left(\frac{\alpha_S}{2\pi}\right)^2 \bar{B}_3 + \left(\frac{\alpha_S}{2\pi}\right)^3 \bar{C}_3\,. \tag{4.6}$$

We can switch to the σ_{tot} normalization to obtain the three-jet rate by multiplying Eq. (4.6) with $\sigma_0/\sigma_{\mathrm{tot}}$, that in perturbation theory is

$$\frac{\sigma_0}{\sigma_{\mathrm{tot}}} = 1 - \frac{\alpha_S}{2\pi} A_{\mathrm{tot}} - \left(\frac{\alpha_S}{2\pi}\right)^2 \left(B_{\mathrm{tot}} - A_{\mathrm{tot}}^2\right). \tag{4.7}$$

The first two perturbative coefficients of the total hadronic cross section σ_{tot} [98, 99] are

$$\begin{aligned} A_{\mathrm{tot}} &= \frac{3}{2} C_F\,, \\ B_{\mathrm{tot}} &= \frac{1}{4}\left[-\frac{3}{2} C_F^2 + \left(\frac{123}{2} - 44\zeta_3\right) C_F C_A + (-22 + 16\zeta_3) C_F n_f T_R\right]. \end{aligned} \tag{4.8}$$

Finally the A_3, B_3 and C_3 perturbative coefficients of the three-jet rate can be obtained with a linear shift according to the following formulae:

$$\begin{aligned} A_3 &= \bar{A}_3\,, \\ B_3 &= \bar{B}_3 - A_{\mathrm{tot}} \bar{A}_3\,, \\ C_3 &= \bar{C}_3 - A_{\mathrm{tot}} \bar{B}_3 - \left(B_{\mathrm{tot}} - A_{\mathrm{tot}}^2\right) \bar{A}_3\,. \end{aligned} \tag{4.9}$$

The renormalization scale dependence of the coefficients can be easily obtained from the coefficients computed at scale $\mu = Q$

$$\begin{aligned} A_3(\mu) &= A_3(Q) \\ B_3(\mu) &= B_3(Q) + \beta_0 \log \xi_R \, A_3(Q) \\ C_3(\mu) &= C_3(Q) + 2\beta_0 \log \xi_R \, B_3(Q) + \left(\frac{1}{2} \beta_1 \log \xi_R + \beta_0^2 \log^2 \xi_R \right) A_3(Q) \,, \end{aligned} \tag{4.10}$$

with $\xi_R \equiv \mu/Q$, while the strong coupling can be evaluated by the three-loop running formula

$$\frac{\alpha_{\mathrm{S}}(\mu)}{2\pi} = \frac{2}{\beta_0 t} \left[1 - \frac{\beta_1}{\beta_0^2 t} \log t + \left(\frac{\beta_1}{\beta_0^2 t} \right)^2 \left(\ln^2 t - \ln t - 1 + \frac{\beta_0 \beta_2}{\beta_0^2} \right) \right] , \tag{4.11}$$

where $t = \ln(\mu^2/\Lambda^2_{\mathrm{QCD}})$. The first two coefficients of the β function appearing Eqs. (4.10) and (4.11) were defined in Eqs. (1.4) and (2.6) while β_2 [100] is

$$\beta_2 = \frac{2857}{54} C_{\mathrm{A}}^3 - \left(\frac{1415}{27} C_{\mathrm{A}}^2 + \frac{205}{9} C_{\mathrm{A}} C_{\mathrm{F}} - 2 C_{\mathrm{F}}^2 \right) T_{\mathrm{R}} n_{\mathrm{f}} + \left(\frac{158}{27} C_{\mathrm{A}} + \frac{44}{9} C_{\mathrm{F}} \right) T_{\mathrm{R}}^2 n_{\mathrm{f}}^2 \,. \tag{4.12}$$

At NNLO accuracy we use $\Lambda^2_{\mathrm{QCD}} = 208$ MeV corresponding to $\alpha_{\mathrm{S}}(m_Z) = 0.118$. The A_3 and B_3 coefficients of the perturbative series have been computed first in Refs. [101, 102] and were also published in Ref. [83]. The C_3 coefficient for the $k_\perp$ algorithm was computed in Refs. [78, 79, 80] and Ref. [81] provided a detailed study on different jet algorithms at NNLO accuracy. In this work we use the CoLoRFulNNLO method to obtain the perturbative coefficients for both $k_\perp$ and anti-$k_\perp$. In our calculation we use the $s_{ij}/Q^2 > 10^{-8}$ scaled invariant mass to cut the phase space.

In Fig. 4.1 we show our perturbative results for the three-jet rate at $\sqrt{Q^2} = 91.2$ GeV center-of-mass energy using the $k_\perp$ jet algorithm and the measured data by the OPAL experiment [103]. In the $y_{\mathrm{cut}} \in (10^{-2}, 1)$ region the perturbative prediction gives a good a description of the data, however at lower values of y_{cut} the differences start to grow and the perturbative predictions become unphysical as they diverge. It indicates the need of resummation in this region. We also plot the NNLO predictions of Ref. [81] with scale uncertainty named as SW. Our NNLO calculation shows good agreement with the predictions of SW.

4.3 Resummation of next-to-double logarithms

Using the coherent branching formalism described in Ref. [8] it is feasible to perform resummation for the jet rates with the $k_\perp$ algorithm. The three-jet rate

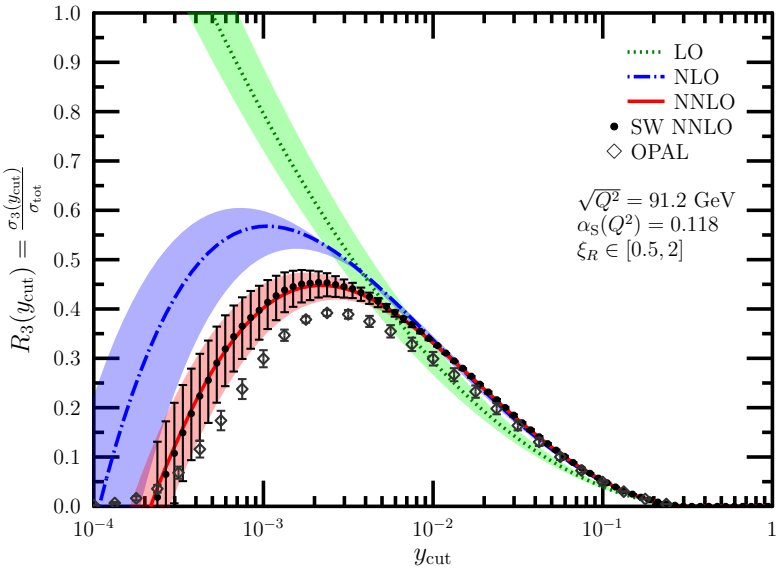

Figure 4.1. LO, NLO and NNLO fixed-order results for the three jet rate using the $k_\perp$ algorithm for clustering compared with OPAL data and theoretical prediction of Ref. [81] (SW). The bands indicate the renormalization scale variation.

at next-to-double logarithmic accuracy can be computed with the following formula as written in Ref [8]:

$$R_3^{\mathrm{NDL}} = 2[\Delta_q(Q)]^2 \int_{Q_0}^{Q} \mathrm{d}Q' \Gamma_q(Q, Q') \Delta_g(Q') \,, \tag{4.13}$$

where $Q_0 = \sqrt{y_{\mathrm{cut}}} Q$.

The so-called decay rates appearing in the resummation of three-jet rate up to NDL accuracy are

$$\begin{aligned} \Gamma_q(Q'', Q') &= \frac{2C_{\mathrm{F}}}{\pi} \frac{\alpha_{\mathrm{S}}(Q')}{Q'} \left[\log \frac{Q''}{Q'} - \frac{3}{4} \right], \\ \Gamma_g(Q'', Q') &= \frac{2C_{\mathrm{A}}}{\pi} \frac{\alpha_{\mathrm{S}}(Q')}{Q'} \left[\log \frac{Q''}{Q'} - \frac{11}{12} \right], \\ \Gamma_f(Q') &= \frac{n_{\mathrm{f}}}{3\pi} \frac{\alpha_{\mathrm{S}}(Q')}{Q'} \,. \end{aligned} \tag{4.14}$$

The Sudakov-factors are defined as

$$\begin{aligned}\Delta_q(Q'') &= \exp\Big(-\int_{Q_0}^{Q''} \mathrm{d}Q' \Gamma_q(Q'',Q') \Big)\,,\\ \Delta_g(Q'') &= \exp\Big(-\int_{Q_0}^{Q''} \mathrm{d}Q' \big[\Gamma_g(Q'',Q') + \Gamma_f(Q')\big] \Big)\,.\end{aligned} \tag{4.15}$$

At NDL accuracy we express the running coupling $\alpha_{\mathrm{S}}(Q')$ in terms of the fixed $\alpha_{\mathrm{S}}(Q)$ coupling at the hard scale Q using the one-loop formula

$$\alpha_{\mathrm{S}}(Q') = \frac{\alpha_{\mathrm{S}}(Q)}{1 - b_0 \alpha_{\mathrm{S}}(Q) \log \frac{Q}{Q'}}\,, \tag{4.16}$$

with $b_0 = \beta_0/(2\pi)$. The two-loop or higher order running of α_{S} would make difference only in subleading terms beyond NDL.

To include scale variation in the resummed prediction we generalize the one-loop formula expressing the running coupling in terms of fixed $\alpha_{\mathrm{S}}(\mu)$, but with an arbitrary chosen $\mu \sim Q$ renormalization scale

$$\alpha_{\mathrm{S}}(Q') = \frac{\alpha_{\mathrm{S}}(\mu)}{1 - b_0 \alpha_{\mathrm{S}}(\mu) \log \frac{\mu}{Q'}} = \frac{\alpha_{\mathrm{S}}(\mu)}{1 - b_0 \alpha_{\mathrm{S}}(\mu) (\log \frac{Q}{Q'} + \log \xi_R)}\,. \tag{4.17}$$

The three-jet rate does not exponentiate, like the two-jet rate or event shapes do, only in the pseudo-Abelian limit with $\Gamma_g\,, \Gamma_f \to 0$

$$R_3 = 2[\Delta_q(Q)]^2 \int_{Q_0}^{Q} \mathrm{d}q \Gamma_q(Q,q) + \Big(\Gamma_g \text{ and } \Gamma_f \text{ terms}\Big)\,. \tag{4.18}$$

The formula (4.13) resums $\alpha_{\mathrm{S}}^n L^{2n}$ and $\alpha_{\mathrm{S}}^n L^{2n-1}$ type logarithmic terms at all orders, where $L = \log 1/y_{\mathrm{cut}}$. It does not classify as NLL accurate in the general definition [49], because it cannot be fully written in the form of Eq. (2.39), namely

$$R_3^{\mathrm{NLL}}(y_{\mathrm{cut}}) = \exp(-L g_1(\alpha_{\mathrm{S}} L) - g_2(\alpha_{\mathrm{S}} L)) \mathcal{F}_{3,\mathrm{NLL}}(L)\,, \tag{4.19}$$

since the function $\mathcal{F}_{3,\mathrm{NLL}}(L)$ is not known yet completely for the three-jet rate.

To perform integrations in the Sudakov-factors and in expression of R_3^{NDL}, it is useful to do an integral transformation with introduction of the following new variables

$$\lambda' = \log \frac{Q'}{Q_0}\,, \quad \lambda = \log \frac{Q}{Q_0}\,, \quad \lambda_R = \log \xi_R\,. \tag{4.20}$$

with $\lambda = L/2$. Using these new variables the decay rates (4.14) become

$$\begin{aligned}
\Gamma_q(\lambda'',\lambda') &= \frac{2C_\mathrm{F}}{\pi}\alpha_\mathrm{S}(\lambda')\Big[(\lambda''-\lambda') - \frac{3}{4}\Big]\,,\\
\Gamma_g(\lambda'',\lambda') &= \frac{2C_\mathrm{A}}{\pi}\alpha_\mathrm{S}(\lambda')\Big[(\lambda''-\lambda') - \frac{11}{12}\Big]\,,\\
\Gamma_f(\lambda') &= \frac{n_\mathrm{f}}{3\pi}\alpha_\mathrm{S}(\lambda')\,.
\end{aligned} \tag{4.21}$$

The Sudakovs (4.15) can be written in the form of

$$\begin{aligned}
\Delta_q(\lambda'') &= \exp\Big(-\int_0^{\lambda''}\mathrm{d}\lambda'\Gamma_q(\lambda'',\lambda')\Big)\,,\\
\Delta_g(\lambda'') &= \exp\Big(-\int_0^{\lambda''}\mathrm{d}\lambda'\big[\Gamma_g(\lambda'',\lambda')+\Gamma_f(\lambda')\big]\Big)\,,
\end{aligned} \tag{4.22}$$

while the one-loop running reads as

$$\alpha_\mathrm{S}(\lambda') = \frac{\alpha_\mathrm{S}(\mu)}{1-b_0\alpha_\mathrm{S}(\mu)(\lambda-\lambda'+\lambda_R)}\,. \tag{4.23}$$

The integrations in the Sudakov-factors can be performed analytically and the result has the following functional form

$$\begin{aligned}
\Delta_q(\lambda'') &= \exp\Bigg\{\frac{C_\mathrm{F}}{2\alpha_\mathrm{S}b_0^2\pi}\Big[4\alpha_\mathrm{S}b_0\lambda'' + \Big[4-\alpha_\mathrm{S}b_0\big(3+4(\lambda-\lambda''+\lambda_R)\big)\Big]\\
&\quad\times\Big[\log\big(1-\alpha_\mathrm{S}b_0(\lambda+\lambda_R)\big)-\log\big(1-\alpha_\mathrm{S}b_0(\lambda-\lambda''+\lambda_R)\big)\Big]\Big]\Bigg\}\,,\\
\Delta_g(\lambda'') &= \exp\Bigg\{\frac{1}{6\alpha_\mathrm{S}b_0^2\pi}\Big[12\alpha_\mathrm{S}C_\mathrm{A}b_0\lambda'' + \Big[12C_\mathrm{A}-\alpha_\mathrm{S}C_\mathrm{A}b_0\big(11+12(\lambda-\lambda''+\lambda_R)\big)\\
&\quad+2\alpha_\mathrm{S}n_\mathrm{f}b_0\Big]\Big[\log\big(1-\alpha_\mathrm{S}b_0(\lambda+\lambda_R)\big)-\log\big(1-\alpha_\mathrm{S}b_0(\lambda-\lambda''+\lambda_R)\big)\Big]\Big]\Bigg\}\,.
\end{aligned} \tag{4.24}$$

where we used the shortnotation $\alpha_\mathrm{S} \equiv \alpha_\mathrm{S}(\mu)$.

The resummed expression of the three-jet rate

$$R_3^\mathrm{NDL}(y_\mathrm{cut}) = 2[\Delta_q(\lambda)]^2\int_0^\lambda \mathrm{d}\lambda'\Gamma_q(\lambda,\lambda')\Delta_g(\lambda') \tag{4.25}$$

cannot be integrated analytically in its full form, one has to use numerical methods to calculate the integral for each different y_cut value.

In Ref. [82] it was shown that an approximate analytic solution can be found for Eq. (4.25) using the following ansatz

$$R_3^{\mathrm{NDL,A}} = R_3^0 + \beta_0 R_3' \,, \tag{4.26}$$

where

$$R_3^0 = R_3^{\mathrm{NDL}}|_{\beta_0=0} \,, \quad R_3' = \frac{\partial R_3^{\mathrm{NDL}}}{\partial \beta_0}\Big|_{\beta_0=0} \,, \tag{4.27}$$

and n_f is expressed as $n_\mathrm{f} = (11C_\mathrm{A} - 3\beta_0)/2$ in R_3^{NDL}. Higher order terms in β_0 give contributes only beyond NDL accuracy, therefore they can be neglected. The final solution at $\mu = Q$ scale is

$$\begin{aligned} R_3^{\mathrm{NDL}}(y_\mathrm{cut}) = &-\frac{C_\mathrm{F}\alpha_\mathrm{S} L}{2\pi} \exp\left(\frac{C_\mathrm{F}\alpha_\mathrm{S} L^2}{2\pi}\right) \Bigg\{ \frac{1}{2}\sqrt{\frac{4\pi^2}{C_\mathrm{A}\alpha_\mathrm{S} L^2}}\,\mathrm{erf}\left(\sqrt{\frac{C_\mathrm{A}\alpha_\mathrm{S} L^2}{4\pi}}\right) \\ &\times \left[3 - 2L + \frac{\beta_0\alpha_\mathrm{S} L^2}{2\pi}\left(\frac{C_\mathrm{F}\alpha_\mathrm{S} L^2}{3\pi} - \frac{1}{2}\right) - 3\frac{C_\mathrm{F}\alpha_\mathrm{S} L^2}{\pi} + \frac{\beta_0}{2C_\mathrm{A}}\right] \\ &+ \frac{1}{C_\mathrm{A}}\left(\exp\left(-\frac{C_\mathrm{A}\alpha_\mathrm{S} L^2}{4\pi}\right) - 1\right) \\ &\times \left[\frac{C_\mathrm{F}\beta_0\alpha_\mathrm{S} L^2}{3\pi} - \frac{\beta_0}{6} - \frac{4\pi}{\alpha_\mathrm{S} L} - 6C_\mathrm{F}\right] - \frac{\beta_0}{2C_\mathrm{A}}\Bigg\} \,. \end{aligned} \tag{4.28}$$

The resulting formula resums all double and next-to-double logarithmic terms, but contains none of further subleading terms. We repeated the calculation and found complete agreement with Eq. (4.28).

The work of Nagy et al. in Ref. [83] included the cusp-anomalous dimension (K-term) in the decay rates, which accounts some part of subleading logarithms beyond NDL accuracy originating from soft emissions

$$\begin{aligned} \Gamma_q(Q'', Q') &= \frac{2C_\mathrm{F}}{\pi}\frac{\alpha_\mathrm{S}(Q')}{Q'}\left[\left(1 + \frac{K}{2\pi}\alpha_\mathrm{S}(Q')\right)\log\frac{Q''}{Q'} - \frac{3}{4}\right] , \\ \Gamma_g(Q'', Q') &= \frac{2C_\mathrm{A}}{\pi}\frac{\alpha_\mathrm{S}(Q')}{Q'}\left[\left(1 + \frac{K}{2\pi}\alpha_\mathrm{S}(Q')\right)\log\frac{Q''}{Q'} - \frac{11}{12}\right] , \\ \Gamma_f(Q') &= \frac{n_\mathrm{f}}{3\pi}\frac{\alpha_\mathrm{S}(Q')}{Q'} \,, \end{aligned} \tag{4.29}$$

where the K-term in the $\overline{\mathrm{MS}}$ scheme reads as

$$K = \left(\frac{67}{18} - \frac{\pi^2}{6}\right)C_\mathrm{A} - \frac{10}{18}n_\mathrm{f} \,. \tag{4.30}$$

Switching to integration variables defined in Eq. (4.20) yields

$$\begin{aligned}
\Gamma_q(\lambda'',\lambda') &= \frac{2C_\mathrm{F}}{\pi}\alpha_\mathrm{S}(\lambda')\left[\left(1+\frac{K}{2\pi}\alpha_\mathrm{S}(\lambda')\right)(\lambda''-\lambda')-\frac{3}{4}\right],\\
\Gamma_g(\lambda'',\lambda') &= \frac{2C_\mathrm{A}}{\pi}\alpha_\mathrm{S}(\lambda')\left[\left(1+\frac{K}{2\pi}\alpha_\mathrm{S}(\lambda')\right)(\lambda''-\lambda')-\frac{11}{12}\right],\\
\Gamma_f(\lambda') &= \frac{n_\mathrm{f}}{3\pi}\alpha_\mathrm{S}(\lambda')\,.
\end{aligned} \tag{4.31}$$

The Sudakov-factors can be calculated analytically performing the integration

$$\begin{aligned}
\Delta_q(\lambda'') = \exp\Bigg\{ & \frac{C_\mathrm{F}}{2\alpha_\mathrm{S}b_0^2\pi}\Big[4\alpha_\mathrm{S}b_0\lambda'' + \Big[4-\alpha_\mathrm{S}b_0\big(3+4(\lambda-\lambda''+\lambda_R)\big)-\frac{2\alpha_\mathrm{S}K}{\pi}\Big]\\
&\times\Big[\log\big(1-\alpha_\mathrm{S}b_0(\lambda+\lambda_R)\big)-\log\big(1-\alpha_\mathrm{S}b_0(\lambda-\lambda''+\lambda_R)\big)\Big]\\
&-\frac{2\alpha_\mathrm{S}K}{\pi}\frac{\alpha_\mathrm{S}b_0\lambda''}{1-\alpha_\mathrm{S}b_0(\lambda+\lambda_R)}\Big]\Bigg\},\\
\Delta_g(\lambda'') = \exp\Bigg\{ & \frac{1}{6\alpha_\mathrm{S}b_0^2\pi}\Big[12\alpha_\mathrm{S}C_\mathrm{A}b_0\lambda'' + \Big[12C_\mathrm{A}-\alpha_\mathrm{S}C_\mathrm{A}b_0\big(11+12(\lambda-\lambda''+\lambda_R)\big)\\
&+2\alpha_\mathrm{S}n_\mathrm{f}b_0-\frac{6\alpha_\mathrm{S}C_\mathrm{A}K}{\pi}\Big]\Big[\log\big(1-\alpha_\mathrm{S}b_0(\lambda+\lambda_R)\big)\\
&-\log\big(1-\alpha_\mathrm{S}b_0(\lambda-\lambda''+\lambda_R)\big)\Big]-\frac{6\alpha_\mathrm{S}C_\mathrm{A}K}{\pi}\frac{\alpha_\mathrm{S}b_0\lambda''}{1-\alpha_\mathrm{S}b_0(\lambda+\lambda_R)}\Big]\Bigg\}.
\end{aligned} \tag{4.32}$$

In the $K\to 0$ limit Eq. (4.32) reduces to Eq. (4.15) as expected. The resummed three-jet rate can be computed using Eq. (4.25) with the modified decay rates and Sudakov-factors and evaluating the λ' integration numerically.

Let us note although all three resummations described in this section are formally equal at NDL accuracy, in fact they give different numerical results. In order to distinguish them in the following, we named them NDL, NDL,A and NDL+K respectively.

4.4 Matching

The most precise theoretical prediction for the three-jet rate is given by the matching of the fixed-order and the resummed calculations. As we discussed in Sect. 2.4 jet rates can be matched using the R-matching scheme [50]. We recall that log R-matching might be feasible as well, but since it is not worked out completely, we do not include any predictions obtained in that scheme.

The R-matching, up to NNLO fixed-order accuracy, is performed according to the following formula

$$R_3^{\mathrm{NNLO+NDL}} = R_3^{\mathrm{NDL}} + \frac{\alpha_{\mathrm{S}}(\mu)}{2\pi}(A_3 - A_3^{\mathrm{NDL}}) + \left(\frac{\alpha_{\mathrm{S}}(\mu)}{2\pi}\right)^2 (B_3 - B_3^{\mathrm{NDL}}) + \left(\frac{\alpha_{\mathrm{S}}(\mu)}{2\pi}\right)^3 (C_3 - C_3^{\mathrm{NDL}})\,, \tag{4.33}$$

where A_3^{NDL}, B_3^{NDL} and C_3^{NDL} are the coefficients of the α_{S} expansion of the resummed formula up to $\mathcal{O}(\alpha_{\mathrm{S}}^3)$.

Applying the CoLoRFulNNLO method we calculated the three-jet rate at NNLO accuracy with the $k_\perp$ algorithm using the `MCCSM` program, what we already showed in Fig. 4.1. We performed the matching of the fixed-order calculation at NLO and NNLO accuracy and various resummed predictions.

In Fig. 4.2 we show our fixed-order and matched results compared to experimental data measured by the OPAL experiment [103]. The plots in Fig. 4.2 show significant difference between the three matched predictions, both using NLO and NNLO fixed-order respectively. On the other hand including the NNLO correction narrows these differences, even between the fixed-order and the matched results. As we mentioned before all three resummed predictions are NDL accurate, they differ only in incomplete subleading contributions. However Fig. 4.2 clearly indicates that these subleading terms can still have an important effect in the $y_{\mathrm{cut}} \in [10^{-4}, 10^{-2}]$ region in matched predictions. This is also supported by the observation that the subleading terms in B_3^{NDL} and C_3^{NDL} have the same numerical order compared to NDL accurate terms. As the NDL,A resummation lacks any of these subleading terms, it loses its predictive power when matched with fixed-order calculation.

Ref. [83] showed that including the K-term into the resummation matched with NLO calculation improves the theoretical prediction compared to data. A similar plot can be seen in Fig. 4.2. In contrast, at NNLO+NDL+K accuracy the K term has the opposite effect: it deviates more from the experimental data compared to the NNLO+NDL prediction. This shows a counterintuitive behavior of the FO+NDL+K matched results: when the accuracy of the fixed-order prediction is increased, the matched prediction becomes worse.

Our study indicates that the improvement of the NLO+NDL+K prediction is not a real physical effect, but a fortunate numerical artifact of the matching. It can be seen from the comparison of the α_{S} series coefficients of the fixed-order and resummed computations in Fig. 4.3. The deviation between NDL and NDL+K accuracy starts only at $\mathcal{O}(\alpha_{\mathrm{S}}^2)$, therefore we only show the B_3 and C_3 coefficients. The fixed-order computation contains all logarithmic terms and power corrections at a given α_{S} order, while the expanded resummation includes only $\alpha_{\mathrm{S}}^n L^n$, $\alpha_{\mathrm{S}}^n L^{n-1}$

type logarithms, and some incomplete sublogarithmic terms. Therefore the fixed-order computation serves as a reference for the resummed calculations.

As shown in Fig. 4.3 the B_3 coefficient of the NDL+K prediction has worse convergence compared to the NDL prediction. However this extra deviation has a favorable numerical effect when the matching is performed: $B_3^{\mathrm{FO}} - B_3^{\mathrm{NDL+K}}$ gives larger negative correction to R_3^{NDL}. The $C_3^{\mathrm{NDL+K}}$ coefficient in Fig. 4.3 shows similar properties, but in this case the overall correction to R_3^{NDL} has an unfortunate larger value. Figs. 4.2 and 4.3 hint that the FO+NDL+K matching has an alternating behavior depending on the perturbative order of the fixed-order calculation. Sometimes it leads to nice looking matched curves, although the origin of the improvement is not physical but an accidental numerical artifact.

While the FO+NDL+K results have a strange behavior when the perturbative order is increased, the FO+NDL behaves consistently and becomes closer to data and overlaps with the NNLO prediction as seen in Fig. 4.2. To make it more enhanced in Fig. 4.4 we plotted the FO+NDL type predictions matched with the NLO and NNLO fixed-order calculations. As we increase the perturbative order, the matched prediction behaves as it expected and gives a better approximation of the data. The left tail of the distribution shows still sizeable differences, which could be decreased including higher order perturbative effects, and more likely using NLL, or NNDL accurate resummation (which are unfortunately not available yet). Non-perturbative hadron corrections are also known to give important contributions for the $k_\perp$-algorithm, especially in the small y_{cut} region [104]. We also mention that in the asymptotic y_{cut} region the matched predictions still behave unphysical, they are divergent due to the mismatch of subleading logarithms beyond NDL accuracy. As discussed in Sect. 2.4 using the $\log R$-matching scheme would help, but it is not yet worked out for jet rates. Thus presently the most precise theoretical prediction in perturbation theory is provided by NNLO+NDL matching as shown in Fig 4.4.

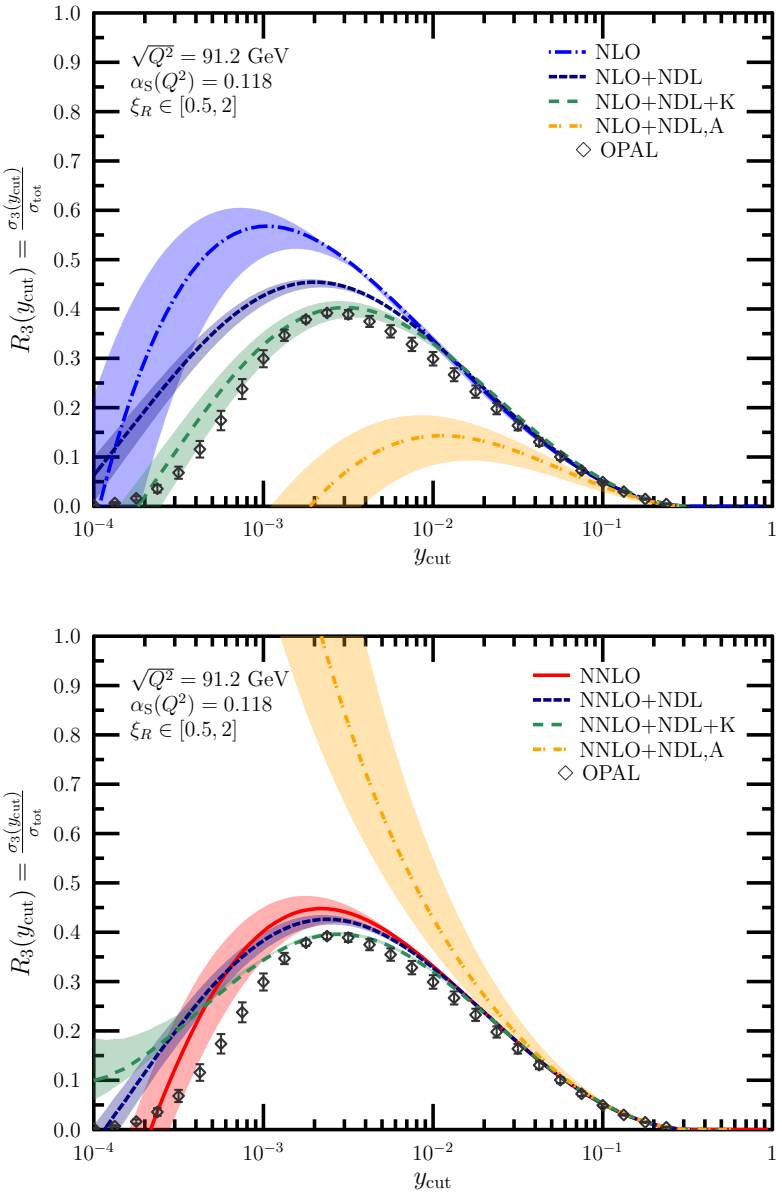

Figure 4.2. NLO and NNLO fixed-order results matched with NDL, NDL+K and NDL,A type resummation respectively using the $k_\perp$ algorithm, compared to OPAL data at $\sqrt{Q^2} = m_Z$ center-of-mass energy. The bands indicate renormalization scale dependence varying ξ_R between 0.5 and 2.

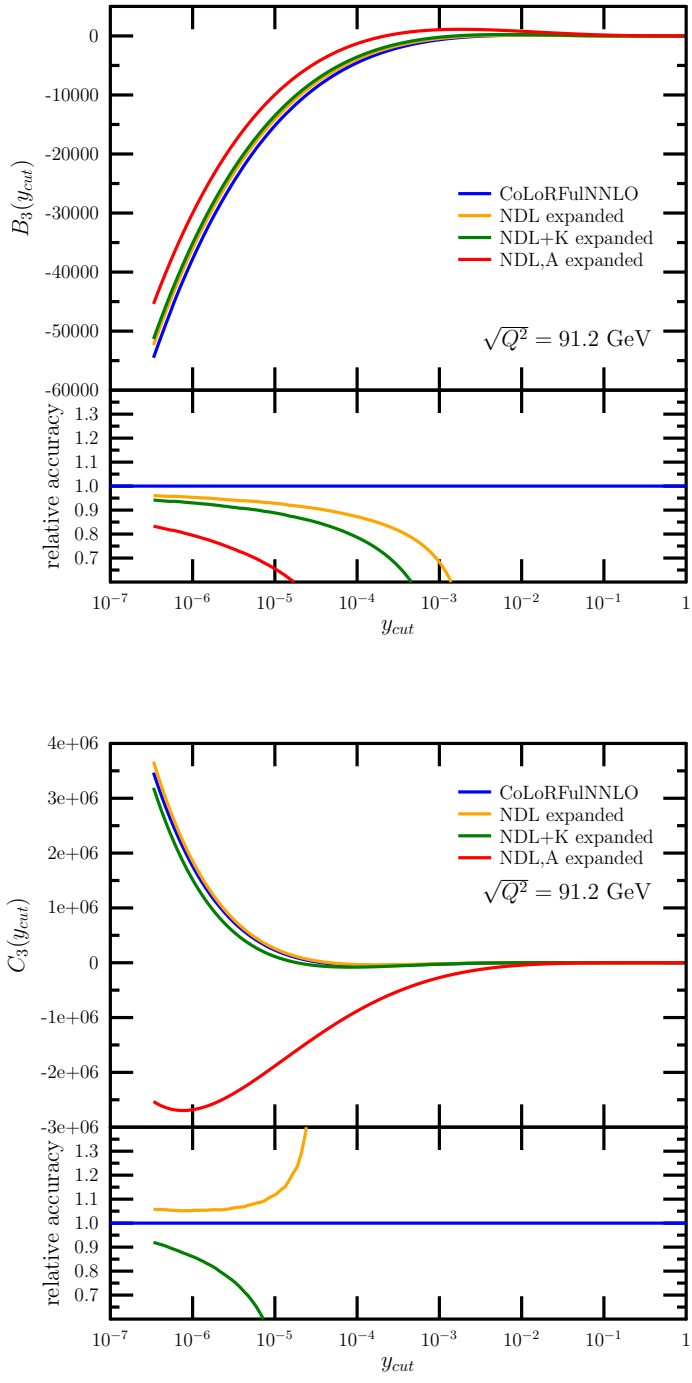

Figure 4.3. B_3 and C_3 coefficients of CoLoRFulNNLO and fixed-order expansions of resummed predictions.

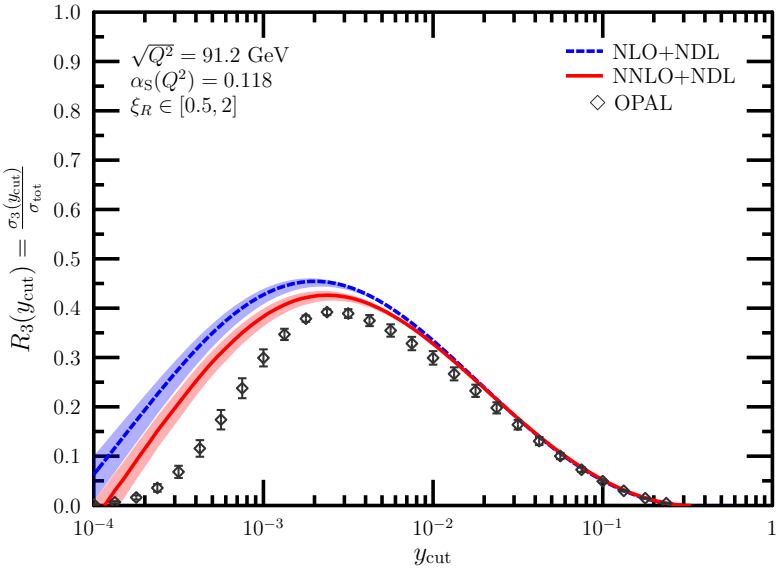

Figure 4.4. NLO and NNLO fixed-order results matched with NDL type resummation compared with OPAL data.

Chapter 5

The three jet rate using the anti-$k_\perp$ algorithm

In proton-proton collisions the used jet algorithms nowadays are various type of general inclusive $k_\perp$ algorithms [105], the most popular choice is the anti-$k_\perp$ [10], because the clustered jets have cone-like shape, that is favored by experimentalists. Although the algorithm was originally developed for hadron colliders it has been adapted to e^+e^- collisions as well. In the literature we can find two different versions of general inclusive $k_\perp$ algorithms for e^+e^- colliders: one is defined in the `FastJet` manual [105] while the other has been introduced by Stefan Weinzierl [81].

5.1 The general inclusive $k_\perp$ algorithm

5.1.1 Type-I definition

The `FastJet` adaptation of the general inclusive $k_\perp$ algorithm in e^+e^- annihilation uses the following measures [105]

$$\begin{aligned} d_{ij} &= \frac{\min(E_i^{2p}, E_j^{2p})(1-\cos\theta_{ij})}{1-\cos R}\,, \\ d_{iB} &= E_i^{2p}\,, \end{aligned} \tag{5.1}$$

and we define $y_{\text{cut}} \equiv 1-\cos R$. The d_{ij} measure is the two particle measure playing a similar role to y_{ij} in the $k_\perp$ algorithm, while d_{iB} is the so-called beam-jet measure which is required in hadron-hadron collisions. Choosing $p = 1, 0, -1$ we get the $k_\perp$ [8], Cambridge/Aachen [9] and anti-$k_\perp$ [10] algorithms.

The iterative clustering steps are the following:

1. Calculate d_{iB} for every particle i and d_{ij} for every particle pair i, j, and find their minimal ones. If there are no more particles in the clustering list, go to Step 4.

2. If d_{kl} is the smallest measure, combine particle k, l according to the chosen recombination scheme, (for example Eq. (4.2))then go to Step 1.

3. If d_{kB} is the smallest measure, particle k is considered as a jet candidate, remove it from the clustering list, then go to Step 1.

4. Apply energy cut(s), every jet candidate with $E_i > E_{\text{cut}}$ is considered as a resolved jet.

For $p = 1, 0$ we get the original jet algorithm with an extra energy cut on jets, but this energy cut is crucial for $p < 0$ choices to make the algorithm infrared safe.

In case of the exclusive $k_\perp$ algorithm we could define transition values, and the number of jets was also monotonic in y_{cut}, which simplified the numerical calculations. Unfortunately we cannot use the same technique here, because, as shown in Fig. 5.1, the number of jets is not always monotonic in y_{cut} due to the presence of E_{cut}. However transition values can be still defined.

We call $y_t \equiv y_{\text{cut}}$ a transition value when the clustered particle configuration changes. It does not necessary imply change in the number of jets, like in the $k_\perp$ algorithm, since the final number of jets also depends on the chosen value of E_{cut}. Using this definition is convenient in practice, since the transition values have to be calculated only once, then we can apply as many different energy cuts as we want without redoing the clusterization steps again. Nevertheless calculating the values of y_t is not straightforward. For the $k_\perp$ algorithm the sequence of clustering is independent of y_{cut}, relevant information can be fully retrieved for any y_{cut} value from one complete clusterization. In contrast, the clusterization sequence of the general inclusive $k_\perp$ algorithm depends on the actual choice of y_{cut}, because of the two different distance measures. The same happens for the Cambridge algorithm. Bentvelsen et al. developed an algorithm [106] which provides transition values for the Cambridge algorithm. We realized that the same algorithm can be applied to general inclusive $k_\perp$ algorithms as well. The philosophy of the original algorithm is the following [106]:

> "While performing the clustering at a particular value of y_{cut}, denoted by y_{ini}, we keep track of the maximum value of y_{ij}, between any two objects i and j encountered in this process, with y_{ij} being always smaller than y_{ini}. By construction this maximum value, which we denote by y_{max}, is smaller than y_{ini}. We now note that for any value of

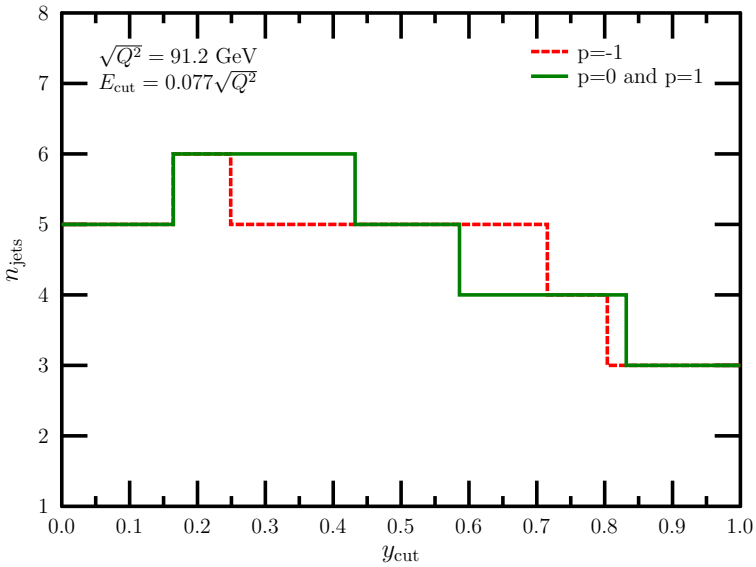

Figure 5.1. The number of jets as a function of $y_{\rm cut}$ with a fixed $E_{\rm cut}$ energy cut clustering the same randomly generated 8-partonic momentum configuration with the inclusive $k_\perp$ ($p = 1$), Cambridge/Aachen ($p = 0$) and anti-$k_\perp$ ($p = -1$) algorithms.

> $y_{\rm cut} \in [y_{\rm max}, y_{\rm ini})$, the Cambridge algorithm will follow the same clustering sequence. Only when the cluster algorithm is performed with a value $y_{\rm cut}$ smaller than $y_{\rm max}$, the condition $y_{ij} \geq y_{\rm cut}$ is satisfied at least once more and the subsequent clustering sequence may change completely. The value $y_{\rm max}$ is therefore one of the $y_{\rm cut}$ transition values. Note that the clustering may also change completely for values of $y_{\rm cut}$ larger than $y_{\rm ini}$."

While the Cambridge algorithm has two different measures, only the y_{ij} is used to decide what to do: cluster two particles, or remove the particle from the clustering list, which has smaller energy. In the general inclusive $k_\perp$ both measures are used in this decision process, however they can be combined into one in the following way

$$y_{ijk} \equiv y_{\rm cut} \frac{\min_{i,j} d_{ij}}{\min_k d_{kB}} = \frac{\min_{i,j}[\min(E_i^{2p}, E_j^{2p})(1 - \cos\theta_{ij})]}{\min_k E_k^{2p}} \tag{5.2}$$

Using this measure we can reformulate the 2nd an the 3rd clusterization steps of the general inclusive $k_\perp$ algorithm as

2. If $y_{ijk} < y_{\text{cut}}$, combine particle i, j according to a chosen recombination scheme, then go to Step 1.

3. If $y_{ijk} > y_{\text{cut}}$, particle k is considered as a jet candidate, remove it from the clustering list, then go to Step 1.

which are equivalent to the original statements.

Now we can apply the algorithm described in Ref. [106] to find transition values for the general inclusive $k_\perp$ algorithm in the following way

1. Set a value for y_{ini} (practically the last bin of the histogram) and set $y_{\text{cut}} = y_{\text{ini}}$.

2. If y_{cut} is less than some preset lower limit (first bin of the histogram), stop the algorithm.

3. Perform the clustering with y_{cut}, and during the process find the maximum value of y_{ijk}.

4. Store the transition value $y_t = y_{ijk}^{max}$ and apply energy cuts to get the corresponding number of jets.

5. Set $y_{\text{cut}} = y_{ijk}^{max}$ and go to Step 2.

The clusterization between two transition values is completely determined, choosing two different y_{cut} in this set will lead to the same jet configuration. It is also worth to mention that the same algorithm can be used in hadron-hadron colliders as well, with the hadron collider definition of d_{ij} in Eq. (5.2). The computing cost of the algorithm scales with the number of transitional values which depends on the number of partons. In Fig. 5.2 we compare the number of jets performing the clusterization bin by bin and using the transition values technique. The two different approaches give the same result, however the latter requires much less computational time.

5.1.2 Type-II definition

An alternative adaptation of the general inclusive $k_\perp$ algorithm for e^+e^- was introduced by S. Weinzierl in his publication about jet rates [81]. In this version the beam jet measure is dropped and we only have the two particle measure defined as

$$y_{ij} = \frac{1}{2}\left(\frac{Q^2}{4}\right)^{-p} \min(E_i^{2p}, E_j^{2p})(1 - \cos\theta_{ij})\,. \tag{5.3}$$

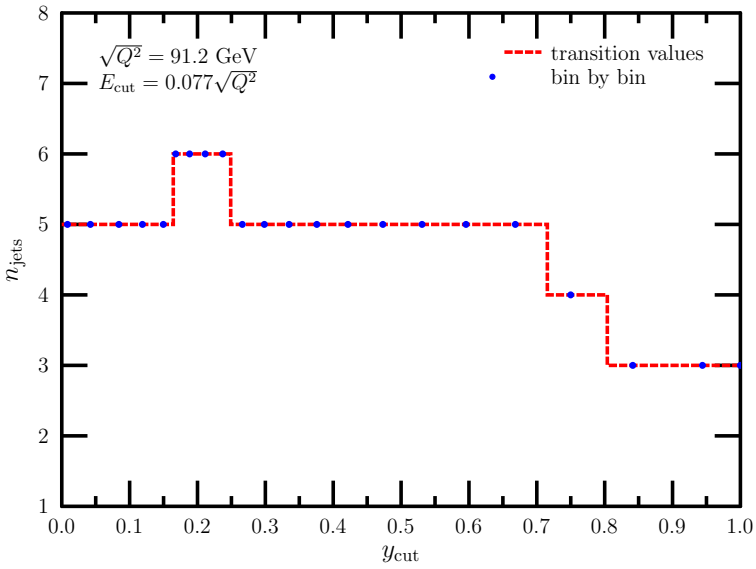

Figure 5.2. The number of jets as a function of $y_{\rm cut}$ calculated with preset values of $y_{\rm cut}$ (dots) and with the transition values technique.

The clusterization follows the steps of the $k_\perp$ algorithm described in Sect. 4.1, with an extra 4th step:

4. Apply energy cuts, jet candidates with $E_i > E_{\rm cut}$ are called jets.

This type of general inclusive $k_\perp$ is also non-monotonic in $y_{\rm cut}$ due to the energy cut. By now we couldn't define transition variables in general which could be found algorithmically for the following reasons. For $p \geq 0$ transition values can be defined in the same fashion, as for the $k_\perp$ algorithm, but the final number of jets also depend on the value of $E_{\rm cut}$. When we choose $p < 0$, the anti-$k_\perp$-like algorithm, the minimal values of y_{ij} do not decrease monotonically as we resolve more and more particles. For example it can happen that $y_{34} > y_{23}$ as illustrated in Table 5.1.2, which indicates that the clusterization of 3 pseudojets into 2 would happen earlier without actually clustering 4 pseudojets into 3. This behavior is completely independent of the energy cut and one can always find such a value that every jet candidates fulfills $E_i > E_{\rm cut}$. Nevertheless choosing $y_{\rm cut} \sim y_{23}$ and running the algorithm, the clusterization would stop at 3 jets because the

requirement to cluster one more particle is not satisfied. Due to this property the transition value cannot be defined based on y_{ij} and there is no other natural candidate. The same algorithm to find transition values for the type-I version of the general inclusive $k_\perp$ algorithm cannot be used here because it runs in infinite loops.

y_{78}	0.365392
y_{67}	0.763364
y_{56}	0.764509
y_{45}	0.850916
y_{34}	0.622647
y_{23}	0.434523

Table 5.1. Values of y_{ij} of a generated 8 partonic event clustered with the type-II anti-$k_\perp$.

5.2 Perturbative expansion

Using the general inclusive $k_\perp$ algorithm (either the type-I or II definition) the three-jet rate can be computed in perturbation theory up to NNLO accuracy in the same way as we described in Sect. 4.2, but there is an extra dependence on $E_{\rm cut}$. The first calculation at such an accuracy was published in Ref. [81] for the type-II general inclusive $k_\perp$ with $p = 1, 0, -1$. With the `MCCSM` numerical code we computed the three-jet rate in e^+e^- collision using both type-I and II anti-$k_\perp$ algorithm with the E-recombination scheme (see Eq. (4.2)). We used two different energy cuts, $E_{\rm cut} = 0.077\sqrt{Q^2}$ and $E_{\rm cut} = 0.0385\sqrt{Q^2}$ with $\sqrt{Q^2} = m_Z$, motivated by experimental considerations. We recall that all perturbative predictions were calculated requiring $s_{ij}/Q^2 > 10^{-8}$ minimal scaled invariant mass, to make the contributions finite.

In Figs. 5.3 and 5.4 we show our fixed-order predictions at $\sqrt{Q^2} = 91.2$ GeV center-of-mass energy. A general trend can be observed in both cases. If we lower the value of the energy cut, we get less events in the smaller $y_{\rm cut}$ regions. In this region events with more than three resolved protojets can still give contribution to the three-jet rate if the energy cut is sufficiently large and softer protojets do not survive. However if we choose a smaller value for $E_{\rm cut}$, these softer protojets will be resolved and contribute to jet rates with higher multiplicities.

In Fig. 5.3 in the upper plot we compare our calculation with results taken from Ref. [81]. The two calculations have a clear difference at NNLO accuracy, however the next-to-leading order accurate predictions agree perfectly as shown in Fig 5.5. Thus the difference is due to the NNLO correction, in fact a bug was found

in the calculation of [81] for anti-$k_\perp$ during the writing of this thesis, which affects the double-real contribution. Since the updated results are not yet available, we can only show the published results, however a new comparision would be required in the future with the updated prediction.

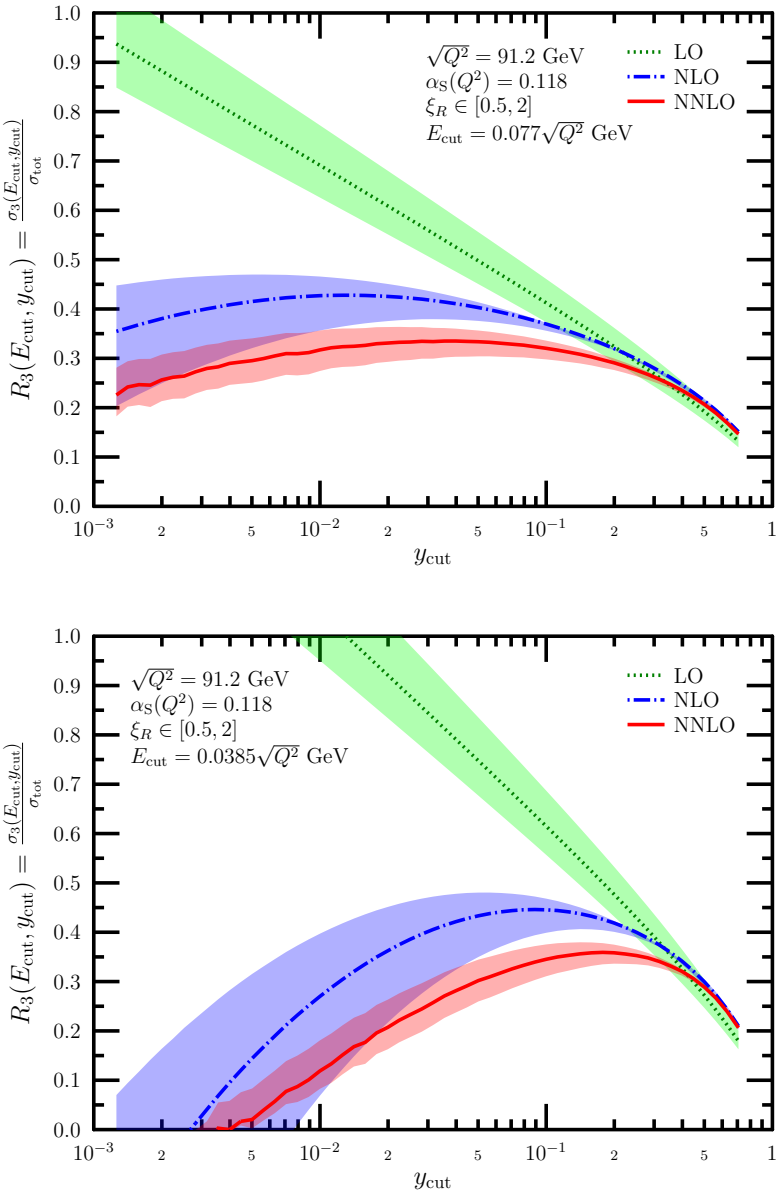

Figure 5.3. LO, NLO and NNLO fixed-order results using the type-I anti-$k_\perp$ algorithm, with two different energy cuts.

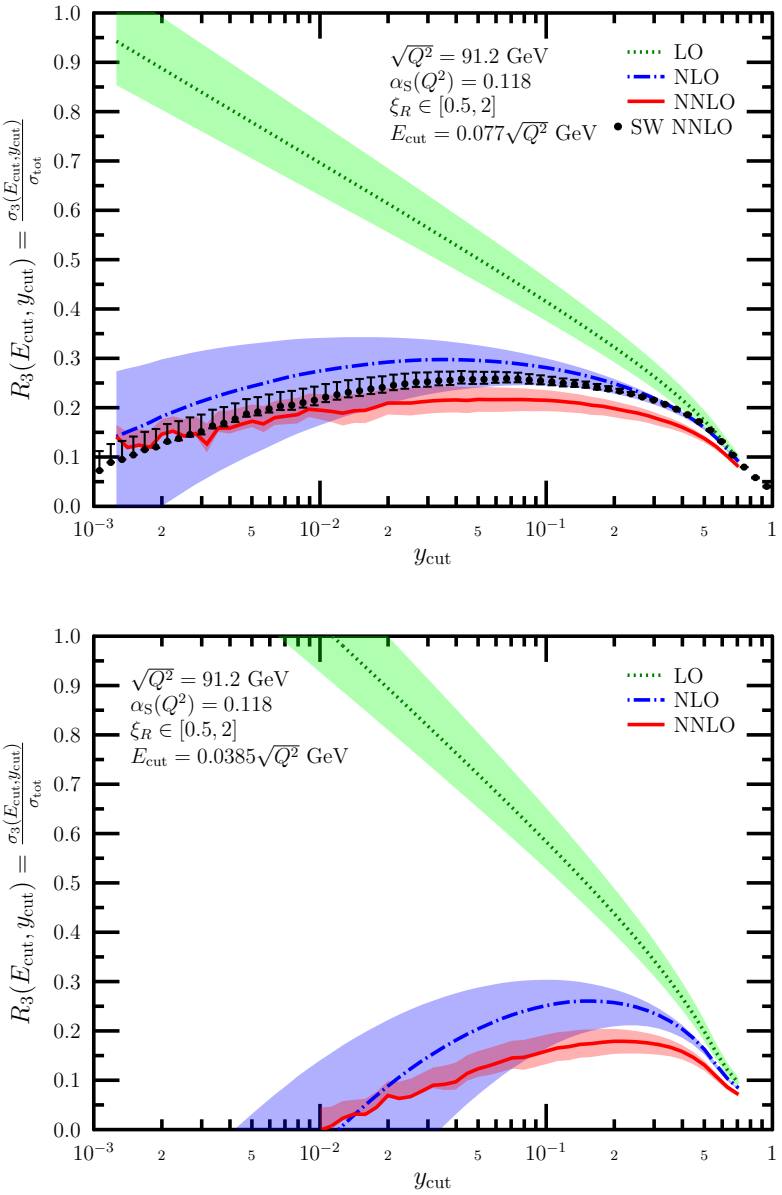

Figure 5.4. LO, NLO and NNLO fixed-order results using the type-II anti-$k_\perp$ algorithm, with two different energy cuts, compared with a previous calculation at next-to-next-to-leading order [81] (SW).

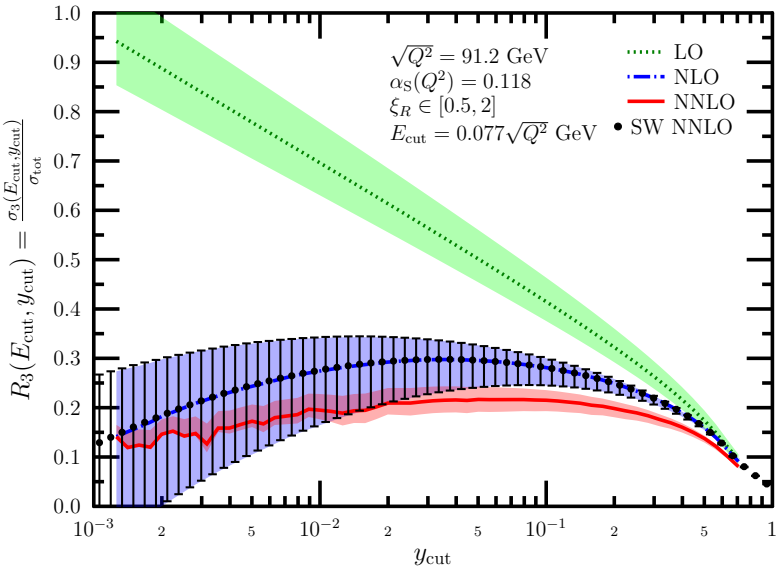

Figure 5.5. LO, NLO and NNLO fixed-order results using the type-II anti-$k_\perp$ algorithm, compared with a previous calculation at next-to-leading order [81] (SW).

5.3 Resummation of next-to-double logarithms

For the general inclusive $k_\perp$ algorithms it is possible to resum double and next-to-double logarithms to all orders applying the coherent branching formalism [59]. It can be shown from Ref. [59] substituting Eqs. (5.7), (5.8) and (5.9) into Eq. (5.10) and then into (5.11), then taking derivatives with respect to u according to Eq. (4.2), that the resummation of the three-jet rate at NDL accuracy, analog to $k_\perp$ case, is given by

$$R_3^{\mathrm{NDL}} = 2[\Delta_q(\kappa,\lambda)]^2 \int_0^\kappa \mathrm{d}\kappa' \int_0^\lambda \mathrm{d}\lambda' \Gamma_q(\kappa',\lambda',\kappa)\Delta_g(\kappa',\lambda')\,, \tag{5.4}$$

where we use the logarithmic variables introduced in the original paper with[1]

$$\kappa = \log\frac{Q}{E_{\mathrm{cut}}}\,, \quad \lambda = \log\frac{1}{y_{\mathrm{cut}}}\,. \tag{5.5}$$

As mentioned in [59], resummation at NDL accuracy is independent of the jet distance measure, therefore it can be used for any kind of general inclusive $k_\perp$ algorithm.

The decay rates appearing in Eq. (5.4) at NDL accuracy are

$$\begin{aligned}
\Gamma_q(\kappa',\lambda',\kappa'') &= \frac{C_{\mathrm{F}}}{\pi}\alpha_{\mathrm{S}}(\kappa',\lambda')\left(1-\frac{3}{4}e^{\kappa'-\kappa''}\right),\\
\Gamma_g(\kappa',\lambda',\kappa'') &= \frac{C_{\mathrm{A}}}{\pi}\alpha_{\mathrm{S}}(\kappa',\lambda')\left(1-\frac{11}{12}e^{\kappa'-\kappa''}\right),\\
\Gamma_f(\kappa',\kappa'') &= \frac{n_{\mathrm{f}}}{6\pi}\alpha_{\mathrm{S}}(\kappa',\lambda')e^{\kappa'-\kappa''}\,.
\end{aligned} \tag{5.6}$$

We note that in the decay rates defined above we kept more terms compared to the definition in Ref. [59], because we are interested not only in the expansion of the resummed formula but in its fully resummed form.

For $\alpha_{\mathrm{S}}(\kappa',\lambda')$ we use the one-loop formula of Eq. (4.16) but expressed in terms of the κ, λ variables and we include scale variation in the same way as in Eq. (4.17)

$$\alpha_{\mathrm{S}}(\kappa',\lambda') = \frac{\alpha_{\mathrm{S}}(\mu)}{1-\frac{b_0}{2}\alpha_{\mathrm{S}}(\mu)[2(\kappa-\kappa'+\log\xi_R)+\lambda-\lambda']}\,, \tag{5.7}$$

where $\xi_R = \mu/Q$.

[1] The original notation uses ξ_R for the angular cut, which is already reserved for scale variation in this work. Using y_{cut} instead also keeps the notation more unified.

The Sudakov-factors are defined as

$$\begin{aligned}\Delta_q(\kappa'',\lambda'') &= \exp\left(-\int_0^{\kappa''}\mathrm{d}\kappa'\int_0^{\lambda''}\mathrm{d}\lambda'\Gamma_q(\kappa',\lambda',\kappa'')\right),\\ \Delta_g(\kappa'',\lambda'') &= \exp\left(-\int_0^{\kappa''}\mathrm{d}\kappa'\int_0^{\lambda''}\mathrm{d}\lambda'\big[\Gamma_g(\kappa',\lambda',\kappa'')+\Gamma_f(\kappa',\kappa'')\big]\right),\end{aligned} \tag{5.8}$$

which can be calculated analytically. The double integral appearing in the resummed formula of Eq. (5.4) similarly to Eq. (4.13) can be evaluated for a given κ and λ only numerically.

5.4 Solving R_3 analytically

In the previous chapter we saw that subleading logarithms, even if they are incomplete, have important effects when we match resummation with fixed-order calculation. We came to this conclusion comparing different versions of resummation in matching, where the difference was the lack or the presence of subleading terms beyond NDL accuracy. We can ask the same question for the general inclusive $k_\perp$ resummation. In order to answer it we would need some approximate analytic formula, similarly to Eq. (4.28), which resums only NDL logarithms but none of the subleading terms. Such a formula was not published before, but it can be computed using the same ansatz as Eq. (4.26), since it is not specific for the $k_\perp$ algorithm.

As we are looking for a formula specifically which has no subleading logarithms in its α_S expansion, it is sufficient to use the original definitions of the decay rates,

the Sudakov-factors and the $\alpha_{\rm S}$ running published in Ref. [59].[2] Explicitly

$$\begin{aligned}
\alpha_{\rm S}(\kappa',\lambda') &= \frac{\alpha_{\rm S}}{\pi} + b_0'\left(\frac{\alpha_{\rm S}}{\pi}\right)^2 [2(\kappa-\kappa')+\lambda-\lambda']\,,\\
\Gamma_q(\kappa',\lambda',\kappa'') &= C_{\rm F}\left(\alpha_{\rm S}(\kappa',\lambda') - \frac{3}{4}\frac{\alpha_{\rm S}}{\pi}e^{\kappa'-\kappa''}\right),\\
\Delta_q(\kappa'',\lambda'') &= \exp\Bigg[-\frac{\alpha_{\rm S}C_{\rm F}\lambda''}{\pi}\left(\kappa''-\frac{3}{4}\right) - \frac{1}{2}\frac{\alpha_{\rm S}^2 C_{\rm F} b_0'\kappa''\lambda''}{\pi^2}\\
&\quad\times(4\kappa-2\kappa''+2\lambda-\lambda'')\Bigg],\\
\Delta_g(\kappa'',\lambda'') &= \exp\Bigg[-\frac{\alpha_{\rm S}\lambda''}{\pi}(C_{\rm A}\kappa''-b_0') - \frac{1}{2}\frac{\alpha_{\rm S}^2 C_{\rm A} b_0'\kappa''\lambda''}{\pi^2}\\
&\quad\times(4\kappa-2\kappa''+2\lambda-\lambda'')\Bigg],
\end{aligned} \tag{5.9}$$

where we use $b_0' = (11C_{\rm A}-2n_{\rm f})/12$ from Ref. [59]. After substituting the formulae (5.9) into Eq. (5.4) and expressing $n_{\rm f} = (11C_{\rm A}-12b_0')/2$, we look for a solution in the form of

$$R_3^{\rm NDL,A} = R_3^0 + b_0' R_3'\,. \tag{5.10}$$

In the followings we calculate the analytic formula for $R_3^{\rm NDL,A}$.

5.4.1 The b_0' independent term

Let us start with the b_0' independent term that is a sum of two contributions

$$R_3^0 = R_3^{\rm NDL}|_{b_0'=0} = \int_0^\kappa {\rm d}\kappa' \int_0^\lambda {\rm d}\lambda' ({\rm d}A_1 + {\rm d}A_2)\,. \tag{5.11}$$

The integrals can be performed analytically, and the resulting expressions for $\mu = Q$ are

$$\begin{aligned}
A_1 &= \frac{2C_{\rm F}}{C_{\rm A}}\exp\left(\frac{\alpha_{\rm S}C_{\rm F}(3-4\kappa)\lambda}{2\pi}\right)\left[\gamma_{\rm E} + \Gamma\left(0,\frac{\alpha_{\rm S}C_{\rm A}\kappa\lambda}{\pi}\right) + \log\left(\frac{\alpha_{\rm S}C_{\rm A}\kappa\lambda}{\pi}\right)\right],\\
A_2 &= \frac{3C_{\rm F}}{2C_{\rm A}}\exp\left(-\kappa + \frac{\alpha_{\rm S}C_{\rm F}(3-4\kappa)\lambda}{2\pi}\right)\left[\Gamma(0,-\kappa) - \Gamma\left(0,\kappa\left(\frac{\alpha_{\rm S}C_{\rm A}\lambda}{\pi}-1\right)\right)\right.\\
&\quad\left.+\log\left(\frac{\pi}{\pi-\alpha_{\rm S}C_{\rm A}\lambda}\right)\right],
\end{aligned} \tag{5.12}$$

[2] Using our extended definitions would result in the same solution in the end, however intermediate steps would be more complicated.

where $\Gamma(a,z)$ is the incomplete gamma function.

A_1 and A_2 still include subleading logarithms beyond NDL accuracy. In order to get rid of these contributions we have to modify the original formulae. Since both A_1 and A_2 involves complicated functions, it is not obvious how to manipulate them and keep only NDL accurate terms. It turned out however that the key is to find infinite series representations for the various pieces and manipulate those. As a guiding principle we have to keep in mind that the product of two double logarithmic terms is double logarithmic as well (at higher order of α_S), while multiplying a double logarithmic term with a next-to-double logarithmic produces a next-to-double logarithm. Thus we only need to keep terms which are in the form of DL $\times$ DL and DL $\times$ NDL, since NDL $\times$ NDL products contribute only beyond NDL accuracy.

Let us start with A_1. Using the series expansion of $\Gamma(0,z)$ in z we can write

$$\gamma_E + \Gamma\left(0, \frac{\alpha_S C_A \kappa\lambda}{\pi}\right) + \log\left(\frac{\alpha_S C_A \kappa\lambda}{\pi}\right) = -\sum_{n=1}^{\infty} \frac{1}{n\,n!}\left(\frac{-\alpha_S C_A \kappa\lambda}{\pi}\right)^n, \tag{5.13}$$

which is a DL type term. However the exponential function

$$\exp\left(\frac{\alpha_S C_F (3-4\kappa)\lambda}{2\pi}\right) = \sum_{n=0}^{\infty} \frac{1}{n!}\left(\frac{\alpha_S C_F (3-4\kappa)\lambda}{2\pi}\right)^n \tag{5.14}$$

includes both DL, NDL and subleading contributions. In order to isolate DL and NDL terms we expand the function

$$\begin{aligned}\exp((c_1\kappa + c_2)\lambda) = \sum_{n=0}^{\infty}(c_1\kappa + c_2)^n\lambda^n = 1 + (c_1\kappa + c_2)\lambda + \frac{1}{2}(c_1\kappa + c_2)^2\lambda^2 \\ + \frac{1}{3!}(c_1\kappa + c_2)^3\lambda^3 + \cdots + \frac{1}{n!}(c_1\kappa + c_2)^n\lambda^n + \ldots .\end{aligned} \tag{5.15}$$

We use the relation $(a+b)^n = a^n + na^{n-1}b + \ldots$ in the expansion, always keeping the first to two terms only

$$\begin{aligned}(5.15) = 1 &+ c_1\kappa\lambda + c_2\lambda \\ &+ \frac{1}{2}c_1^2\kappa^2\lambda^2 + \frac{1}{2}2c_1c_2\kappa\lambda^2 + \ldots \\ &+ \frac{1}{3!}c_1^3\kappa^3\lambda^3 + \frac{1}{3!}3c_1^2c_2\kappa^2\lambda^3 + \ldots \\ &+ \frac{1}{n!}c_1^n\kappa^n\lambda^n + \frac{1}{n!}nc_1^{n-1}c_2\kappa^{n-1}\lambda^n + \ldots .\end{aligned} \tag{5.16}$$

Rearranging the result into two groups and factoring $c_2\lambda$ out from the second part

we obtain

$$\begin{aligned}(5.16) = (1 + c_1\kappa\lambda + \frac{1}{2}c_1^2\kappa^2\lambda^2 + \cdots + \frac{1}{n!}c_1^n\kappa^n\lambda^n + \dots)\\ + c_2\lambda(1 + c_1\kappa\lambda + \frac{1}{2}c_1^2\kappa^2\lambda^2 + \cdots + \frac{1}{(n-1)!}c_1^{n-1}\kappa^{n-1}\lambda^{n-1} + \dots) \qquad (5.17)\\ + \text{other subleading terms}\,.\end{aligned}$$

After relabeling $m = n - 1$ in the second part and resumming to all orders we obtain the following formula

$$\begin{aligned}\exp((c_1\kappa + c_2)\lambda) &= \sum_{n=0}^{\infty}\frac{1}{n!}(c_1\kappa\lambda)^n + c_2\lambda\sum_{m=0}^{\infty}\frac{1}{m!}(c_1\kappa\lambda)^m\\ &\quad + \text{other subleading terms}\\ &= (1 + c_2\lambda)\exp(c_1\kappa\lambda) + \text{other subleading terms}\,,\end{aligned} \qquad (5.18)$$

where we isolated the DL and NDL terms. Choosing the c_1 and c_2 coefficients as

$$c_1 = \frac{-2\alpha_S C_F}{\pi}\,, \quad c_2 = \frac{3\alpha_S C_F}{2\pi}\,, \qquad (5.19)$$

we find the following substitution rule for the exponential function in A_1

$$\exp\left(\frac{\alpha_S C_F(3-4\kappa)\lambda}{2\pi}\right) \to \left(1 + \frac{3\alpha_S C_F}{2\pi}\right)\exp\left(\frac{-2\alpha_S C_F\kappa\lambda}{\pi}\right), \qquad (5.20)$$

which contains DL and NDL logarithms only. Using this we define

$$\tilde{A}_1 \equiv \frac{2C_F}{C_A}\left(1+\frac{3\alpha_S C_F}{2\pi}\right)\exp\left(\frac{-2\alpha_S C_F\kappa\lambda}{\pi}\right)\left[\gamma_E+\Gamma\left(0,\frac{\alpha_S C_A\kappa\lambda}{\pi}\right)+\log\left(\frac{\alpha_S C_A\kappa\lambda}{\pi}\right)\right], \qquad (5.21)$$

that is free of subleading logarithms.

Now we turn to A_2 and we derive a formula for $\tilde{A}_2$. Our first observation is that

$$\exp\left(-\kappa + \frac{\alpha_S C_F(3-4\kappa)\lambda}{2\pi}\right)\log\left(\frac{\pi}{\pi - \alpha_S C_A\lambda}\right)$$

contributes only beyond NDL, therefore it can be dropped completely. We saw previously that the exponential

$$\exp\left(\frac{\alpha_S C_F(3-4\kappa)\lambda}{2\pi}\right)$$

gives DL, NDL and subleading terms as well. In order to know how to manipulate it, first we need some information about the Γ functions. The α_S expansion of those terms gives

$$e^{-\kappa}\left[\Gamma(0,-\kappa)-\Gamma\left(0,\kappa\left(\frac{\alpha_S C_A\lambda}{\pi}-1\right)\right)\right]=-\frac{\alpha_S C_A\lambda}{\pi}+\frac{\alpha_S^2 C_A^2\lambda^2(\kappa-1)}{2\pi^2} - \frac{\alpha_S^3 C_A^3\lambda^3(\kappa^2-2\kappa-2)}{6\pi^3}+\frac{\alpha_S^4 C_A^4\lambda^4(\kappa^3-3\kappa^2+6\kappa-6)}{24\pi^4}+\dots, \tag{5.22}$$

which can be actually written as an infinite sum in the form of

$$e^{-\kappa}\left[\Gamma(0,-\kappa)-\Gamma\left(0,\kappa\left(\frac{\alpha_S C_A\lambda}{\pi}-1\right)\right)\right]=\sum_{n=1}^{\infty}\frac{1}{n!}\left(-\frac{\alpha_S C_A\lambda}{\pi}\right)^n\sum_{i=0}^{n-1}(-1)^i\frac{\mathrm{d}^i\kappa^{n-1}}{\mathrm{d}\kappa^i}, \tag{5.23}$$

where $\mathrm{d}^0\kappa^{n-1}/\mathrm{d}\kappa^0=\kappa^{n-1}$. From the series representation we can see that the first term at any n is an NDL type logarithm followed by other subleading ones. Therefore it is sufficient to keep only the first term from the second summation

$$\begin{aligned}(5.23)&=\sum_{n=1}^{\infty}\frac{1}{n!}\left(-\frac{\alpha_S C_A\lambda}{\pi}\right)^n\kappa^{n-1}+\dots=\frac{1}{\kappa}\sum_{n=1}^{\infty}\frac{1}{n!}\left(-\frac{\alpha_S C_A\lambda\kappa}{\pi}\right)^n+\dots\\&=\frac{1}{\kappa}\left[\exp\left(-\frac{\alpha_S C_A\lambda\kappa}{\pi}\right)-1\right]+\dots.\end{aligned} \tag{5.24}$$

Since the second part of A_2 contributes as NDL, we only need DL terms from the exponential part

$$\exp\left(\frac{\alpha_S C_F(3-4\kappa)\lambda}{2\pi}\right)\to\exp\left(\frac{-2\alpha_S C_F\kappa\lambda}{\pi}\right), \tag{5.25}$$

thus we can define

$$\tilde{A}_2\equiv\frac{3C_F}{2C_A\kappa}\exp\left(\frac{-2\alpha_S C_F\kappa\lambda}{\pi}\right)\left[\exp\left(-\frac{\alpha_S C_A\lambda\kappa}{\pi}\right)-1\right]. \tag{5.26}$$

Finally the b_0' independent part is simply

$$R_3^0=\tilde{A}_1+\tilde{A}_2\,. \tag{5.27}$$

5.4.2 The linear b_0' term

The linear term in b_0' is a sum of 16 different integrals

$$R_3'=\frac{\partial R_3}{\partial b_0'}\Big|_{b_0'=0}\int_0^{\kappa}\mathrm{d}\kappa'\int_0^{\lambda}\mathrm{d}\lambda'\sum_{i=1}^{16}\mathrm{d}B_i\,, \tag{5.28}$$

that can be also computed analytically. 7 out of the 16 integrals contributes only beyond NDL accuracy, therefore we can neglect them. The remaining 9 integrals are the following:

$$\begin{aligned}
B_1 &= -\frac{4\alpha_{\mathrm{S}}^2 C_{\mathrm{F}}^2 \kappa^2 \lambda}{C_{\mathrm{A}} \pi^2} e^{\mathcal{A}+\mathcal{C}} \Big[\gamma_{\mathrm{E}} + \Gamma(0,\mathcal{B}) + \log \mathcal{B}\Big] \,, \\
B_3 &= \frac{\lambda}{2\kappa} B_1 \\
B_5 &= -\frac{4\alpha_{\mathrm{S}} C_{\mathrm{F}} \kappa}{C_{\mathrm{A}} \pi} e^{\mathcal{A}+\mathcal{C}} \Big[e^{-\mathcal{B}} - 1 + \gamma_{\mathrm{E}} + \Gamma(0,\mathcal{B}) + \log \mathcal{B}\Big] \,, \\
B_7 &= \frac{2C_{\mathrm{F}}}{C_{\mathrm{A}}^2 \pi \lambda} e^{\mathcal{A}-\mathcal{B}+\mathcal{C}} (\alpha_{\mathrm{S}} C_{\mathrm{A}} \kappa \lambda + 2\pi + (\alpha_{\mathrm{S}} C_{\mathrm{A}} \kappa \lambda - 2\pi) e^{\mathcal{B}}) \,, \\
B_9 &= \frac{\lambda}{2\kappa} B_5 \,, \\
B_{11} &= \frac{\lambda}{2\kappa} B_7 \,, \\
B_{13} &= -\frac{\pi}{\alpha_{\mathrm{S}} C_{\mathrm{F}} \kappa \lambda} B_1 \,, \\
B_{14} &= -\frac{4C_{\mathrm{F}}}{C_{\mathrm{A}}^2 \pi \lambda} e^{\mathcal{A}+\mathcal{C}} (\alpha_{\mathrm{S}} C_{\mathrm{A}} \kappa \lambda - \pi(1 - e^{-\mathcal{B}})) \,, \\
B_{15} &= -\frac{\pi}{2\alpha_{\mathrm{S}} C_{\mathrm{F}} \kappa^2} B_1 \,,
\end{aligned} \tag{5.29}$$

where we introduced the shortnotation

$$\mathcal{A} = -\frac{2\alpha_{\mathrm{S}} C_{\mathrm{F}} \kappa \lambda}{\pi} \,, \quad \mathcal{B} = \frac{\alpha_{\mathrm{S}} C_{\mathrm{A}} \kappa \lambda}{\pi} \,, \quad \mathcal{C} = \frac{3\alpha_{\mathrm{S}} C_{\mathrm{F}} \lambda}{2\pi} \,. \tag{5.30}$$

These integrals still contain subleading logarithms, but fortunately there is a universal way to get rid of them setting $\mathcal{C} = 0$ in the expressions. Applying this rule we define

$$\tilde{B}_i = B_i|_{\mathcal{C}=0} \,, \tag{5.31}$$

and the linear term in b_0' becomes

$$R_3' = \tilde{B}_1 + \tilde{B}_3 + \tilde{B}_5 + \tilde{B}_7 + \tilde{B}_9 + \tilde{B}_{11} + \tilde{B}_{13} + \tilde{B}_{14} + \tilde{B}_{15} \,. \tag{5.32}$$

Summing up all the contributions and doing some algebraic manipulations, the approximate solution for R_3^{NDL} has a simple analytic form

$$R_3^{\mathrm{NDL,A}}(\kappa,\lambda) = \frac{C_\mathrm{F}}{6C_\mathrm{A}\pi^2} e^{\mathcal{A}} \Big[12\pi^2 + 18\alpha_\mathrm{S} C_\mathrm{F}\pi\lambda - \alpha_\mathrm{S}^2 C_\mathrm{F}\kappa\lambda(2\kappa+\lambda)(11C_\mathrm{A}-2n_\mathrm{f}) \Big] \times \Big[\gamma_\mathrm{E} + \Gamma(0,\mathcal{B}) + \log\mathcal{B} \Big] - \frac{C_\mathrm{F}}{12C_\mathrm{A}^2\pi} e^{\mathcal{A}-\mathcal{B}} \Big[\frac{4\pi(10C_\mathrm{A}-n_\mathrm{f})}{\kappa} \big(e^{\mathcal{B}}-1\big) - \alpha_\mathrm{S} C_\mathrm{A}(11C_\mathrm{A}-2n_\mathrm{f}) \Big(2\kappa\big(e^{\mathcal{B}}-1\big) + \lambda\big(3e^{\mathcal{B}}-1\big) \Big) \Big] . \tag{5.33}$$

The fixed-order expansions in α_S up to $\mathcal{O}(\alpha_\mathrm{S}^3)$ gives back exactly the same logarithmic coefficients that were published in Ref [59].

In order to compare the approximate formula with the original, we computed the resummed three-jet rate as a function of y_cut with a fix energy cut $E_\mathrm{cut} = 0.0385\sqrt{Q^2}$ at $\mu = \sqrt{Q^2}$ performing the integral in Eq. (5.4) numerically and evaluating the approximate solution (5.33). The results are plotted on Fig. 5.6. The plot shows clearly the effect of the missing subleading logarithms, which will be much more enhanced in matched predictions (see Figs. 5.7, 5.8, 5.9 and 5.10). At $y_\mathrm{cut} \sim 10^{-3}$ the difference reaches a factor of 2. Although it is not clearly visible in Fig. 5.6, the NDL,A solution also approaches 0 in the small y_cut limit. This can be checked explicitly taking the $\lambda \to \infty$ limit of Eq. (5.33).

5.5 Matching

We performed the matching of the NDL and NDL,A accurate resummed results with fixed-order predictions using the R-matching formula (4.33). We calculated the resummed three-jet rate at $\sqrt{Q^2} = 91.2$ GeV center-of-mass energy evaluating Eqs. 5.4 and 5.33 respectively. We used two different energy cuts previously introduced for fixed-order calculations $E_\mathrm{cut} = 0.077\sqrt{Q^2}$, and $E_\mathrm{cut} = 0.0385\sqrt{Q^2}$, and we chose 56 different y_cut values in the $(10^{-3}, 1)$ region. For the matching we used our fixed-order predictions shown in Figs. (5.3) and (5.4), with the two different type of anti-$k_\perp$ algorithm.

The matched predictions are shown in Figs. 5.7, 5.8, 5.9 and 5.10. Unfortunately for the anti-$k_\perp$ three-jet rate there are no data published yet, we do not have any reference distribution. Similarly to the $k_\perp$ case, the matched result calculated with the NDL,A approximate resummation starts to diverge, and behave unphysical at quite large values of y_cut. As discussed before this is the consequence of missing subleading logarithms and the R-matching scheme, which is known to be sensitive to these subleading terms.

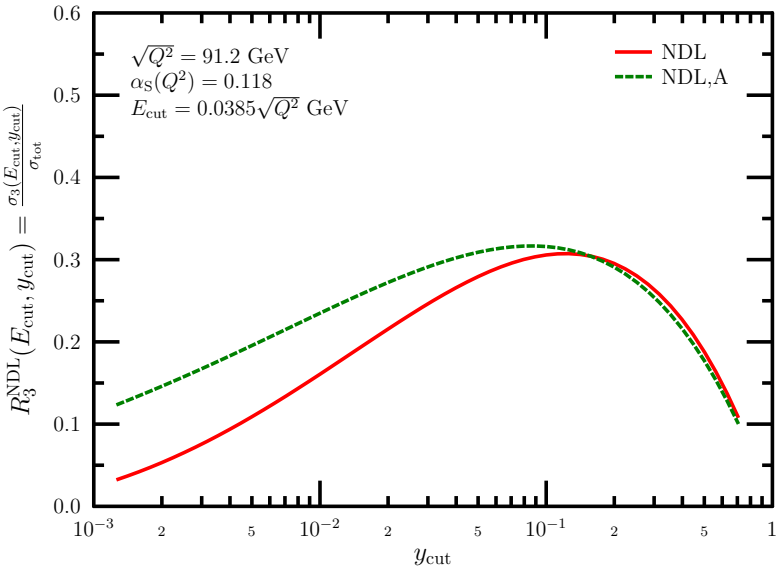

Figure 5.6. Comparision of the full resummed three-jet rate calculated numerically and the analytic approximate solution as function of $y_{\rm cut}$ using a fixed energy cut.

In Fig. 5.7 there is clear gap between the fixed-order and the resummed prediction, however in Fig. 5.9 on the upper panel the two coincide for the $E_{\rm cut} = 0.077\sqrt{Q^2}$ energy cut. This suggested that fixed-order predictions calculated with the type-II anti-$k_\perp$ algorithm might be closer to the resummed prediction in general, which was the main reason to calculate the three-jet rate using this algorithm. Note that the resummed prediction is independent of the jet distance measure at NDL accuracy. In the end our expectation turned out to be not true as visible in the lower panel of Fig. 5.9 and in both panels of Fig. 5.10, it was just rather a random coincidence.

Finally we note that the R-matched predictions still suffer from the mismatch of subleading terms, which could be fixed by using resummation at higher accuracy or possibly using the $\log R$-matching scheme. The NNLO predictions in 5.10 are still noisy in the smaller $y_{\rm cut}$ regions, the NNLO correction would require further statistics.

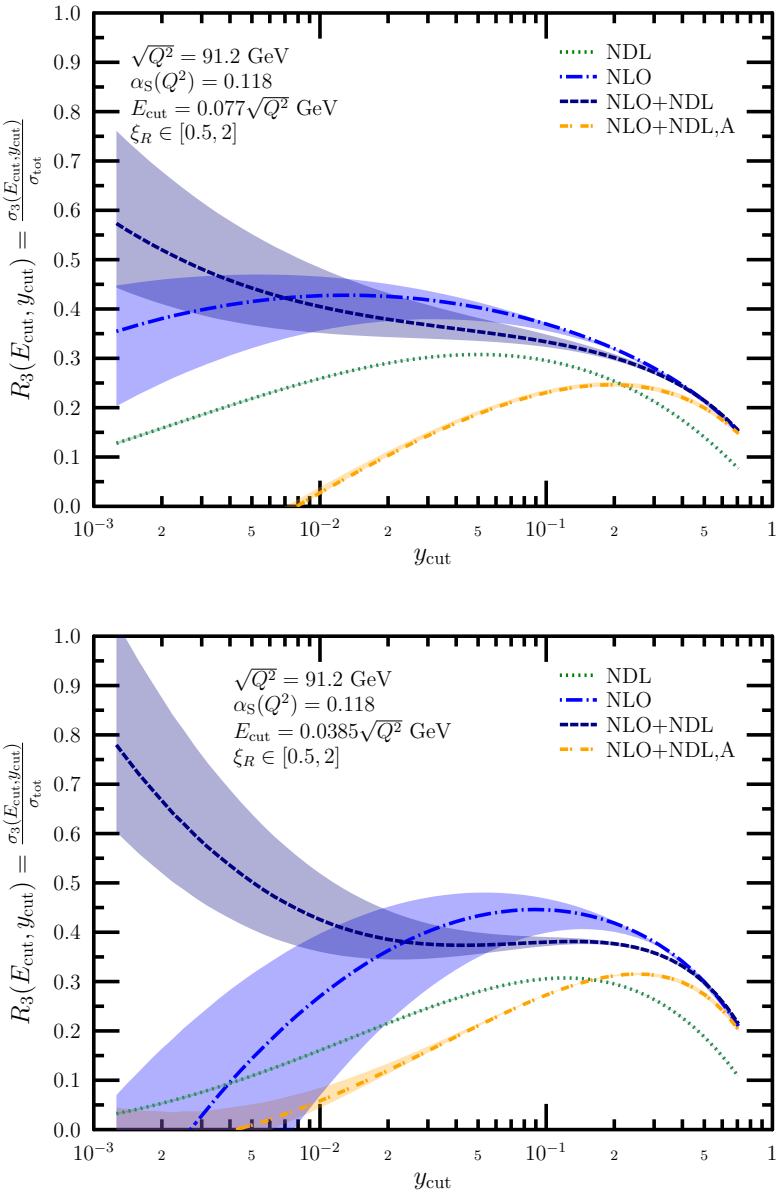

Figure 5.7. Matching of fixed-order NLO and resummed NDL and NDL,A predictions using the type I. anti-$k_\perp$ algorithm with two different energy cuts.

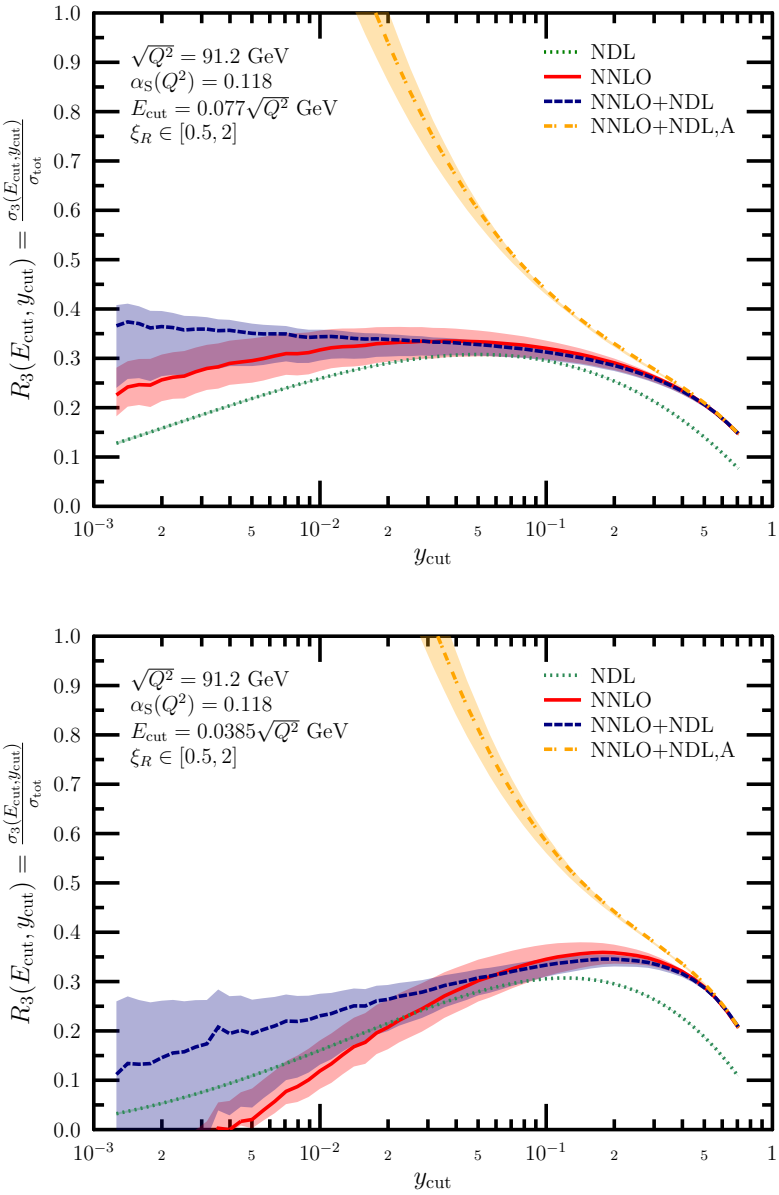

Figure 5.8. Matching of fixed-order NNLO and resummed NDL and NDL,A predictions using the type I. anti-$k_\perp$ algorithm with two different energy cuts.

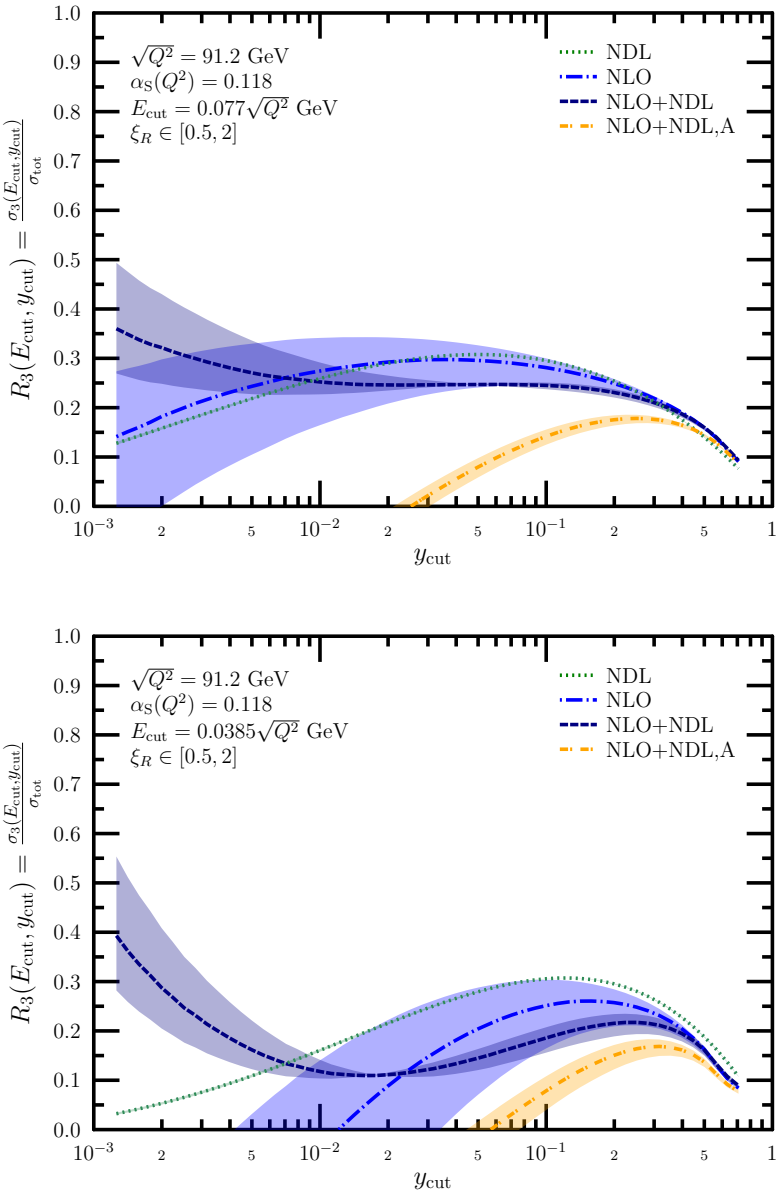

Figure 5.9. Matching of fixed-order NLO and resummed NDL and NDL,A predictions using the type II. anti-$k_\perp$ algorithm with two different energy cuts.

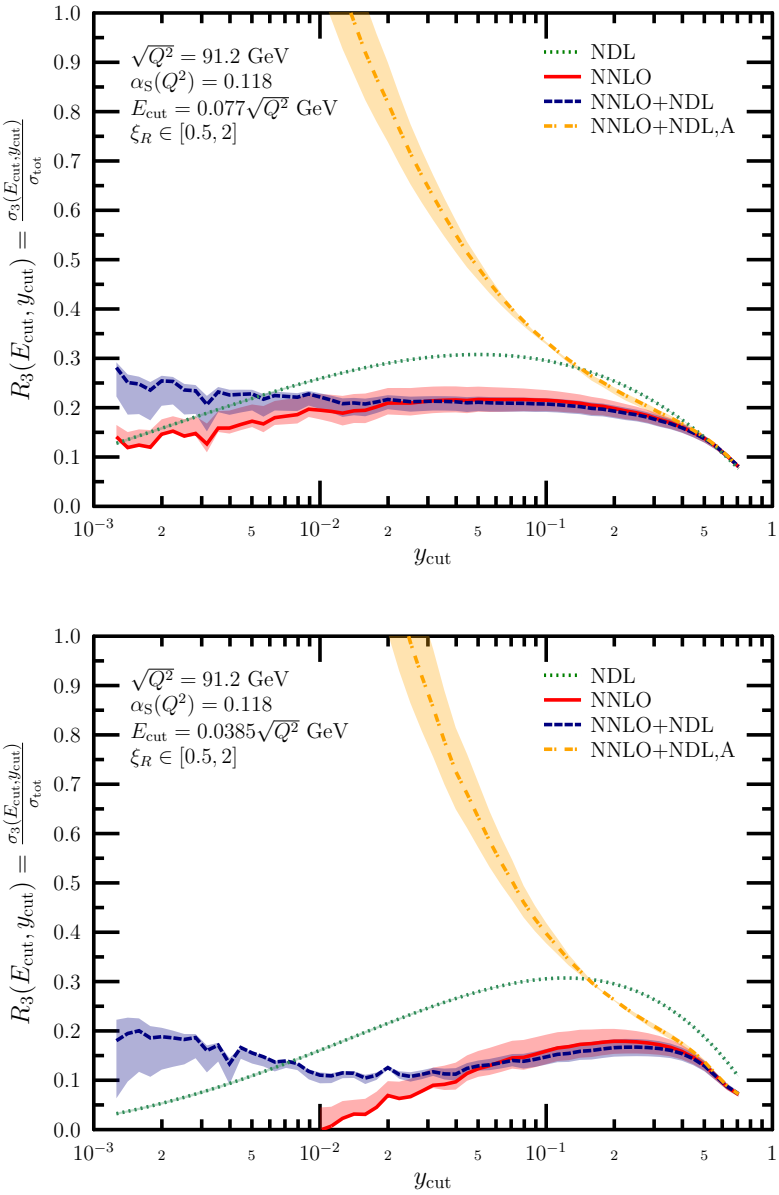

Figure 5.10. Matching of fixed-order NNLO and resummed NDL and NDL,A predictions using the type II. anti-$k_\perp$ algorithm with two different energy cuts.

Chapter 6

Towards hadron collisions

As we mentioned the CoLoRFulNNLO scheme is worked out for processes involving colorful particles in the final state only. Recently the largest particle collider is the LHC, hence the hot topics of contemporary particle phenomenology are related to hadron collisions. Thus the natural step forward is to extend the CoLoRFulNNLO scheme onto the class of hadron-initiated processes. This work has been started already but not finished yet. In this chapter we present our intermediate results related to the regularization of the real-virtual contribution, namely the definition of the single-unresolved one-loop subtraction term.

6.1 NNLO cross section in hadron collisions

In hadron collisions the colliding particles are composite, however when hadron A and B collide, the elementary collision process is due to hard scattering of parton a and b originating from the hadrons. The latter can be calculated in QCD, using the same methods we described earlier. The initial hadrons to the hard scattering partons are related via the parton distribution functions (PDF) $f_{a/A}(x, \mu_F^2)$. The quantity $f_{a/A,\mu_F^2}(x)$ gives the probability of parton a obtaining momentum fraction x from the hadron A. In $2 \to m$ hadron scattering the total jet cross section (denoted by $\widetilde{\sigma}$ here) is given by the convolution of the PDFs and the partonic cross section

$$\widetilde{\sigma}_m(p_A, p_B, \mu_F^2, \mu_R^2) = \sum_{a,b} \int_0^1 \mathrm{d}\eta_a \mathrm{d}\eta_b f_{a/A}(\eta_a, \mu_F^2) f_{b/B}(\eta_b, \mu_F^2) \sigma_{a,b;m}(p_a, p_b, \mu_F^2, \mu_R^2)\,, \tag{6.1}$$

where we sum over all possible constituents of the colliding hadrons. A new scale μ_F is introduced which separates the hadron level and the parton level physics,

or in other words the scale where the non-perturbative effects factorize from the perturbative region, hence it is called the factorization scale. This scale, similarly to the renormalization scale μ_R is also unphysical, therefore cross sections must be independent of μ_F up to the given perturbative order.

The partonic cross section can be computed in perturbation theory as in Eq. (2.9), but σ_m^{NLO} and σ_m^{NNLO} defined as

$$\sigma_m^{\mathrm{NLO}} = \int_{m+1} \mathrm{d}\sigma_{m+1}^{\mathrm{R}} J_{m+1} + \int_m \mathrm{d}\sigma_m^{\mathrm{V}} J_m + \int \mathrm{d}\sigma_m^{\mathrm{C,V}} J_m \,, \tag{6.2}$$

$$\sigma_m^{\mathrm{NNLO}} = \int_{m+2} \mathrm{d}\sigma_{m+2}^{\mathrm{RR}} J_{m+2} + \int_{m+1} \left(\mathrm{d}\sigma_{m+1}^{\mathrm{RV}} + \mathrm{d}\sigma_{m+1}^{\mathrm{C,RV}}\right) J_{m+1} + \int_m \left(\mathrm{d}\sigma_m^{\mathrm{VV}} + \mathrm{d}\sigma_m^{\mathrm{C,VV}}\right) J_m \,, \tag{6.3}$$

where the σ^{C} terms are the collinear counterterms which cancel the remaining collinear singularities coming from the mismatch of the real type and the loop type contributions. At NNLO accuracy the collinear counterterm also has singularities in the infrared limits, namely $\mathrm{d}\sigma_{m+1}^{\mathrm{C,RV}}$ is divergent in the single-unresolved limits. Therefore the subtraction terms for the real-virtual contribution are

$$\begin{aligned} \mathrm{d}\sigma_{m+1}^{\mathrm{NNLO}} = \Bigg\{ & \left[\mathrm{d}\sigma_{m+1}^{\mathrm{RV}} + \mathrm{d}\sigma_{m+1}^{\mathrm{C,RV}} + \int_1 \mathrm{d}\sigma_{m+2}^{\mathrm{RR,A_1}}\right] J_{m+1}^{(m)} \\ & - \left[\mathrm{d}\sigma_{m+1}^{\mathrm{RV,A_1}} + \left(\mathrm{d}\sigma_{m+1}^{\mathrm{C,RV}}\right)^{A_1} + \left(\int_1 \mathrm{d}\sigma_{m+2}^{\mathrm{RR,A_1}}\right)^{A_1}\right] J_m^{(m)} \Bigg\}_{d=4} , \end{aligned} \tag{6.4}$$

and integral of $\left(\mathrm{d}\sigma_{m+1}^{\mathrm{C,RV}}\right)^{A_1}$ is added back in the double-virtual line

$$\begin{aligned} \mathrm{d}\sigma_m^{\mathrm{NNLO}} = \Bigg\{ & \mathrm{d}\sigma_m^{\mathrm{VV}} + \mathrm{d}\sigma_m^{\mathrm{C,VV}} + \int_2 \left[\mathrm{d}\sigma_{m+2}^{\mathrm{RR,A_2}} - \mathrm{d}\sigma_{m+2}^{\mathrm{RR,A_{12}}}\right] \\ & + \int_1 \left[\mathrm{d}\sigma_{m+1}^{\mathrm{RV,A_1}} + \left(\mathrm{d}\sigma_{m+1}^{\mathrm{C,RV}}\right)^{A_1} + \left(\int_1 \mathrm{d}\sigma_{m+2}^{\mathrm{RR,A_1}}\right)^{A_1}\right] \Bigg\}_{d=4} J_m^{(m)} \,. \end{aligned} \tag{6.5}$$

In the following we will define the subtraction term $\mathrm{d}\sigma_{m+1}^{\mathrm{RV,A_1}}$ including initial state counterterms based on the infrared factorization properties of QCD matrix elements. Thus first we start with reviewing the infrared behavior of the one-loop squared matrix element.

6.2 The single unresolved limits of one-loop matrix element

6.2.1 The final-final collinear limit

First we consider the limit when two final state particles i and r become collinear. In this limit we can express the corresponding momenta with the usual Sudakov parametrization using an auxiliary light-like vector n^μ ($n^2 = 0$)

$$p_i^\mu = z_i p_{ir}^\mu - k_\perp^\mu - \frac{k_\perp^2}{z_i}\frac{n^\mu}{2p_{ir}n}, \quad p_r^\mu = z_r p_{ir}^\mu + k_\perp^\mu - \frac{k_\perp^2}{z_r}\frac{n^\mu}{2p_{ir}n}\,, \tag{6.6}$$

where p_{ir}^μ is a light-like momentum which points into the collinear direction, $k_\perp$ is the transverse momentum component orthogonal both to p_{ir}^μ and n^μ. z_i and z_r are the momentum fractions related to particle i and r and their sum is 1 required by momentum conservation. The collinear limit is defined by rescaling $k_\perp \to \lambda k_\perp$ and taking the $\lambda \to 0$ limit, when the one-loop squared matrix element factorizes in the following way [107]:

$$\begin{aligned}
&2\mathrm{Re}\langle \mathcal{M}_{m+1}^{(0)}(p_i, p_r, \dots)|\mathcal{M}_{m+1}^{(1)}(p_i, p_r, \dots)\rangle \simeq \\
&8\pi\alpha_\mathrm{S}\mu^{2\epsilon}\frac{1}{s_{ir}}2\mathrm{Re}\Bigg[\langle \mathcal{M}_m^{(0)}(p_{ir}, \dots)|\hat{P}_{f_i f_r}^{(0)}|\mathcal{M}_m^{(1)}(p_{ir}, \dots)\rangle \\
&+ 8\pi\alpha_\mathrm{S}c_\Gamma\Big(\frac{\mu^2}{-s_{ir}}\Big)^\epsilon\langle \mathcal{M}_m^{(0)}(p_{ir}, \dots)|\hat{P}_{f_i f_r}^{(1)}|\mathcal{M}_m^{(0)}(p_{ir}, \dots)\rangle\Bigg]\,,
\end{aligned} \tag{6.7}$$

where we only keep the leading $1/\lambda^2$ singular terms, and

$$c_\Gamma = \frac{1}{(4\pi)^{2-\epsilon}}\frac{\Gamma(1+\epsilon)\Gamma^2(1-\epsilon)}{\Gamma(1-\epsilon)}\,. \tag{6.8}$$

Based on Eq. (6.7) we define the symbolic $\mathbf{C}_{ir}$ operator which takes the the collinear limit of the one-loop squared matrix element and keeps the leading singular terms

$$\begin{aligned}
&\mathbf{C}_{ir}2\mathrm{Re}\langle \mathcal{M}_{m+1}^{(0)}(p_i, p_r, \dots)|\mathcal{M}_{m+1}^{(1)}(p_i, p_r, \dots)\rangle = \\
&8\pi\alpha_\mathrm{S}\mu^{2\epsilon}\frac{1}{s_{ir}}2\mathrm{Re}\Bigg[\langle \mathcal{M}_m^{(0)}(p_{ir}, \dots)|\hat{P}_{f_i f_r}^{(0)}|\mathcal{M}_m^{(1)}(p_{ir}, \dots)\rangle \\
&+ 8\pi\alpha_\mathrm{S}c_\Gamma\Big(\frac{\mu^2}{-s_{ir}}\Big)^\epsilon\langle \mathcal{M}_m^{(0)}(p_{ir}, \dots)|\hat{P}_{f_i f_r}^{(1)}|\mathcal{M}_m^{(0)}(p_{ir}, \dots)\rangle\Bigg]\,.
\end{aligned} \tag{6.9}$$

The $\hat{P}^{(0)}_{f_i f_r}$ and $\hat{P}^{(1)}_{f_i f_r}$ functions in Eqs. (6.7) and (6.9) are the final state d-dimensional tree-level and one-loop Altarelli-Parisi splitting kernels. In our notation we label the splitting kernels by the flavor of the two daughter partons, where the flavor of the mother parton are determined through the flavor summation rules: anything plus gluon gives anything, and quark plus an antiquark gives a gluon. The tree-level kernels are defined as

$$\langle r|\hat{P}^{(0)}_{qg}(z_i,z_r,;\epsilon)|s\rangle = \delta_{rs}C_{\rm F}\left[\frac{1+z_i^2}{z_r}-\epsilon z_r\right],, \tag{6.10}$$

$$\langle \mu|\hat{P}^{(0)}_{q\bar{q}}(z_i,z_r,k^\mu_\perp;\epsilon)|\nu\rangle = T_{\rm R}\left[-g^{\mu\nu}+4z_iz_r\frac{k^\mu_\perp k^\nu_\perp}{k^2_\perp}\right], \tag{6.11}$$

$$\langle \mu|\hat{P}^{(0)}_{gg}(z_i,z_r,k^\mu_\perp;\epsilon)|\nu\rangle = 2C_{\rm A}\left[-g^{\mu\nu}\left(\frac{z_i}{z_r}+\frac{z_r}{z_i}\right)-2(1-\epsilon)z_iz_r\frac{k^\mu_\perp k^\nu_\perp}{k^2_\perp}\right], \tag{6.12}$$

while the one-loop kernels [107] are

$$\begin{aligned}\langle r|\hat{P}^{(1)}_{qg}(z_i,z_r;\epsilon)|s\rangle &= r^{qg}_{S,ren}(z_i,z_r;\epsilon)\langle r|\hat{P}^{(0)}_{qg}(z_i,z_r;\epsilon)|s\rangle \\ &\quad+\delta_{rs}C_{\rm F}r^{qg}_{NS}\Big[1-\epsilon z_r\Big],\end{aligned} \tag{6.13}$$

$$\langle \mu|\hat{P}^{(1)}_{q\bar{q}}(z_i,z_r,k^\mu_\perp;\epsilon)|\nu\rangle = r^{q\bar{q}}_{S,ren}(z_i,z_r;\epsilon)\langle \mu|\hat{P}^{(0)}_{q\bar{q}}(z_i,z_r,k^\mu_\perp;\epsilon)|\nu\rangle\,, \tag{6.14}$$

$$\begin{aligned}\langle \mu|\hat{P}^{(1)}_{gg}(z_i,z_r,k^\mu_\perp;\epsilon)|\nu\rangle &= r^{gg}_{S,ren}(z_i,z_r;\epsilon)\langle \mu|\hat{P}^{(0)}_{gg}(z_i,z_r,k^\mu_\perp;\epsilon)|\nu\rangle \\ &\quad-4C_{\rm A}r^{gg}_{NS}\Big[1-2\epsilon z_iz_r\Big]\frac{k^\mu_\perp k^\nu_\perp}{k^2_\perp}\,.\end{aligned} \tag{6.15}$$

The renormalized $r_{S,ren}(z_i,z_r;\epsilon)$ singular factors appearing in the one-loop kernels are expressed in terms of unrenormalized ones with the relation:

$$r_{S,ren}(z_i,z_r;\epsilon) = r_S(z_i,z_r;\epsilon)-\frac{\beta_0}{2\epsilon}\frac{S^{\overline{\rm MS}}_\epsilon}{(4\pi)^2c_\Gamma}\Big(\frac{\mu^2}{(-1)^{\lambda_{i,r}}s_{ir}}\Big)^{-\epsilon}. \tag{6.16}$$

Please note that here all momenta are in the physical region ($E_i>0$), therefore s_{ir} is always positive. The $\lambda_{i,r}$ exponent takes care about the sign change of the kinematic invariant when the final state kernels are crossed into the initial state kinematics. $\lambda_{i,j}=1$ if both particles are in the final or the initial state and it is 0 otherwise.

The unrenormalized singular terms can be written as [107]

$$r^{qg}_S(z_i,z_r;\epsilon) = -\frac{1}{\epsilon^2}\left[C_{\rm A}\Big(\frac{z_i}{z_r}\Big)^\epsilon\frac{\pi\epsilon}{\sin(\pi\epsilon)}+\sum_{m=1}^{\infty}\epsilon^m\Big[(1+(-1)^m)C_{\rm A}-2C_{\rm F}\Big]{\rm Li}_m\Big(\frac{-z_r}{z_i}\Big)\right], \tag{6.17}$$

$$r_S^{q\bar{q}}(z_i,z_r;\epsilon) = \frac{1}{\epsilon^2}(C_\mathrm{A}-2C_\mathrm{F}) + \frac{C_\mathrm{A}}{\epsilon^2}\sum_{m=1}^{\infty}\epsilon^m\left[\mathrm{Li}_m\Big(\frac{-z_i}{z_r}\Big)+\mathrm{Li}_m\Big(\frac{-z_r}{z_i}\Big)\right] + \frac{1}{1-2\epsilon}\left[\frac{1}{\epsilon}\Big(\frac{11}{3}C_\mathrm{A}-\frac{4T_\mathrm{R}}{3}n_\mathrm{f}-3C_\mathrm{F}\Big)+C_\mathrm{A}-2C_\mathrm{F}+\frac{C_\mathrm{A}+4T_\mathrm{R}n_\mathrm{f}}{3(3-2\epsilon)}\right], \tag{6.18}$$

$$r_S^{gg}(z_i,z_r;\epsilon) = -\frac{C_\mathrm{A}}{\epsilon^2}\left[\Big(\frac{z_i}{z_r}\Big)^{\epsilon}\frac{\pi\epsilon}{\sin(\pi\epsilon)}-\sum_{m=1}^{\infty}2\epsilon^{2m-1}\mathrm{Li}_{2m-1}\Big(\frac{-z_r}{z_i}\Big)\right]. \tag{6.19}$$

The non-singular r_{NS} factors appearing in the definition of the one-loop kernels are independent of the kinematics, and they read as

$$r_{NS}^{qg} = \frac{C_A-C_F}{1-2\epsilon}\,, \quad r_{NS}^{gg} = \frac{C_A(1-\epsilon)-2T_Rn_f}{(1-2\epsilon)(2-2\epsilon)(3-2\epsilon)}\,. \tag{6.20}$$

6.2.2 Analytic continuation of the final state one-loop kernels

The $\left(\frac{\mu^2}{-s_{ir}}\right)^{\epsilon}$ factor appearing in Eq. (6.7) and in Eq. (6.16) needs analytic continuation in the final state kinematics. We will also use the final state one-loop kernels in the initial-final collinear limit, using the crossing relation[1]

$$\hat{P}^{(i)}_{f_{ar}f_r}(x,k_\perp;\epsilon) = -(-1)^{F(f_a)+F(f_{ar})}x\hat{P}^{(f)}_{f_a\bar{f}_r}\left(\frac{1}{x},k_\perp;\epsilon\right), \tag{6.21}$$

with the same flavor sum rules that we described in the final state splitting. The $F(f_i)$ factors ($F(q)=1, F(g)=0$) take care of the crossing of fermionic lines. When we cross the kernels into initial state kinematics $z_r = 1-1/x$ becomes negative, as $0<x<1$, which leads to negative arguments in Eqs. (6.17,6.18) and (6.19), therefore they would require analytic continuation. To do so, first we rewrite the unrenormalized singular terms in a slightly different form

$$r_S^{qg}(z_i,z_r;\epsilon) = -\frac{1}{\epsilon^2}\left[C_\mathrm{A}Z_\epsilon\frac{\pi\epsilon}{\sin(\pi\epsilon)}+\mathcal{P}_{qg}\right], \tag{6.22}$$

$$r_S^{q\bar{q}}(z_i,z_r;\epsilon) = \frac{1}{\epsilon^2}(C_\mathrm{A}-2C_\mathrm{F}) + \frac{C_\mathrm{A}}{\epsilon^2}\mathcal{P}_{q\bar{q}} + \frac{1}{1-2\epsilon} \times\left[\frac{1}{\epsilon}\Big(\frac{11}{3}C_\mathrm{A}-\frac{4T_\mathrm{R}}{3}n_\mathrm{f}-3C_\mathrm{F}\Big)+C_\mathrm{A}-2C_\mathrm{F}+\frac{C_\mathrm{A}+4T_\mathrm{R}n_\mathrm{f}}{3(3-2\epsilon)}\right], \tag{6.23}$$

[1]Here we only indicated the z_i dependence of the final state kernels explicitly, since z_r is related via momentum conservation $z_r = 1-z_i$.

$$r_S^{gg}(z_i, z_r; \epsilon) = -\frac{C_\mathrm{A}}{\epsilon^2}\left[Z_\epsilon \frac{\pi\epsilon}{\sin(\pi\epsilon)} - \mathcal{P}_{gg}\right], \tag{6.24}$$

where we introduced the factors that need analytic continuation as

$$Z_\epsilon = \left(\frac{z_i}{z_r}\right)^\epsilon, \tag{6.25}$$

$$\mathcal{P}_{qg} = \sum_{m=1}^{\infty} \epsilon^m \Big[(1+(-1)^m)C_A - 2C_F\Big] \mathrm{Li}_m\left(\frac{-z_r}{z_i}\right), \tag{6.26}$$

$$\mathcal{P}_{q\bar{q}} = \sum_{m=1}^{\infty} \epsilon^m \left[\mathrm{Li}_m\left(\frac{-z_i}{z_r}\right) + \mathrm{Li}_m\left(\frac{-z_r}{z_i}\right)\right], \tag{6.27}$$

$$\mathcal{P}_{gg} = \sum_{m=1}^{\infty} 2\epsilon^{2m-1} \mathrm{Li}_{2m-1}\left(\frac{-z_r}{z_i}\right). \tag{6.28}$$

First we expand formally the factors defined above in ϵ up to second order and neglect $\mathcal{O}(\epsilon^3)$ and higher order terms, which is sufficient in one-loop calculations since the leading pole starts at ϵ^{-2}. In our calculations we use the $s_{ij} + i0$ prescription for the propagator, hence the corresponding analytic continuation of the logarithm is $\log(x) \to \log|x| - i\pi\theta(-x)$, where θ is the Heaviside-function with $\theta(x) = 1$ if the argument is positive, 0 otherwise. We found that the same rule can be applied for $\log(z_i)$, since the ration of momentum fractions z_i/z_r can be defined as ratio of kinematic invariants and therefore we can use the same prescription. For momentum fraction ratios appearing in logarithms first we use the $\log a/b = \log a - \log b$ identity then apply analytic continuation. After applying these rules on the ϵ expansions and performing some algebra we obtain

$$\left(\frac{\mu^2}{-s_{ir}}\right)^\epsilon = 1 + \left(\log\frac{\mu^2}{s_{ir}} + i\pi\right)\epsilon + \frac{1}{2}\left(\log^2\frac{\mu^2}{s_{ir}} - 2i\pi\log\frac{\mu^2}{s_{ir}} - \pi^2\right)\epsilon^2 + \mathcal{O}(\epsilon^3), \tag{6.29}$$

$$\begin{aligned} Z_\epsilon = 1 &+ \Big[\log|z_i| - \log|z_r| - i\pi\Big(\theta(-z_i) - \theta(-z_r)\Big)\Big]\epsilon \\ &+ \frac{1}{2}\Big[(\log|z_i| - \log|z_r|)^2 - 2i\pi(\log|z_i| - \log|z_r|)\Big(\theta(-z_i) - \theta(-z_r)\Big) \\ &- \pi^2\Big(\theta(-z_i) + \theta(-z_r) - 2\theta(-z_i)\theta(-z_r)\Big)\Big]\epsilon^2, \end{aligned} \tag{6.30}$$

$$\begin{aligned} \mathcal{P}_{qg} = 2\epsilon\Big[&C_\mathrm{F}\Big[\log|z_i + z_r| - \log|z_i| - i\pi\Big(\theta(-z_i - z_r) - \theta(-z_i)\Big)\Big] \\ &+ \epsilon(C_\mathrm{A} - C_\mathrm{F})\mathrm{Li}_2\left(\frac{-z_r}{z_i}\right)\Big] + \mathcal{O}(\epsilon^3), \end{aligned} \tag{6.31}$$

$$\begin{aligned}\mathcal{P}_{q\bar{q}} = \epsilon\Big[&\log|z_i| + \log|z_r| - 2\log|z_i + z_r| - i\pi\Big(\theta(-z_i) + \theta(-z_r) \\ &- 2\theta(-z_i - z_r)\Big) + \epsilon \mathrm{Li}_2\left(\frac{-z_i}{z_r}\right) + \epsilon \mathrm{Li}_2\left(\frac{-z_r}{z_i}\right)\Big] + \mathcal{O}(\epsilon^3)\,,\end{aligned} \tag{6.32}$$

$$\mathcal{P}_{gg} = -2\epsilon\Big[\log|z_i + z_r| - \log|z_i| - i\pi\Big(\theta(-z_i - z_r) - \theta(-z_i)\Big)\Big] + \mathcal{O}(\epsilon^3)\,. \tag{6.33}$$

The $\mathrm{Li}_2(x)$ function also requires analytic continuation, when the argument is $x > 1$, and the real part can be computed as

$$\mathrm{ReLi}_2(x) = \frac{\pi^2}{6} - \log\big(|x|\big)\log\big(|1-x|\big) - \mathrm{Li}_2(1-x)\,, \tag{6.34}$$

while the imaginary part is

$$\mathrm{ImLi}_2(x) = -\log(x)\,\mathrm{Im}\log(1-x)\,. \tag{6.35}$$

6.2.3 The initial-final collinear limit

Now let us consider the initial-final collinear limit, when a final state particle r radiated from the initial state becomes collinear to its radiator a, which splits into ar and r. We define the collinear limit using the following parametrization

$$p_r^\mu = (1-x_a)p_a^\mu + k_\perp^\mu - \frac{k_\perp^2}{1-x_a}\frac{n^\mu}{2p_a n}\,, \quad p_{ar}^\mu = x_a p_a^\mu\,, \tag{6.36}$$

with $k_\perp \to 0$.

In the initial-final collinear limit the universal factorization of the one-loop matrix element is violated. However at one-loop order the terms which violate factorization cancel for the $2\mathrm{Re}\langle\mathcal{M}^{(0)}|\mathcal{M}^{(1)}\rangle$ interference term at the squared amplitude level, and in the initial-final limit this interference term obeys strict factorization similarly to the final-final collinear limit [108]:

$$\begin{aligned}&2\mathrm{Re}\langle\mathcal{M}^{(0)}_{m+1}(p_a, p_r, \dots)|\mathcal{M}^{(1)}_{m+1}(p_a, p_r, \dots)\rangle \simeq \\ &8\pi\alpha_\mathrm{S}\mu^{2\epsilon}\frac{1}{x_a}\frac{1}{s_{ar}}2\mathrm{Re}\Bigg[\langle\mathcal{M}^{(0)}_m(p_{ar}, \dots)|\hat{P}^{(0)}_{f_{ar}f_r}|\mathcal{M}^{(1)}_m(p_{ar}, \dots)\rangle \\ &+ 8\pi\alpha_\mathrm{S}c_\Gamma\left(\frac{\mu^2}{s_{ar}}\right)^\epsilon\langle\mathcal{M}^{(0)}_m(p_{ar}, \dots)|\hat{P}^{(1)}_{f_{ar}f_r}|\mathcal{M}^{(0)}_m(p_{ar}, \dots)\rangle\Bigg]\,.\end{aligned} \tag{6.37}$$

The initial state $\hat{P}^{(i)}_{f_{ar}f_r}(x_a, k_\perp; \epsilon)$ splitting kernels are related to the final state ones by Eq. (6.21), both at tree and at one-loop level. Since we took care about the

proper definition of the final state kernels in the crossed kinematics already, we can simply use them in Eq. (6.37) with the crossing relation.

Based on Eq. (6.37) we define the symbolic $\mathbf{C}_{ar}$ operator that takes the initial-final collinear limit and keeps only the leading singular terms

$$\begin{aligned}\mathbf{C}_{ar} 2\mathrm{Re}\langle \mathcal{M}^{(0)}_{m+1}(p_a,p_r,\dots)|\mathcal{M}^{(1)}_{m+1}(p_a,p_r,\dots)\rangle = \\ 8\pi\alpha_{\mathrm{S}}\mu^{2\epsilon}\frac{1}{x_a}\frac{1}{s_{ar}}2\mathrm{Re}\Bigg[\langle \mathcal{M}^{(0)}_{m}(p_{ar},\dots)|\hat{P}^{(0)}_{f_{ar}f_r}|\mathcal{M}^{(1)}_{m}(p_{ar},\dots)\rangle \\ + 8\pi\alpha_{\mathrm{S}}c_\Gamma\Big(\frac{\mu^2}{s_{ar}}\Big)^{\epsilon}\langle \mathcal{M}^{(0)}_{m}(p_{ar},\dots)|\hat{P}^{(1)}_{f_{ar}f_r}|\mathcal{M}^{(0)}_{m}(p_{ar},\dots)\rangle\Bigg].\end{aligned} \tag{6.38}$$

6.2.4 The soft limit

We consider the soft limit of the squared one-loop matrix element. When a gluon r either coming from the initial or the final state becomes soft, the squared matrix element factorizes universally in both cases [109]

$$\begin{aligned}2\mathrm{Re}\langle \mathcal{M}^{(0)}_{m+1}(p_r,\dots)|\mathcal{M}^{(1)}_{m+1}(p_r,\dots)\rangle \simeq -8\pi\alpha_S\mu^{2\epsilon}\sum_{i,j\neq i}\frac{1}{2}\mathcal{S}_{ij}(r)\Bigg\{|\mathcal{M}^{(0,1)}_{m,(i,j)}(\dots)|^2 + \\ - 8\pi\alpha_S\mu^{2\epsilon}c_\Gamma\Bigg[\Bigg(\frac{C_A}{\epsilon^2}\frac{\pi\epsilon}{\sin(\pi\epsilon)}\cos(\pi\epsilon)\Big(\frac{1}{2}\mathcal{S}_{ij}(r)\Big)^{\epsilon}+\frac{1}{2}\frac{\beta_0}{(4\pi)^2\epsilon}\frac{S_\epsilon}{\mu^{2\epsilon}c_\Gamma}\Bigg)|\mathcal{M}^{(0)}_{m,(i,j)}(\dots)|^2 \\ + \frac{2\pi}{\epsilon}\sum_{k\neq i,j}\Big(\frac{1}{2}\mathcal{S}_{jk}(r)\Big)^{\epsilon}(\lambda_{j,k}-\lambda_{j,r}-\lambda_{k,r})|\mathcal{M}^{(0)}_{m,(i,j,k)}(\dots)|^2\Bigg]\Bigg\}.\end{aligned} \tag{6.39}$$

where p_r is simply dropped on the right hand side of the equation and we sum over both initial and final state colored partons. The color correlated squared matrix elements are defined as

$$\begin{aligned}|\mathcal{M}^{(0,1)}_{m,(i,j)}|^2 &= 2\mathrm{Re}\langle \mathcal{M}^{(0)}_{m}|\mathbf{T}_i\mathbf{T}_j|\mathcal{M}^{(1)}_{m}\rangle\,, \\ |\mathcal{M}^{(0)}_{m,(i,j)}|^2 &= \langle \mathcal{M}^{(0)}_{m}|\mathbf{T}_i\mathbf{T}_j|\mathcal{M}^{(0)}_{m}\rangle\,, \\ |\mathcal{M}^{(0)}_{m,(i,j,k)}|^2 &= \langle \mathcal{M}^{(0)}_{m}|\mathbf{T}_i\mathbf{T}_j\mathbf{T}_k|\mathcal{M}^{(0)}_{m}\rangle\,.\end{aligned} \tag{6.40}$$

The $\lambda_{i,j}$ factors in Eq. (6.39) have the same purpose as in Eq. (6.16). The triple sum gives contribution only in processes involving four or more hard colored

partons. We define the soft limit by introducing the $\mathbf{S}_r$ operator

$$\mathbf{S}_r 2\mathrm{Re}\langle\mathcal{M}^{(0)}_{m+1}(p_r,\dots)|\mathcal{M}^{(1)}_{m+1}(p_r,\dots)\rangle = -8\pi\alpha_{\mathrm{S}}\mu^{2\epsilon}\sum_{i,j\neq i}\frac{1}{2}\mathcal{S}_{ij}(r)\Bigg\{|\mathcal{M}^{(0,1)}_{m,(i,j)}(\dots)|^2+$$
$$-8\pi\alpha_{\mathrm{S}}\mu^{2\epsilon}c_\Gamma\Bigg[\left(\frac{C_{\mathrm{A}}}{\epsilon^2}\frac{\pi\epsilon}{\sin(\pi\epsilon)}\cos(\pi\epsilon)\Big(\frac{1}{2}\mathcal{S}_{ij}(r)\Big)^{\epsilon}+\frac{1}{2}\frac{\beta_0}{(4\pi)^2\epsilon}\frac{S_\epsilon}{\mu^{2\epsilon}c_\Gamma}\right)|\mathcal{M}^{(0)}_{m,(i,j)}(\dots)|^2$$
$$+\frac{2\pi}{\epsilon}\sum_{k\neq i,j}\Big(\frac{1}{2}\mathcal{S}_{jk}(r)\Big)^{\epsilon}(\lambda_{j,k}-\lambda_{j,r}-\lambda_{k,r})|\mathcal{M}^{(0)}_{m,(i,j,k)}(\dots)|^2\Bigg]\Bigg\}. \tag{6.41}$$

6.2.5 Collinear limits of the soft formula

The collinear and the soft limits overlap, a collinear particle can become soft simultaneously and a soft gluon also can be collinear to another particle. In order to avoid double counting in the subtraction, we have to introduce a new term to cancel the overlapping. It can be either the soft limit of the collinear formula or the collinear limit of the soft formula. One can check that the latter gives a more general expression and cancel the overlapping region for both the collinear and the soft limit. Thus we have to compute the collinear limits of the soft limit.

We start with the final-final collinear limit. When the soft parton r becomes collinear to the final state parton i we can use the parametrization (6.6) neglecting the $k_{\perp,r}$ terms. Substituting the Sudakov-parametrization into the eikonal factors we get

$$\mathbf{C}_{ir}\mathcal{S}_{ij}(r) = \frac{2z_i}{s_{ir}(1-z_i)}\,, \quad \mathbf{C}_{ir}\mathcal{S}_{jk}(r) = \frac{\mathcal{S}_{jk}(ir)}{(1-z_i)^2}\,. \tag{6.42}$$

After taking the final-final limit of Eq. (6.41) and substituting the eikonals we find

$$\mathbf{C}_{ir}\mathbf{S}_r 2\mathrm{Re}\langle\mathcal{M}^{(0)}_{m+1}(p_i,p_r,\dots)|\mathcal{M}^{(1)}_{m+1}(p_i,p_r,\dots)\rangle = 8\pi\alpha_{\mathrm{S}}\mu^{2\epsilon}\mathbf{T}_i^2\frac{2}{s_{ir}}\frac{z_i}{1-z_i}$$
$$\times\Bigg[|\mathcal{M}^{(0,1)}_m(p_i,\dots)|^2-8\pi\alpha_{\mathrm{S}}\mu^{2\epsilon}c_\Gamma\Bigg(\frac{C_{\mathrm{A}}}{\epsilon^2}\frac{\pi\epsilon}{\sin(\pi\epsilon)}\cos(\pi\epsilon)\Big(\frac{1}{s_{ir}}\frac{z_i}{1-z_i}\Big)^{\epsilon}$$
$$+\frac{1}{2}\frac{\beta_0}{(4\pi)^2\epsilon}\frac{S_\epsilon}{\mu^{2\epsilon}c_\Gamma}\Bigg)|\mathcal{M}^{(0)}_m(p_i,\dots)|^2\Bigg], \tag{6.43}$$

where we performed summation over j and we used color conservation

$$\mathbf{T}_i^2|\mathcal{M}\rangle = -\sum_j \mathbf{T}_i\mathbf{T}_j|\mathcal{M}\rangle\,. \tag{6.44}$$

The triple color correlated squared matrix element $|\mathcal{M}^{(0)}_{m,(i,j,k)}|^2$ is antisymmetric in j,k, while its coefficients are symmetric, therefore the total sum over j,k gives no contribution.

To compute the initial-final collinear limit of the soft formula we use the parametrization of Eq. (6.36) in the eikonal factors

$$\mathbf{C}_{ar}\mathcal{S}_{aj}(r) = \frac{2}{s_{ar}(1-x_a)}\,, \quad \mathbf{C}_{ar}\mathcal{S}_{jk}(r) = \frac{x_a}{1-x_a}\mathcal{S}_{jk}(ar)\,. \tag{6.45}$$

When a soft gluon r becomes simultaneously collinear to the initial state particle a, the squared matrix element factorizes as

$$\begin{aligned}\mathbf{C}_{ar}\mathbf{S}_r 2\mathrm{Re}\langle\mathcal{M}^{(0)}_{m+1}(p_a,p_r,\dots)|\mathcal{M}^{(1)}_{m+1}(p_a,p_r,\dots)\rangle &= 8\pi\alpha_{\mathrm{S}}\mu^{2\epsilon}\mathbf{T}_b^2\frac{2}{s_{ar}}\frac{1}{1-x_a}\\ &\times\Bigg[|\mathcal{M}^{(0,1)}_m(p_a,\dots)|^2 - 8\pi\alpha_{\mathrm{S}}\mu^{2\epsilon}c_\Gamma\Bigg(\frac{C_A}{\epsilon^2}\frac{\pi\epsilon}{\sin(\pi\epsilon)}\cos(\pi\epsilon)\Big(\frac{1}{s_{ar}}\frac{1}{1-x_a}\Big)^{\epsilon}\\ &+\frac{1}{2}\frac{\beta_0}{(4\pi)^2\epsilon}\frac{S_\epsilon}{\mu^{2\epsilon}c_\Gamma}\Bigg)|\mathcal{M}^{(0)}_m(p_a,\dots)|^2\Bigg]\,,\end{aligned} \tag{6.46}$$

where we repeated the same steps as in the $\mathbf{C}_{ir}\mathbf{S}_r$ limit to obtain this expression.

Based on the single unresolved factorization properties of the one-loop squared matrix element discussed previously we define the subtraction candidate for the $m+1$ partonic single-unresolved one-loop contribution as

$$\begin{aligned}\mathbf{A}_1 2\mathrm{Re}\langle\mathcal{M}^{(0)}_{m+1}|\mathcal{M}^{(1)}_{m+1}\rangle = \Bigg[&\sum_{i\in F}\sum_{r\neq i\in F}\frac{1}{2}\mathbf{C}_{ir} + \sum_{a\in I}\sum_{r\in F}\mathbf{C}_{ar}\\ &+\sum_{r\in F}\Big(\mathbf{S}_r - \sum_{i\neq r\in F}\mathbf{C}_{ir}\mathbf{S}_r - \sum_{a\in I}\mathbf{C}_{ar}\mathbf{S}_r\Big)\Bigg]2\mathrm{Re}\langle\mathcal{M}^{(0)}_{m+1}|\mathcal{M}^{(1)}_{m+1}\rangle\,.\end{aligned} \tag{6.47}$$

6.3 The one-loop single-unresolved counterterm

The subtraction candidate $\mathbf{A}_1$ given in Eq. (6.47) is only valid in the strict infrared limits. The true subtraction term must be defined over the whole space, therefore we have to extend the factorization formulae away from the strict limits. Thus we introduce phase space mappings which map the $m+1$ particle momenta configurations into the m particle phase space.

6.3.1 The final-final collinear counterterm

For the final-final collinear counterterm we use the phase space mapping already introduced in the CoLoRFulNNLO scheme [34]

$$\{p\}_{m+1} \overset{\mathbf{C}_{ir}}{\to} \{\hat{p}\}_m^{(ir)}\,, \tag{6.48}$$

where $\{p\}_{m+1}$ denotes the set of $m+1$ momenta and set of final state momenta is $\{\hat{p}\}^{(ir)} \equiv (\hat{p}_1, \ldots, \hat{p}_{ir}, \ldots, \hat{p}_{m+1})$, p_r missing from the list. The mapped final state momenta entering the m particle squared matrix elements are

$$\hat{p}_{ir}^{\mu} = \frac{1}{1-\alpha_{ir}}(p_i^{\mu} + p_r^{\mu} - \alpha_{ir} Q^{\mu})\,, \quad \hat{p}_n^{\mu} = \frac{1}{1-\alpha_{ir}} p_n^{\mu}\,, \quad n \neq i, r\,, \tag{6.49}$$

while the initial state momenta remains unchanged. The factor α_{ir} appearing in the momentum mapping is set by momentum conservation

$$\alpha_{ir} = \frac{1}{2}\left(y_{(ir)Q} - \sqrt{y_{(ir)Q}^2 - 4y_{ir}}\right), \tag{6.50}$$

with $y_{(ir)Q} = y_{iQ} + y_{rQ}$. The momentum fractions $z_{i,r}$ and $z_{r,i}$ are defined as

$$z_{i,r} = \frac{y_{iQ}}{y_{(ir)Q}}\,, \quad z_{r,i} = \frac{y_{rQ}}{y_{(ir)Q}}\,, \tag{6.51}$$

while the transverse momentum is

$$k_{\perp,i,r}^{\mu} = \zeta_{i,r} p_r^{\mu} - \zeta_{r,i} p_i^{\mu}\,, \quad \zeta_{i,r} = z_{i,r} - \frac{y_{ir}}{\alpha_{ir} y_{(ir)Q}}\,, \quad \zeta_{r,i} = z_{r,i} - \frac{y_{ir}}{\alpha_{ir} y_{(ir)Q}}\,. \tag{6.52}$$

We mention that the phase space mapping defined here leads to phase space factorization, but we neglect the discussion of this property since we do not exploit it in this work.

The final-final collinear counterterms are then defined as

$$\mathcal{C}_{ir}^{(0,1)}(\{p\}) = 8\pi\alpha_{\mathrm{S}}\mu^{2\epsilon}\frac{1}{s_{ir}} 2\mathrm{Re}\langle \mathcal{M}_m^{(0)}(\{\hat{p}\}^{(ir)})|\hat{P}_{f_i f_r}^{(0)}(z_{i,r}, z_{r,i}, k_{\perp,i,r}; \epsilon)|\mathcal{M}_m^{(1)}(\{\hat{p}\}^{(ir)})\rangle\,, \tag{6.53}$$

$$\begin{aligned}\mathcal{C}_{ir}^{(1,0)}(\{p\}) = (8\pi\alpha_{\mathrm{S}})^2\mu^{2\epsilon} c_\Gamma \frac{1}{s_{ir}}\Big(\frac{\mu^2}{-s_{ir}}\Big)^{\epsilon} \\ 2\mathrm{Re}\langle \mathcal{M}_m^{(0)}(\{\hat{p}\}^{(ir)})|\hat{P}_{f_i f_r}^{(1)}(z_{i,r}, z_{r,i}, k_{\perp,i,r}; \epsilon)|\mathcal{M}_m^{(0)}(\{\hat{p}\}^{(ir)})\rangle\,.\end{aligned} \tag{6.54}$$

The superscript (a, b) in the notation of the counterterms indicates the number of loops present in the splitting kernel and in the squared matrix element respectively.

6.3.2 The initial-final collinear counterterm

In the initial-final collinear limit we extend our factorization formula over the whole space via the phase space mapping introduced in Ref. [39]

$$\{p\}_{m+1} \overset{\mathbf{C}_{ar}}{\to} \{\tilde{p}\}_m^{(ar)}\,, \tag{6.55}$$

with $\{\tilde{p}\}^{(ar)} \equiv (\tilde{p}_1, \ldots, \tilde{p}_{m+1})$ and p_r dropped from the list. The mapped momenta is defined as[2]

$$\tilde{p}_{ar}^{\mu} = \tilde{x}_a p_a^{\mu}\,, \quad \tilde{p}_n^{\mu} = \Lambda[Q-(1-\tilde{x}_a)p_a, Q-p_r]_{\nu}^{\mu} p_n^{\nu}\,, \quad n \neq a,b,r\,, \tag{6.56}$$

where the Lorentz-transformation matrix $\Lambda(K,\hat{K})_{\nu}^{\mu}$ is

$$\Lambda(K,\hat{K})_{\nu}^{\mu} = g_{\nu}^{\mu} - \frac{2(K+\hat{K})^{\mu}(K+\hat{K})_{\nu}}{(K+\hat{K})^2} + \frac{K^{\mu}\hat{K}_{\nu}}{K^2}\,. \tag{6.57}$$

This matrix is a Lorentz-boost, it maps $\hat{K}^{\mu}$ to K^{μ} when $K^2 = \hat{K}^2$. The momentum fraction and the transverse momentum in the mapping are given by

$$\tilde{x}_a = 1 - y_{rQ}\,, \quad \tilde{k}_{\perp,a}^{\mu} = p_r^{\mu} - y_{rQ} p_a^{\mu} - y_{ar} Q^{\mu}\,. \tag{6.58}$$

The mapping leads to phase space convolution, similarly to Eq. (6.65).

The initial-final collinear counterterms are defined as

$$\begin{aligned}\mathcal{C}_{ar}^{(0,1)}(\{p\},p_a,p_b) &= 8\pi\alpha_{\mathrm{S}}\mu^{2\epsilon}\frac{1}{x_a}\frac{1}{s_{ar}} \\ &\times 2\mathrm{Re}\langle \mathcal{M}_m^{(0)}(\{\hat{p}\}^{(ar)},\tilde{p}_{ar},p_b)|\hat{P}_{f_{ar}f_r}^{(0)}(\tilde{x}_a,\tilde{k}_{\perp,a};\epsilon)|\mathcal{M}_m^{(1)}(\{\hat{p}\}^{(ar)},\tilde{p}_{ar},p_b)\rangle\,,\end{aligned} \tag{6.59}$$

$$\begin{aligned}\mathcal{C}_{ar}^{(1,0)}(\{p\},p_a,p_b) &= (8\pi\alpha_{\mathrm{S}}\mu^{2\epsilon})^2 c_{\Gamma}\frac{1}{\tilde{x}_a}\frac{1}{s_{ar}^{1+\epsilon}} \\ &\times 2\mathrm{Re}\langle \mathcal{M}_m^{(0)}(\{\hat{p}\}^{(ar)},\tilde{p}_{ar},p_b)|\hat{P}_{f_{ar}f_r}^{(1)}(\tilde{x}_a,\tilde{k}_{\perp,a};\epsilon)|\mathcal{M}_m^{(0)}(\{\hat{p}\}^{(ar)},\tilde{p}_{ar},p_b)\rangle\,.\end{aligned} \tag{6.60}$$

6.3.3 The soft and soft-collinear counterterms

In the soft limit we replace the original phase space mapping of the CoLoRFulNNLO method defined in Ref. [34], because that mapping cannot be applied for processes involving only one massive particle in the final state (e.g. Drell-Yan

[2] Please note that the arguments of the boost in Eq. (5.17) of Ref. [39] are exchanged compared to here due to a typing error.

processes). Here we introduce a new soft phase space mapping for the extended CoLoRFulNNLO scheme[3]

$$\{p\}_{m+1} \xrightarrow{\mathbf{S}_r} \{\tilde{p}\}_m^{(r)} \,. \tag{6.61}$$

In this mapping we simply rescale the initial state momenta

$$\tilde{p}_n^\mu = \lambda_r p_n^\mu \,, \quad n = a, b \,, \tag{6.62}$$

with

$$\lambda_r = \sqrt{1 - y_{rQ}} \,, \tag{6.63}$$

while the final state particles get boosted using the Lorentz-transformation defined in Eq. (6.57)

$$\tilde{p}_i^\mu = \Lambda(\lambda_r Q, Q - p_r)^\mu_\nu p_i^\nu \,, \quad i \neq r \,, \tag{6.64}$$

and p_r is simply dropped. It can be shown that this mapping leads to the phase space convolution of the m particle phase space and the one-particle unresolved phase space

$$\mathrm{d}\Phi_{m+1} = \int_0^1 \mathrm{d}\lambda \, \mathrm{d}\Phi_m(\{\tilde{p}\}, \lambda Q) \Big[\mathrm{d}p_1^{(1)}(p_a, p_b, p_r, \lambda) \Big] \,. \tag{6.65}$$

The derivation of the formula and the definition of $\Big[\mathrm{d}p_1^{(1)}(p_a, p_b, p_r, \lambda) \Big]$ is given in the Appendix B.

The soft counterterms are defined as

$$\mathcal{S}_r^{(0,1)}(\{p\}) = -8\pi\alpha_\mathrm{S}\mu^{2\epsilon} \sum_{i,j\neq i} \frac{1}{2} \mathcal{S}_{ij}(r) |\mathcal{M}^{(0,1)}_{m,(i,j)}(\{\tilde{p}^{(r)}\})|^2 \,, \tag{6.66}$$

$$\begin{aligned}
\mathcal{S}_r^{(1,0)}(\{p\}) = (8\pi\alpha_\mathrm{S}\mu^{2\epsilon})^2 c_\Gamma \sum_{i,j\neq i} \frac{1}{2} \mathcal{S}_{ij}(r) \\
\times \Bigg[\left(\frac{C_\mathrm{A}}{\epsilon^2} \frac{\pi\epsilon}{\sin(\pi\epsilon)} \cos(\pi\epsilon) \Big(\frac{1}{2} \mathcal{S}_{ij}(r) \Big)^\epsilon + \frac{1}{2} \frac{\beta_0}{(4\pi)^2\epsilon} \frac{S_\epsilon}{\mu^{2\epsilon} c_\Gamma} \right) |\mathcal{M}^{(0)}_{m,(i,j)}(\{\tilde{p}^{(r)}\})|^2 \\
+ \frac{2\pi}{\epsilon} \sum_{k\neq i,j} \Big(\frac{1}{2} \mathcal{S}_{jk}(r) \Big)^\epsilon (\lambda_{j,k} - \lambda_{j,r} - \lambda_{k,r}) |\mathcal{M}^{(0)}_{m,(i,j,k)}(\{\tilde{p}^{(r)}\})|^2 \Bigg] \,.
\end{aligned} \tag{6.67}$$

The final-final soft-collinear counterterms share the same soft mapping and have the following form

$$\mathcal{C}_{ir}\mathcal{S}_r^{(0,1)}(\{p\}) = 8\pi\alpha_\mathrm{S}\mu^{2\epsilon} \mathbf{T}_i^2 \frac{2}{s_{ir}} \frac{z_i}{1 - z_i} |\mathcal{M}_m^{(0,1)}(\{\tilde{p}^{(r)}\})|^2 \,, \tag{6.68}$$

[3] A similar mapping was introduced in the work of Nagy et al. [110].

$$\mathcal{C}_{ir}\mathcal{S}_r^{(1,0)}(\{p\}) = -(8\pi\alpha_{\rm S}\mu^{2\epsilon})^2 c_\Gamma \mathbf{T}_i^2 \frac{2}{s_{ir}}\frac{z_i}{1-z_i}\left(\frac{C_{\rm A}}{\epsilon^2}\frac{\pi\epsilon}{\sin(\pi\epsilon)}\cos(\pi\epsilon)\Big(\frac{1}{s_{ir}}\frac{z_i}{1-z_i}\Big)^{\epsilon} + \frac{1}{2}\frac{\beta_0}{(4\pi)^2\epsilon}\frac{S_\epsilon}{\mu^{2\epsilon}c_\Gamma}\right)|\mathcal{M}_m^{(0)}(\{\tilde{p}^{(r)}\})|^2\,. \tag{6.69}$$

The initial-final soft-collinear counterterms are

$$\mathcal{C}_{ar}\mathcal{S}_r^{(0,1)}(\{p\}) = 8\pi\alpha_{\rm S}\mu^{2\epsilon}\mathbf{T}_a^2\frac{2}{s_{ar}}\frac{1}{1-x_a}|\mathcal{M}_m^{(0,1)}(\{\tilde{p}^{(r)}\})|^2\,. \tag{6.70}$$

$$\mathcal{C}_{ar}\mathcal{S}_r^{(1,0)}(\{p\}) = -(8\pi\alpha_{\rm S}\mu^{2\epsilon})^2 c_\Gamma \mathbf{T}_a^2 \frac{2}{s_{ar}}\frac{1}{1-x_a}\left(\frac{C_{\rm A}}{\epsilon^2}\frac{\pi\epsilon}{\sin(\pi\epsilon)}\cos(\pi\epsilon)\Big(\frac{1}{s_{ar}}\frac{1}{1-x_a}\Big)^{\epsilon} + \frac{1}{2}\frac{\beta_0}{(4\pi)^2\epsilon}\frac{S_\epsilon}{\mu^{2\epsilon}c_\Gamma}\right)|\mathcal{M}_m^{(0)}(\{\tilde{p}^{(r)}\})|^2\,, \tag{6.71}$$

and again we use the soft mapping on the right hand side of the equations.

Finally the singly-unresolved real-virtual counterterm is

$$\mathrm{d}\sigma_{m+1}^{\mathrm{RV,A_1}} = \mathrm{d}\Phi_m \otimes \Big[\mathrm{d}p_1\Big]\mathcal{A}_1 2\mathrm{Re}\langle\mathcal{M}_{m+1}^{(0)}|\mathcal{M}_{m+1}^{(1)}\rangle\,, \tag{6.72}$$

where $\otimes$ denotes exact factorization of the phase space in the final-final collinear limits, and phase space convolution otherwise. The $\mathcal{A}_1 2\mathrm{Re}\langle\mathcal{M}_{m+1}^{(0)}|\mathcal{M}_{m+1}^{(1)}\rangle$ subtraction candidate has the following form

$$\begin{aligned}\mathcal{A}_1 2\mathrm{Re}\langle\mathcal{M}_{m+1}^{(0)}|\mathcal{M}_{m+1}^{(1)}\rangle &= \\ &= \sum_{r\in F}\left[\sum_{i\neq r\in F}\frac{1}{2}\mathcal{C}_{ir}^{(0,1)} + \sum_{a\in I}\mathcal{C}_{ar}^{(0,1)} + \Big(\mathcal{S}_r^{(0,1)} - \sum_{i\neq r\in F}\mathcal{C}_{ir}\mathcal{S}_r^{(0,1)} - \sum_{a\in I}\mathcal{C}_{ar}\mathcal{S}_r^{(0,1)}\Big)\right] \\ &+ \sum_{r\in F}\left[\sum_{i\neq r\in F}\frac{1}{2}\mathcal{C}_{ir}^{(1,0)} + \sum_{a\in I}\mathcal{C}_{ar}^{(1,0)} + \Big(\mathcal{S}_r^{(1,0)} - \sum_{i\neq r\in F}\mathcal{C}_{ir}\mathcal{S}_r^{(1,0)} - \sum_{a\in I}\mathcal{C}_{ar}\mathcal{S}_r^{(1,0)}\Big)\right].\end{aligned} \tag{6.73}$$

6.4 Numerical test of the subtraction candidate in deeply-inelastic scattering

We implemented the subtraction candidates defined in the previous section in a numerical program written in `Fortran90` language. We chose deeply-inelastic

scattering (DIS) as a test process, because it involves colored particles both in the initial and in the final state. We used the Bern-Dixon-Kosower four partonic one-loop matrix elements [111], and crossed it into DIS kinematics. To test all possible type of initial state single-unresolved limits we used three subprocesses summarized in Table 6.4. We computed the $\mathcal{C}_{25}$ collinear limit for the third subprocess, the $\mathcal{C}_{26}$

Type	1	2	3	4	5	6
I	e^-	u	e^-	u	g	g
II	e^-	d	e^-	u	$\bar{u}$	d
III	e^-	g	e^-	u	$\bar{u}$	g

collinear limit for all three subprocesses, the $\mathcal{S}_5$, $\mathcal{S}_6$ soft limit and finally the $\mathcal{C}_{26}\mathcal{S}_6$ soft-collinear limit for the I. and III. subprocesses. We generated 10000 unresolved phase space configurations and plotted the ratio of the subtraction term and the one-loop squared matrix element in the various limits. The results are shown in Figs. 6.4, 6.4, 6.4 and 6.4 as histograms. As visible in the plots the subtraction terms matches the squared matrix element more and more as we go deeper into the infrared limits.

We note that soft limits shown in Fig. 6.4, have an asymmetric form, which looks unusual compared to the other plots that are symmetric. The reason of this behavior is not known, it might be related to some numerics or the phase space mapping of the soft counterterms, namely final state momenta are always boosted, which could introduce some systematic shift in the squared matrix element. However one should not worry about this asymmetry, first of all there is not such a requirement that the counterterms should approach the full squared matrix element from both directions. Secondly this asymmetry could be actually useful in integration, since the regulated squared matrix element would be either positive or negative definite, which is easier to integrate compared to the case when counterterms converges from both direction, which results an oscillating function.

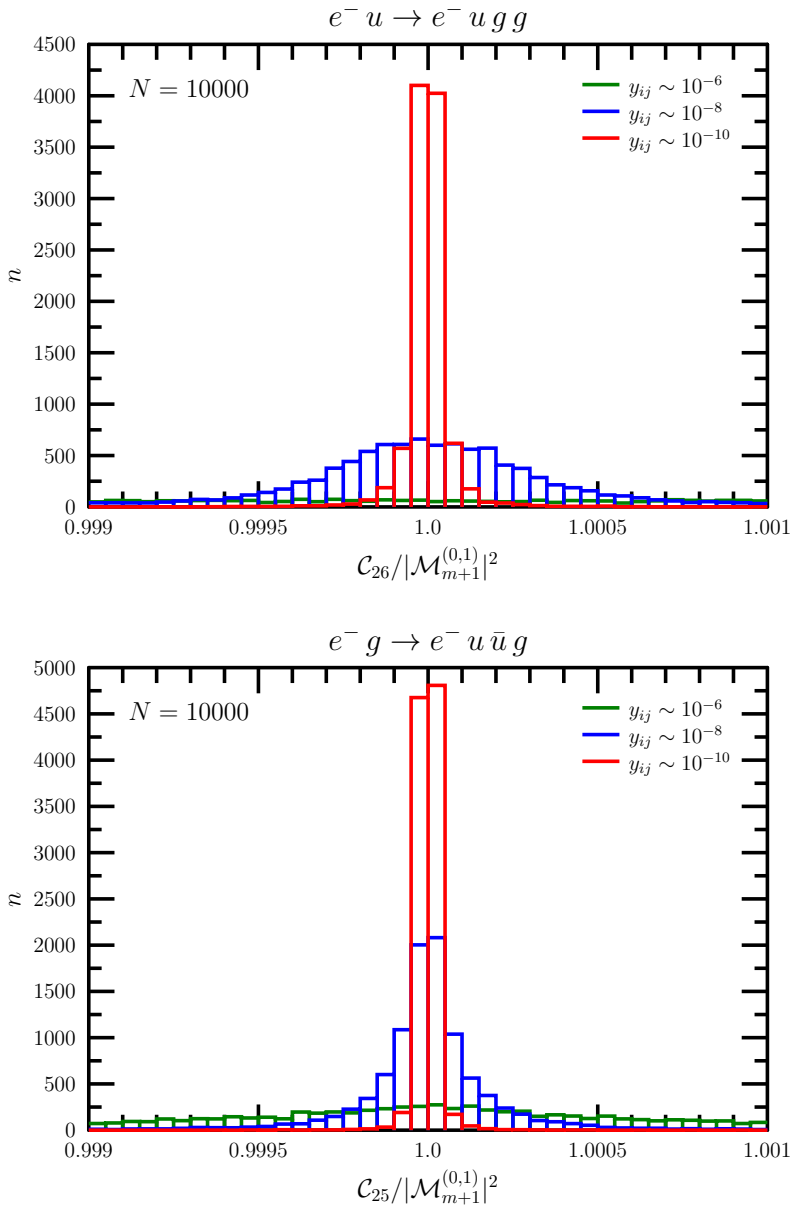

Figure 6.1. Spike plots with $N = 10000$ randomly generated phase space points in the initial-final collinear limit $q||g$ and $q||\bar{q}$ (lower).

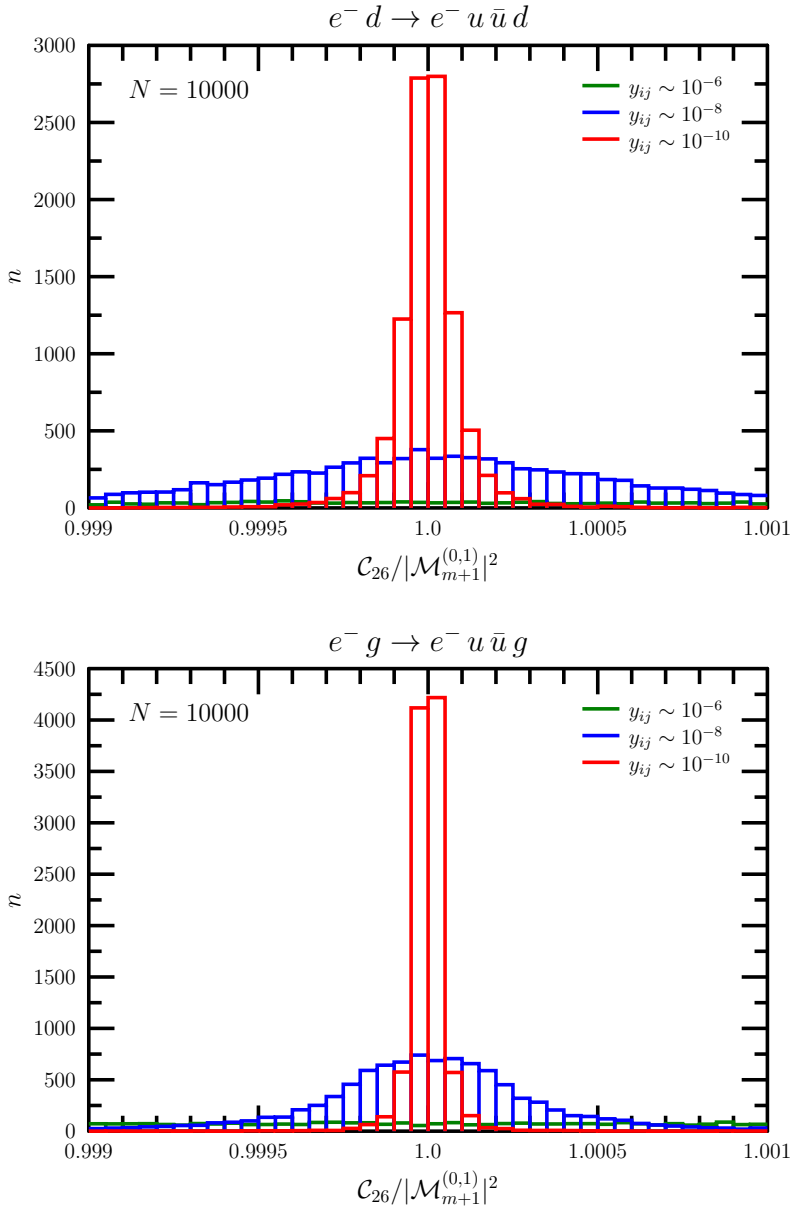

Figure 6.2. Spike plots with $N = 10000$ randomly generated phase space points in the initial-final collinear limit $g||q$ (upper) and $g||g$ (lower).

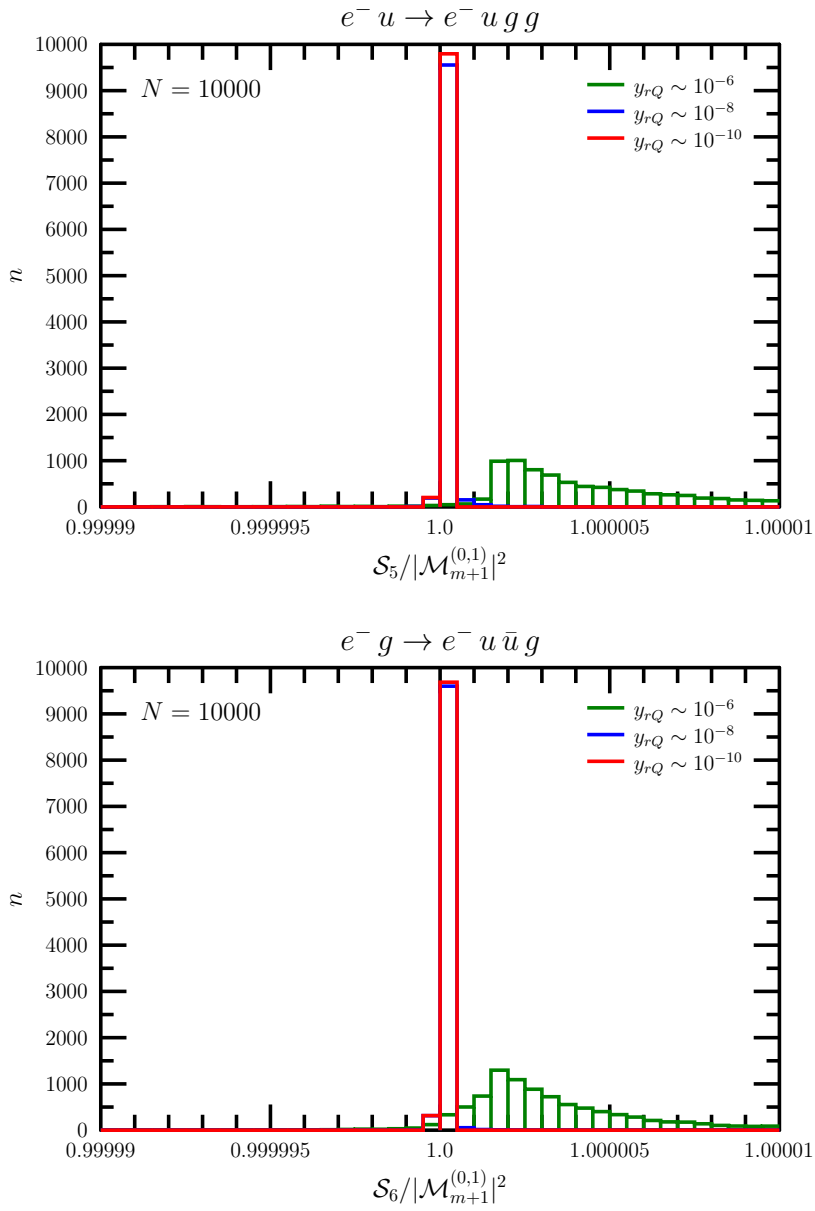

Figure 6.3. Spike plots $N = 10000$ randomly generated phase space points in the soft limit with two different subprocesses.

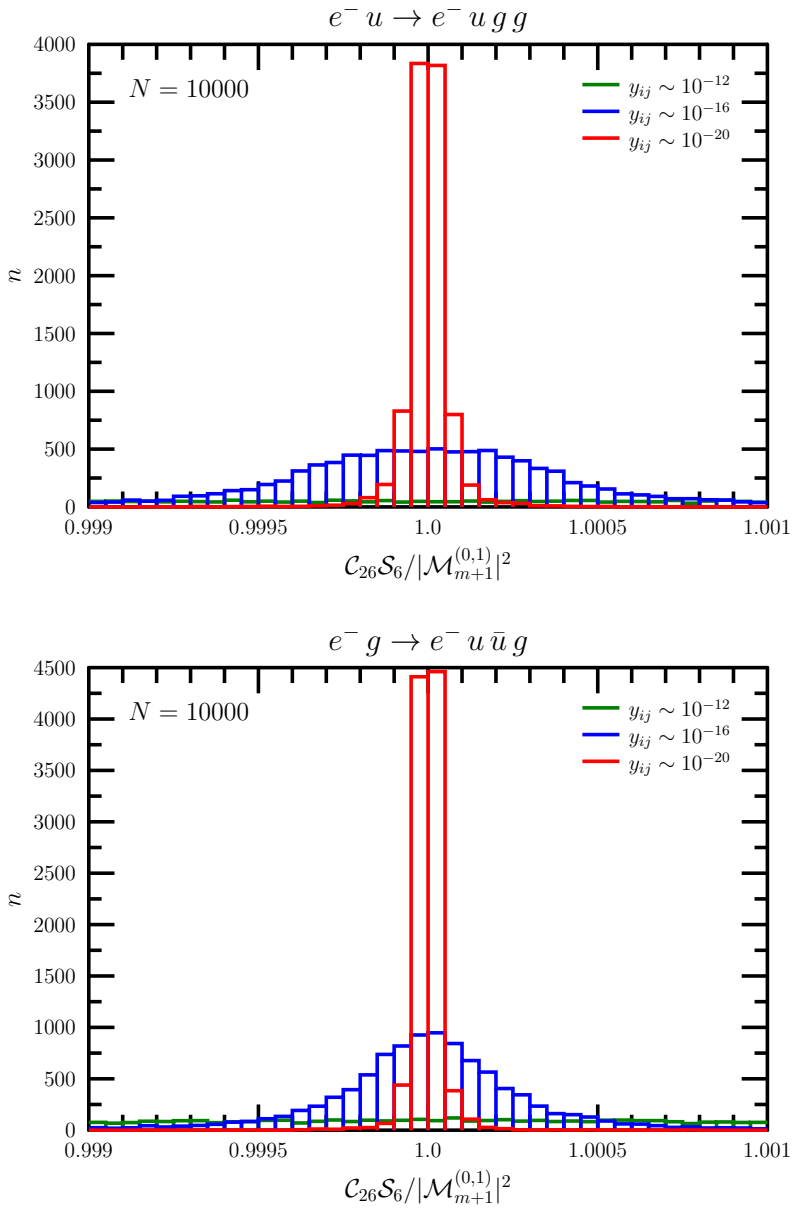

Figure 6.4. Spike plots with $N = 10000$ randomly generated phase space points in the initial-final collinear limit $q||g$ (upper) and $g||g$ (lower) with gluon also being soft.

Chapter 7

Summary and outlook

Three-jet production in electron-positron annihilation provides a clear environment to measure the α_S coupling of QCD. Precise theoretical calculations are key elements in this measurement. Presently the state-of-the-art predictions are next-to-next-to-leading order accurate in perturbation theory for both event shape and jet rate observables and next-to-next-to-leading logarithmic accurate resummation of logarithmic terms for event shapes. Resummation of jet rates is only available at next-to-double logarithmic accuracy for the $k_\perp$ and the general inclusive $k_\perp$ algorithm. In the literature there are no matched predictions for the three-jet rate either using the $k_\perp$ or the anti-$k_\perp$ jet clustering algorithm at $\sqrt{Q^2} = 91.2$ GeV center-of-mass energy. Also various versions of resummation are available formally equal at NDL accuracy but different numerically due to subleading logarithmic terms, which needs a comparison.

Furthermore presently new results in high energy physics are related mostly for hadron-hadron collisions due to the operation of LHC. This requires to extend the CoLoRFulNNLO subtraction scheme for hadron initiated processes in order to make predictions for hadron colliders.

In my thesis I collected my calculations and results performed in QCD perturbation theory using the CoLoRFulNNLO subtraction scheme, which I shortly summarize here again emphasizing my personal contributions.

First I calculated the finite part of integrated subtraction terms numerically, which is necessary to make predictions with the CoLoRFulNNLO method at NNLO accuracy. I developed and implemented a `python` and `Mathematica` framework based on the program `SecDec` to manage calculations of integrated subtraction terms numerically in large numbers in a fully automated way. I used my automated tools to compute master integrals numerically required for the $\mathbf{I}_1^{(0)}$, $\mathbf{I}_{1,1}^{(0,0)}$, $\mathbf{I}_1^{(1)}$ and $\mathbf{I}_2^{(0)}$ color insertion operators appearing in the CoLoRFulNNLO method.

Using the results of the master integrals I computed these operators for the three-jet kinematics and fit the results using logarithmic and polynomial functions. I implemented the resulting functions into the `MCCSM` code.

The CoLoRFulNNLO method was applied to three-jet production in e^+e^- collisions to calculate event shapes at NNLO accuracy. Using the same process I calculated the three-jet rate at NNLO accuracy using the $k_\perp$ jet clustering algorithm at $\sqrt{Q^2} = 91.2\,\mathrm{GeV}$ center-of-mass energy. I matched the fixed-order results with resummation at NDL accuracy available in the literature using the so-called R-matching scheme. I compared three different resummations, all three formally NDL accurate but different in subleading terms beyond NDL accuracy therefore different numerically. I showed that even incomplete subleading logarithms have an important effect in matched results. I also showed that although including the cusp anomalous dimension (K-term) into the resummation improves the matched physical prediction at NLO+NLL accuracy, this effect comes from an unphysical numerical behavior. It is also confirmed by matched predictions using NNLO fixed-order results. The predictions at NNLO+NDL accuracy provides better description of the data measured by the OPAL experiment compared to pure fixed-order prediction, however inclusion of further resummed logarithmic terms would be still necessary, and using the $\log R$-matching scheme would probably also improve the results.

I also calculated the three-jet rate at NNLO accuracy using two different versions of the anti-$k_\perp$ algorithm adapted for e^+e^- colliders. I calculated the fully resummed prediction for the general inclusive $k_\perp$ algorithm using two different energy cuts and I made matched predictions for three-jet rate for the first time using these algorithms. I calculated and provided an approximate analytic formula for the resummed prediction, which resums all NDL type logarithms but do not include any further subleading logarithmic terms. Using this resummed formula in matching, I showed that subleading logarithms have an important effect in matched prediction similarly to the $k_\perp$ algorithm.

In the work of extension of the CoLoRFulNNLO method to hadron colliders, I defined the single-unresolved one-loop subtraction term for the real-virtual squared matrix element with $m+1$ partons, which regularizes both the initial and final state single-unresolved singularities. The subtraction term is based on the factorization properties of one-loop QCD amplitudes in the infrared limits. The splitting kernels present in the initial-final collinear subtraction terms are obtained from the final state splitting kernels using the crossing relation. For this purpose I performed analytic continuation for the final state splitting kernel in order to use them in the initial state kinematics. The subtraction terms are defined over the whole phase space using phase space mappings. For the soft limit I introduced a new phase space mapping for the CoLoRFulNNLO method, which can be used in Drell-Yan processes as well. I checked the defined counterterms numerically in deeply inelas-

tic scattering and I showed that they match the squared matrix element in the possible infrared limits.

As I mentioned in my thesis, the use of the log R-matching scheme seems to be feasible, however it requires more work to be finished. This would be a major step forward, since the log R-matching scheme is less sensitive for missing subleading logarithms, therefore our predictions would be more stable and they would provide a physical behavior in the small y_{cut} region, not to mention that log R-matching was never used before for jet rates.

The regularization of the real-virtual contribution is not complete. Presently only the single-unresolved one-loop subtraction terms is defined, and for example the integrated single-unresolved double-real subtraction term also has infrared divergences in the single unresolved limits and has to be regularized by subtraction.

Chapter 8

Magyar nyelvű összefoglaló

A kvantum-színdinamika (QCD) az erős kölcsönhatás kvantum-térelmélete. Az elmélet lokális nem-ábeli $SU(N_c)$ mértékszimmetriával rendelkezik, ahol N_c a színek számát jelöli. Az elmélet a színes fermionok, a kvarkok kölcsönhatását írja le, melyet a szintén színtöltéssel rendelkező mértékbozonok, a gluonok közvetítenek. A QCD renormálható, ami technikai szempontból azt jelenti, hogy az elméletben megjelenő ultraibolya divergenciák szisztematikusan eltávolíthatóak a perturbációszámítás minden rendjében véges számú paraméter renormálásával. A renormálás eredményeként az elmélet fizikai paraméterei, mint például a csatolás vagy a kvark tömegek energiafüggőek lesznek, mért értékük függ az adott ütközetési energiától. Mivel a gluonok is rendelkeznek színtöltéssel, ezért az elméletben megjelenik a gluonok önkölcsönhatása is, ami az aszimptotikus szabadsághoz vezet. Ez azt jelenti, hogy ahogyan egyre magasabb és magasabb ütközési energiákra lépünk, az elmélet csatolása egyre kisebbé válik.

A természetben azonban nem figyelhetőek meg szabad kvarkok és gluonok (együttes nevükön partonok), csak kötött részecskeállapotban találhatóak meg, melyeket hadronoknak nevezünk, továbbá az ütközési kísérletekben a hadronok energikus, közel párhuzamos záporát, az úgynevezett jeteket figyelhetjük meg.

A hadronikus jetek keletkezése az ütközési kísérletek általános sajátossága és vizsgálatuk fontos, mivel: a jetek felhasználhatók a standard modell paramétereinek a mérésére és a modell tesztelésére; a jetek új fizikára utaló nyomot tartalmazhatnak, emiatt a standard modell típusú folyamatokban való keltésük fontos háttérbecslésként szolgál az új fizika kereséséhez.

Mérhető mennyiségekre a nagy energiás fizikában a perturbációszámítás elméletében tehetünk jóslatokat. A QCD aszimptotikus szabadsága miatt a hatáskeresztmetszet kiszámolható az α_S csatolás Taylor-soraként. Azonban az erős csatolás még nagy energiákon sem túl kicsi, például $\alpha_S(91.2\,\mathrm{GeV}) = 0.118$, ezért a

magasabb rendű sugárzási korrekciók ismerete elengedhetetlen hadronos folyamatok kvantitatív leírásához. Ellenben ezen sugárzási korrekciók számítása bonyolult a számolás során megjelenő ultraibolya és infravörös szingularitások miatt. Ahogy korábban említettem az ultraibolya divergenciák renormálás segítségével szisztematikusan eltávolíthatóak a perturbációszámítás minden rendjében véges számú paraméter újranormálásával. A Kinoshita-Lee-Nauenberg tétel kimondja, hogy a hatáskeresztmetszet QCD-ben véges minden infravörös véges mennyiségre, azaz olyan mennyiségekre, amelyek érzéketlenek lágy és kollineáris sugárzás jelenlétére. Ezzel szemben a tétel nem biztosítja a számolás közbenső lépéseiben megjelenő egyes járulékok végességét, és sajnos nincsen egy, a renormáláshoz hasonló általános módszer, amellyel szisztematikusan eltávolíthatóak lennének az infravörös divergenciák a perturbációszámítás minden rendjében. Az első (NLO) sugárzási korrekciók automatizált számítása már több éve elérhető különböző szoftverek formájában, melyek segítségével a részecskefizikai folyamatok egy széles skálája könnyen kiszámolható.

A jelenlegi kutatási frontvonal a QCD perturbációszámításban a második (NNLO) sugárzási korrekciók meghatározása, melyre több megoldás is született az elmúlt 15 évben, azonban még egyik sem képes az NLO korrekciók számításához hasonló fokú automatizációra.

Az egyik lehetséges megoldás az úgynevezett CoLoRFulNNLO levonási séma. A módszer alapja az infravörös divergens mátrixelemnégyzet levonással való regularizálása. A levonási tagok a QCD mátrixelemek univerzális faktorizációs tulajdonságain alapulnak, és az infravörös határértékekben való viselkedésük d-dimenzióban megegyezik az eredeti mátrixelemével. A CoLoRFulNNLO módszer jelenleg csak olyan részecskefizikai folyamatokra alkalmazható, amelyek csak a végállapotban tartalmaznak színtöltött részecskéket.

Az elektron-pozitron ütköztetésekben keletkező három jetes események tiszta laboratóriumi körülményeket kínálnak a QCD elméletének kísérleti ellenőrzésére, mivel csak a végállapotban találhatóak színtöltéssel rendelkező részecskék. Emellett a három jetes események gyakorisága már a perturbációszámítás vezető rendjében arányos az α_S csatolással. Az ebben a folyamatban mért alakváltozó és jet hányad mennyiségek még a mai napig az egyik legpontosabb eszközöknek számítanak az erős csatolás mérésére. A csatolás meghatározásának pontossága függ a kísérleti mérés és az elméleti jóslat pontosságától egyaránt. Az elmúlt években megnőtt kísérleti precizitás megköveteli a hasonlóan pontos elméleti számításokat. A CoLoRFulNNLO módszerrel lehetőségünk nyílik differenciális hatáskeresztmetszetek NNLO pontosságú kiszámítására.

A CoLoRFulNNLO módszerben azonban, több más fontos feladat mellett, szükség van az úgynevezett integrált levonási tagok ismeretére. Ezen tagok pólusegyütthatói már ismertek analitikusan, viszont a véges rész teljesen analitikus módon

történő kiszámítása nehéz a kifejezés bonyolultsága miatt, így az ehhez kapcsolódó integrálokat numerikusan kell elvégezni. Ez a feladat több száz bonyolult integrál, nagy számú pontban numerikus módszerekkel történő meghatározását igényli, amely miatt az egész folyamat teljes fokú automatizálása szükséges.

Ennek a feladatnak az elvégzésére létrehoztam egy `python` és `Mathematica` nyelveneken írt automatizált rendszert, amely a `SecDec` programot használja alapul. A kifejlesztett automatizált eszköz segítségével numerikusan kiszámoltam az $\mathbf{I}_1^{(0)}$, az $\mathbf{I}_{1,1}^{(0,0)}$, az $\mathbf{I}_1^{(1)}$ és az $\mathbf{I}_2^{(0)}$ színtéren ható operátorokhoz szükséges mester integrálokat. A mester integrálok eredményeit felhasználva, kiszámítottam a fent említett operátorokat három jet végállapot esetén, és a numerikus eredményeket logaritmikus és polinom függvényekkel illesztettem meg. A kapott függvényt implementáltam az `MCCSM` Monte Carlo programba. Végül a kész levonási módszerrel alakváltozó mennyiségekre NNLO pontosságú jóslatokat tettünk e^+e^- ütközésben keletkező három jet esetén.

Az alakváltozó mennyiségek mellett az α_S csatolás mérése gyakran az úgynevezett három jet hányad vizsgálatán alapszik. A perturbációszámítás vezető rendjében a jeteket partonok segítségével modellezzük, minden jethez egy-egy partont rendelünk. Magasabb rendű sugárzási korrekciók figyelembevételével újabb partonokat rendelünk az egyes jetekhez, azonban az egy jetben jelenlévő partonok száma még mindig nagyságrendileg $\mathcal{O}(1)$. Bizonyos kinematikai tartományokban ez a közelítés nem megfelelő, mivel a domináns járulék újabb és újabb lágy-kollineáris partonok kibocsájtásából származik. Ez a viselkedés figyelembe vehető az ezekhez a tartományokhoz kapcsolódó logaritmikus tagok minden rendben történő felösszegzésével, vagy parton záporok alkalmazásával. A parton zápor NNLO pontosságú rögzített rendű számolással való illesztése jelenleg még nem megoldott, azonban az úgynevezett dupla logaritmus melletti (NDL) tagok felösszegzése több éve ismert jet hányad esetén. A szélesebb kinematikai tartományon érvényes jóslat a rögzített rendű és a felösszegzett számítás illesztésével kapható meg.

A $k_\perp$ jet algoritmust használva NNLO pontosságú jóslatot tettem a három jet hányadra $\sqrt{Q^2} = 91.2$ GeV ütköztetési energián. A kapott eredményt illesztettem NDL pontosságú felösszegzett jóslattal az úgynevezett R-illesztési sémát felhasználva. Összehasonlítottam három, formálisan azonos felösszegzett számítást, amelyek NDL pontosságon túli logaritmikus tagokban térnek el. Megmutattam, hogy ezek a logaritmikus tagok nem elhanyagolható módon befolyásolják a kapott illesztett eredményeket. Emellett megmutattam, hogy habár az úgynevezett K-tag figyelembevétele a felösszegzésben javít az NLO+NDL típusú illesztett eredményen, ez valójában egy véletlen numerikus összjáték eredménye, amelyet az NNLO+NDL típusú illesztett eredmények is alátámasztanak. Az NNLO+NDL illesztett eredmény jobban leírja a kísérleti adatokat, mint a rögzített rendű NNLO számolás, azonban további logaritmikus tagok felösszegzése még szükséges lenne,

és az úgynevezett log R-illesztési séma használata is javíthat az eredményeken.

Az anti-$k_\perp$ jet algoritmus e^+e^- ütköztetőkre adaptált két különböző verzióját használva kiszámoltam a három jet hányadot ezen algoritmusokra is. Kiszámítottam a teljes felösszegzett eredményt két különböző energia vágást alkalmazva és ezeket illesztettem rögzített rendű számolásokkal. Megadtam egy analitikus közelítő képletet a felösszegzett jóslatra, amely kizárólag csak az NDL típusú logaritmusokat tartalmazza. Ezt a felösszegzett alakot felhasználva az illesztésben megmutattam, hogy ebben az esetben is jelentős eltérést okoznak az éppen jelen lévő vagy hiányzó NDL pontosságon túli tagok, hasonlóan a $k_\perp$ algoritmus esetéhez.

A mai, új részecskefizikai eredmények döntő része, az LHC proton-proton ütköztetőhöz kapcsolódik, ami szükségessé teszi a CoLoRFulNNLO módszer ilyen típusú folyamatokra való kiterjesztését. Ebben a munkában részt véve definiáltam az egyszeresen feloldatlan egyhurok levonási tagot, amely az $m + 1$ partonos egyhurok mátrixelemnégyzet kezdeti és végállapoti infravörös szingularitásait egyaránt regularizálja. A levonási tag az egyhurok mátrixelemnégyzet infravörös faktorizációs tulajdonságain alapszik, amely impulzus leképezések segítségével kiterjeszthetőek az egész fázistérre. A kezdeti-végállapoti kollineáris levonási tagban jelen lévő Altarelli-Parisi függvények megkaphatóak a végállapoti Altarelli-Parisi függvényekből a keresztezési összefüggés segítségével. Hogy ezt alkalmazhassam, analitikusan elfolytattam a végállapoti Altarelli-Parisi függvények kifejezéseit, így azok használhatóak kezdeti állapoti kinematikában is. A lágy levonási tag számára bevezettem egy új impulzus leképezést a CoLoRFulNNLO módszerben, amely alkalmazható Drell-Yan folyamatok számolásánál is. A definiált levonási tagokat mélyen rugalmatlan szórás folyamatán teszteltem le numerikusan, és megmutattam, hogy az egyes ellentagok infravörös viselkedése azonos az eredeti mátrixelemnégyzetével.

Ahogy a disszertációmban is említettem a log R-illesztési séma is alkalmazhatónak tűnik jet hányad esetén, azonban ebben a témában még további munka szükséges. Mindenesetre ennek a sémának a használata jelentős előrelépés lenne, mivel a log R-illesztési séma kevésbé érzékeny a hiányzó NDL pontosságon túli tagok hiányára, így az illesztett jóslatok stabilabbak lennének és a kis y_{cut} tartományban is fizikai viselkedést mutatnának. Fontos még megemlíteni, hogy eddig még senki nem használta ezt az illesztési sémát a jet hányad mennyiségre.

A valós-virtuális járulék regularizációja még nincs befejezve. Jelenleg csak egy levonási tag, az egyszeresen feloldatlan egyhurok levonási tag definiált, azonban a szintén $m + 1$ partonos járulékot adó integrált egyszeresen feloldatlan duplán valós levonási tag is rendelkezik infravörös szingularitásokkal, amelyeket szintén regularizálni kell levonás segítségével.

Appendix A

Auxiliary figures

In this appendix we show two examples for fitting the master integrals, referred previously in Sect. 3.1. The first one is the $\mathcal{I}_{2\mathcal{C},1}^{(-1,0,-1,1)}$ integral which has been defined in Eq. (3.8) and it is a function of y_{iQ} kinematic variable, here labeled with x. The integral was evaluated in a list of points numerically and then fitted by the following function:

$$\mathcal{F}(x) = \sum_{i=0}^{l} P_i^{(m)}(x) \log^i x \,, \quad P_i^{(m)}(x) = \sum_{k=0}^{m} a_{i,k}\, x^k \,, \tag{A.1}$$

where l is the order of the logarithmic function determined by the pole coefficient of the Laurent-series, while m sets the order of polynomials in x and it is a free parameter. We found that $m = 2, 3$ for the polynomial order provides a good fit in general, an example shown in Fig A.1.

The second example is the master integral $\mathcal{I}_{2\mathcal{C},6}^{(-1,0)}$, which comes from the integration of double collinear limits. The integral depends on two kinematic variables y_{iQ} and y_{jQ}, here denoted with $x_{\widetilde{is}}$ and $x_{\widetilde{js}}$. The fit function can be easily extended into two dimensions:

$$\mathcal{F}(x,y) = \sum_{i=0}^{l} \sum_{j=0}^{l-i} P_i^{(m)}(x) P_j^{(m)}(y) \log^i x \log^j y \,, \tag{A.2}$$

where we used that the function is symmetric in x and y, therefore symmetric terms share the same coefficients. The $\mathcal{I}_{2\mathcal{C},6}^{(-1,0)}$ master integral was calculated numerically in a list of points, then fitted with the two-dimensional fit function. Results for the finite part are shown in Fig. A.2.

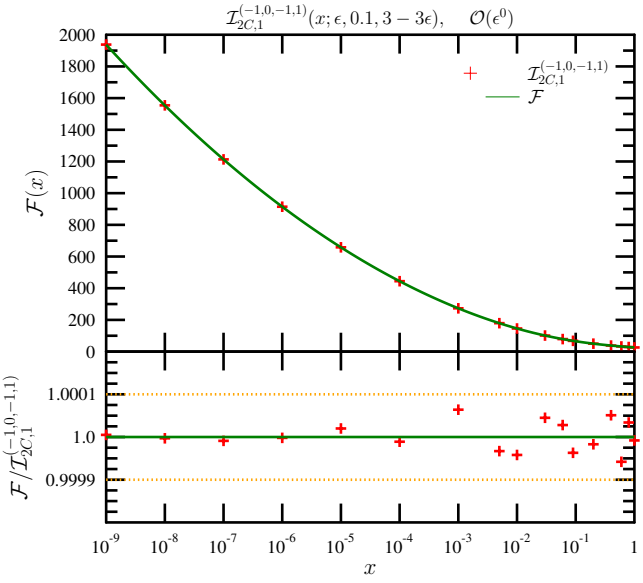

Figure A.1. The finite part of the $\mathcal{I}^{(-1,0,-1,1)}_{2\mathcal{C},1}$ integral calculated numerically (red crosses). The points are fitted using the functional form of Eq. (A.1) choosing $l = 4$ and $m = 2$ (denoted by the green line). On the lower panel we show the relative accuracy of the fit compared to the results of numerical integrations.

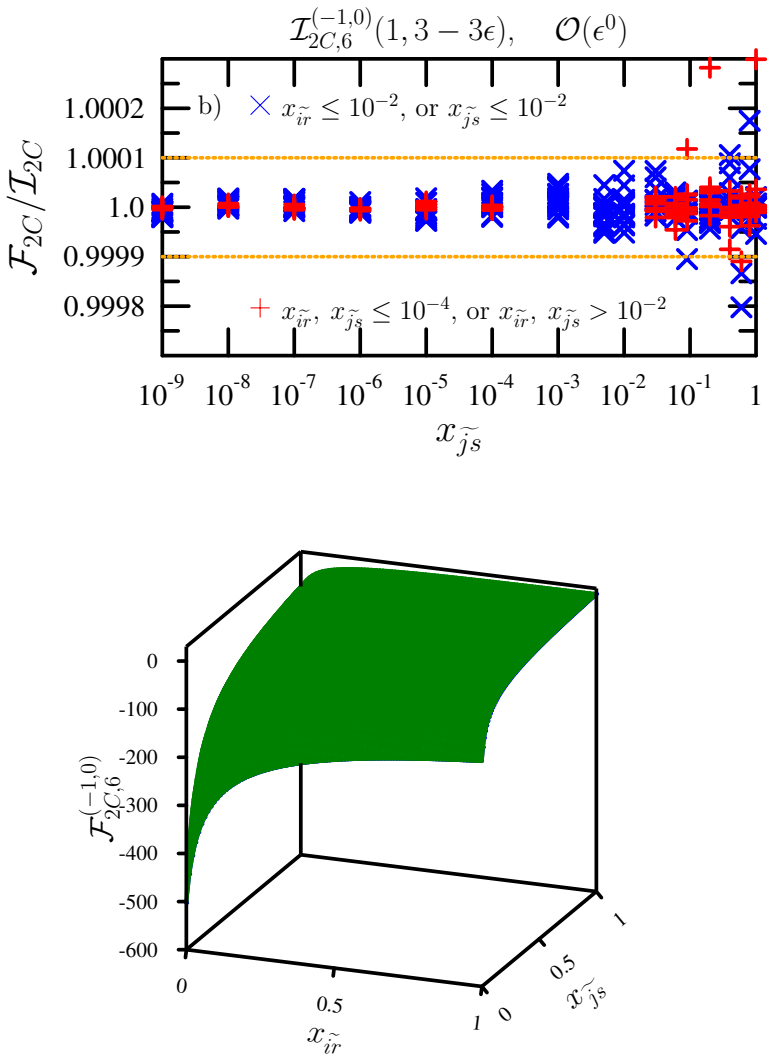

Figure A.2. The finite part of the $\mathcal{I}^{(-1,0)}_{2C,6}$ integral calculated numerically. The $x_{\tilde{is}} - x_{\tilde{js}}$ plane is cut into three different regions, and points in each region are fitted using the functional form of Eq. A.2 separately. On the upper panel we show the goodness of the fit plotted as a function of only one variable (hence the multiple points to one $x_{\tilde{js}}$ value), while the lower panel shows the shape of the function.

Appendix B

Soft phase space mapping

In this appendix chapter we discuss the new phase space mapping in CoLoRFulNNLO introduced for the soft type subtractions in Chapter 6. The new mapping has the advantage that it can be used in Drell-Yan processes as well, in contrast of the original soft mapping of the method.

The momenta of the incoming partons are simply rescaled

$$\tilde{p}_n^\mu = \lambda_r p_n^\mu \,, n = a, b \,, \tag{B.1}$$

while particles in the final states get boosted

$$\tilde{p}_i = \Lambda(p_i) \,, i \neq r \,, \tag{B.2}$$

except p_r which is simply dropped. The scaling factor λ_r can be calculated from energy conservation:

$$(\tilde{p}_a + \tilde{p}_b)^2 = \lambda_r^2 (p_a + p_b)^2 = \lambda_r^2 Q^2 \,. \tag{B.3}$$

On the other hand it is also true that

$$(\tilde{p}_a + \tilde{p}_b)^2 = \Big(\Lambda(p_1) + \cdots + \Lambda(p_m)\Big)^2 = \Big(\Lambda(p_1 + \cdots + p_m)\Big)^2 = (Q - p_r)^2 \,, \tag{B.4}$$

where we used the Lorentz-invariance of the invariant mass. Combining Eqs. (B.3) and (B.4) we get

$$\lambda_r = \sqrt{1 - \frac{2 p_r Q}{Q^2}} = \sqrt{1 - y_{rQ}} \,. \tag{B.5}$$

The desired boost can be omitted from the requirement of momentum conservation:

$$\tilde{p}_a + \tilde{p}_b = \lambda_r (p_a + p_b) = \lambda_r Q \,, \tag{B.6}$$

and

$$\tilde{p}_a + \tilde{p}_b = \sum_i \tilde{p}_i = \sum_i \Lambda(p_i) = \Lambda\Big(\sum_i p_i\Big) = \Lambda(Q - p_r)\,, \tag{B.7}$$

which gives the $\Lambda(Q - p_r) = \lambda_r Q$ condition for the desired boost. The Lorentz-transformation matrix

$$\Lambda(K, \hat{K})^\mu_\nu = g^\mu_\nu - \frac{2(K + \hat{K})^\mu (K + \hat{K})_\nu}{(K + \hat{K})^2} + \frac{K^\mu \hat{K}_\nu}{K^2} \tag{B.8}$$

maps $\hat{K}$ to K if $\hat{K}^2 = K^2$. Therefore the boost we looked for is $\Lambda(\lambda_r Q, Q - p_r)^\mu_\nu$.

Using the mapping defined above we can rewrite the $m + 1$ partonic phase space in terms of the $\hat{p}_i$ mapped momenta. The phase space for $m + 1$ partons by definition is

$$\mathrm{d}\Phi_{m+1} = \left(\prod_{i=1}^{m} \frac{\mathrm{d}^d p_i}{(2\pi)^{d-1}} \delta_+(p_i^2)\right) \frac{\mathrm{d}^d p_r}{(2\pi)^{d-1}} \delta_+(p_r^2) (2\pi)^d \delta^{(d)}\Big(\sum_i p_i + p_r - p_a - p_b\Big)\,. \tag{B.9}$$

Inserting the factors

$$\int \mathrm{d}^d \tilde{p}_i \delta^{(d)}(\tilde{p}_i - \Lambda(p_i))\,, \quad \int \mathrm{d}\lambda \delta(\lambda - 1 + y_{rQ})\,, \tag{B.10}$$

into the previous equation we get

$$\begin{aligned}
\mathrm{d}\Phi_{m+1} &= \left(\prod_{i=1}^{m} \int \frac{\mathrm{d}^d \tilde{p}_i}{(2\pi)^{d-1}} \mathrm{d}^d p_i \delta^{(d)}(\Lambda^{-1}(\tilde{p}_i) - p_i) \delta_+(p_i^2)\right) \\
&\times \int \mathrm{d}\lambda \delta(\lambda - 1 + y_{rQ}) \frac{\mathrm{d}^d p_r}{(2\pi)^{d-1}} \delta_+(p_r^2) (2\pi)^d \delta^{(d)}\Big(\sum_i p_i + p_r - p_a - p_b\Big) \\
&= \left(\prod_{i=1}^{m} \frac{\mathrm{d}^d \tilde{p}_i}{(2\pi)^{d-1}} \delta_+(\tilde{p}_i^2)\right) \int \mathrm{d}\lambda \delta(\lambda - 1 + y_{rQ}) \frac{\mathrm{d}^d p_r}{(2\pi)^{d-1}} \delta_+(p_r^2) \\
&\times (2\pi)^d \delta^{(d)}\Big(\sum_i \Lambda^{-1}(p_i) + p_r - p_a - p_b\Big)\,,
\end{aligned} \tag{B.11}$$

where we used $\delta^{(d)}(\tilde{p}_i - \Lambda(p_i)) = J\delta^{(d)}(\Lambda^{-1}(\tilde{p}_i) - p_i)$ with $J = 1$ for proper Lorentz-transformation and we evaluated the $\mathrm{d}^d p_i$ integral.

The argument of the d-dimensional delta function in Eq. (B.11) can be rewritten as:

$$\sum_i \Lambda^{-1}(p_i) + p_r - p_a - p_b = \Lambda^{-1}(\sum_i \tilde{p}_i) - (Q - p_r) = \Lambda^{-1}\Big(\sum_i \tilde{p}_i - \Lambda(Q - p_r)\Big)\,. \tag{B.12}$$

Using this we obtain

$$\delta^{(d)}\left(\Lambda^{-1}\Big(\sum_i \tilde{p}_i - \Lambda(Q-p_r)\Big)\right) = J\delta^{(d)}\Big(\sum_i \tilde{p}_i - \lambda Q\Big)\,,\ \text{with}\ J=1\,. \tag{B.13}$$

Therefore the $m+1$ particle phase space becomes

$$\begin{aligned}\mathrm{d}\Phi_{m+1} = \int_0^1 \mathrm{d}\lambda\left(\prod_{i=1}^{m}\frac{\mathrm{d}^d\tilde{p}_i}{(2\pi)^{d-1}}\delta_+(\tilde{p}_i^2)\right)(2\pi)^d\delta^{(d)}\Big(\sum_i \tilde{p}_i - \lambda Q\Big)\\ \times\frac{\mathrm{d}^d p_r}{(2\pi)^{d-1}}\delta_+(p_r^2)\delta(\lambda-\tilde{\lambda}_r)\Theta(\lambda)\Theta(1-\lambda)\,.\end{aligned} \tag{B.14}$$

The Θ functions comes from changing the integration borders of λ from $(-\infty,\infty)$ to $(0,1)$ since $\tilde{\lambda}_r$ is physically limited to $(0,1)$.

Defining the one particle unresolved phase space as

$$\big[\mathrm{d}p_1^{(1)}(p_a,p_b,p_r,\lambda)\big] \equiv \frac{\mathrm{d}^d p_r}{(2\pi)^{d-1}}\delta_+(p_r^2)\delta(\lambda-\tilde{\lambda}_r)\Theta(\lambda)\Theta(1-\lambda)\,, \tag{B.15}$$

the original $m+1$ phase space expressed in terms of the mapped momenta turns into a convolution of the mapped m partonic and the one particle unresolved phase space

$$\mathrm{d}\Phi_{m+1} = \int_0^1 \mathrm{d}\lambda\mathrm{d}\Phi_m(\{\tilde{p}\},\lambda Q)\big[\mathrm{d}p_1^{(1)}(p_a,p_b,p_r,\lambda)\big]\,. \tag{B.16}$$

Bibliography

[1] S. Brandt, C. Peyrou, R. Sosnowski, and A. Wroblewski, Phys. Lett. **12**, 57 (1964).

[2] E. Farhi, Phys. Rev. Lett. **39**, 1587 (1977).

[3] S. Catani, G. Turnock, and B. R. Webber, Phys. Lett. **B295**, 269 (1992).

[4] J. F. Donoghue, F. E. Low, and S.-Y. Pi, Phys. Rev. **D20**, 2759 (1979).

[5] G. P. Salam and G. Soyez, JHEP **05**, 086 (2007), 0704.0292.

[6] JADE, W. Bartel *et al.*, Z. Phys. **C33**, 23 (1986), [,53(1986)].

[7] JADE, S. Bethke *et al.*, Phys. Lett. **B213**, 235 (1988).

[8] S. Catani, Y. L. Dokshitzer, M. Olsson, G. Turnock, and B. R. Webber, Phys. Lett. **B269**, 432 (1991).

[9] Y. L. Dokshitzer, G. D. Leder, S. Moretti, and B. R. Webber, JHEP **08**, 001 (1997), hep-ph/9707323.

[10] M. Cacciari, G. P. Salam, and G. Soyez, JHEP **04**, 063 (2008), 0802.1189.

[11] T. Binoth and G. Heinrich, Nucl. Phys. **B585**, 741 (2000), hep-ph/0004013.

[12] V. A. Smirnov, Phys. Lett. **B460**, 397 (1999), hep-ph/9905323.

[13] S. Catani and M. H. Seymour, Nucl. Phys. **B485**, 291 (1997), hep-ph/9605323, [Erratum: Nucl. Phys.B510,503(1998)].

[14] S. Frixione, Z. Kunszt, and A. Signer, Nucl. Phys. **B467**, 399 (1996), hep-ph/9512328.

[15] S. Frixione, Nucl. Phys. **B507**, 295 (1997), hep-ph/9706545.

[16] Z. Nagy and D. E. Soper, JHEP **09**, 055 (2003), hep-ph/0308127.

[17] Z. Nagy and Z. Trócsányi, Nucl. Phys. **B486**, 189 (1997), hep-ph/9610498.

[18] S. Frixione and B. R. Webber, JHEP **06**, 029 (2002), hep-ph/0204244.

[19] C. F. Berger *et al.*, Phys. Rev. **D78**, 036003 (2008), 0803.4180.

[20] M. Czakon, C. G. Papadopoulos, and M. Worek, JHEP **08**, 085 (2009), 0905.0883.

[21] G. Cullen *et al.*, Eur. Phys. J. **C72**, 1889 (2012), 1111.2034.

[22] G. Bevilacqua *et al.*, Comput. Phys. Commun. **184**, 986 (2013), 1110.1499.

[23] S. Actis, A. Denner, L. Hofer, A. Scharf, and S. Uccirati, JHEP **04**, 037 (2013), 1211.6316.

[24] G. Bevilacqua, M. Czakon, M. Kubocz, and M. Worek, JHEP **10**, 204 (2013), 1308.5605.

[25] J. Alwall *et al.*, JHEP **07**, 079 (2014), 1405.0301.

[26] G. Cullen *et al.*, Eur. Phys. J. **C74**, 3001 (2014), 1404.7096.

[27] S. Actis *et al.*, Comput. Phys. Commun. **214**, 140 (2017), 1605.01090.

[28] A. Gehrmann-De Ridder, T. Gehrmann, and E. W. N. Glover, JHEP **09**, 056 (2005), hep-ph/0505111.

[29] M. Czakon and D. Heymes, Nucl. Phys. **B890**, 152 (2014), 1408.2500.

[30] S. Catani and M. Grazzini, Phys. Rev. Lett. **98**, 222002 (2007), hep-ph/0703012.

[31] J. Gaunt, M. Stahlhofen, F. J. Tackmann, and J. R. Walsh, JHEP **09**, 058 (2015), 1505.04794.

[32] C. W. Bauer, S. Fleming, D. Pirjol, and I. W. Stewart, Phys. Rev. **D63**, 114020 (2001), hep-ph/0011336.

[33] G. Somogyi, Z. Trócsányi, and V. Del Duca, JHEP **0506**, 024 (2005), hep-ph/0502226.

[34] G. Somogyi and Z. Trócsányi, (2006), hep-ph/0609041.

[35] G. Somogyi, Z. Trócsányi, and V. Del Duca, JHEP **01**, 070 (2007), hep-ph/0609042.

[36] G. Somogyi and Z. Trócsányi, JHEP **01**, 052 (2007), hep-ph/0609043.

[37] G. Somogyi and Z. Trócsányi, JHEP **08**, 042 (2008), 0807.0509.

[38] U. Aglietti, V. Del Duca, C. Duhr, G. Somogyi, and Z. Trócsányi, JHEP **09**, 107 (2008), 0807.0514.

[39] G. Somogyi, JHEP **05**, 016 (2009), 0903.1218.

[40] P. Bolzoni, S.-O. Moch, G. Somogyi, and Z. Trócsányi, JHEP **08**, 079 (2009), 0905.4390.

[41] P. Bolzoni, G. Somogyi, and Z. Trócsányi, JHEP **01**, 059 (2011), 1011.1909.

[42] V. Del Duca, G. Somogyi, and Z. Trócsányi, JHEP **06**, 079 (2013), 1301.3504.

[43] G. Somogyi, JHEP **04**, 010 (2013), 1301.3919.

[44] V. Del Duca *et al.*, Phys. Rev. **D94**, 074019 (2016), 1606.03453.

[45] V. Del Duca, C. Duhr, G. Somogyi, F. Tramontano, and Z. Trócsányi, JHEP **04**, 036 (2015), 1501.07226.

[46] V. Del Duca, C. Duhr, A. Kardos, G. Somogyi, and Z. Trócsányi, Phys. Rev. Lett. **117**, 152004 (2016), 1603.08927.

[47] G. Somogyi, A. Kardos, Z. Szőr, and Z. Trócsányi, In preparation (2017).

[48] G. Somogyi, A. Kardos, Z. Szőr, and Z. Trócsányi, Under publication in Acta Physica Polonica B (2017), 1706.01688.

[49] A. Banfi, G. P. Salam, and G. Zanderighi, JHEP **03**, 073 (2005), hep-ph/0407286.

[50] S. Catani, L. Trentadue, G. Turnock, and B. R. Webber, Nucl. Phys. **B407**, 3 (1993).

[51] R. Bonciani, S. Catani, M. L. Mangano, and P. Nason, Phys. Lett. **B575**, 268 (2003), hep-ph/0307035.

[52] S. Catani, G. Turnock, B. Webber, and L. Trentadue, Physics Letters B **263**, 491 (1991).

[53] S. Catani, G. Turnock, and B. R. Webber, Phys. Lett. **B272**, 368 (1991).

[54] S. Catani and B. R. Webber, Phys. Lett. **B427**, 377 (1998), hep-ph/9801350.

[55] Y. L. Dokshitzer, A. Lucenti, G. Marchesini, and G. P. Salam, JHEP **01**, 011 (1998), hep-ph/9801324.

[56] G. Dissertori and M. Schmelling, Phys. Lett. **B361**, 167 (1995).

[57] C. F. Berger, T. Kucs, and G. F. Sterman, Phys. Rev. **D68**, 014012 (2003), hep-ph/0303051.

[58] A. J. Larkoski, D. Neill, and J. Thaler, JHEP **04**, 017 (2014), 1401.2158.

[59] E. Gerwick, S. Schumann, B. Gripaios, and B. Webber, JHEP **04**, 089 (2013), 1212.5235.

[60] T. Becher and M. D. Schwartz, JHEP **07**, 034 (2008), 0803.0342.

[61] P. F. Monni, T. Gehrmann, and G. Luisoni, JHEP **08**, 010 (2011), 1105.4560.

[62] Y.-T. Chien and M. D. Schwartz, JHEP **08**, 058 (2010), 1005.1644.

[63] T. Becher and G. Bell, JHEP **11**, 126 (2012), 1210.0580.

[64] S. Alioli *et al.*, JHEP **09**, 120 (2013), 1211.7049.

[65] D. de Florian and M. Grazzini, Nucl. Phys. **B704**, 387 (2005), hep-ph/0407241.

[66] A. Banfi, H. McAslan, P. F. Monni, and G. Zanderighi, JHEP **05**, 102 (2015), 1412.2126.

[67] OPAL, M. Z. Akrawy *et al.*, Phys. Lett. **B235**, 389 (1990).

[68] R. K. Ellis, W. J. Stirling, and B. R. Webber, Camb. Monogr. Part. Phys. Nucl. Phys. Cosmol. **8**, 1 (1996).

[69] DELPHI, P. Abreu *et al.*, Phys. Lett. **B456**, 322 (1999).

[70] O. Biebel, Phys. Rept. **340**, 165 (2001).

[71] OPAL, G. Abbiendi *et al.*, Eur. Phys. J. **C40**, 287 (2005), hep-ex/0503051.

[72] S. Kluth, Rept. Prog. Phys. **69**, 1771 (2006), hep-ex/0603011.

[73] JADE, S. Bethke, S. Kluth, C. Pahl, and J. Schieck, Eur. Phys. J. **C64**, 351 (2009), 0810.1389.

[74] S. Bethke, Eur. Phys. J. **C64**, 689 (2009), 0908.1135.

[75] G. Dissertori *et al.*, Phys. Rev. Lett. **104**, 072002 (2010), 0910.4283.

[76] OPAL, G. Abbiendi *et al.*, Eur. Phys. J. **C71**, 1733 (2011), 1101.1470.

[77] JADE, J. Schieck, S. Bethke, S. Kluth, C. Pahl, and Z. Trócsányi, Eur. Phys. J. **C73**, 2332 (2013), 1205.3714.

[78] A. Gehrmann-De Ridder, T. Gehrmann, E. W. N. Glover, and G. Heinrich, Phys. Rev. Lett. **100**, 172001 (2008), 0802.0813.

[79] S. Weinzierl, Phys. Rev. Lett. **101**, 162001 (2008), 0807.3241.

[80] S. Weinzierl, JHEP **06**, 041 (2009), 0904.1077.

[81] S. Weinzierl, Eur. Phys. J. **C71**, 1565 (2011), 1011.6247, [Erratum: Eur. Phys. J.C71,1717(2011)].

[82] C. N. Lovett-Turner, Phys. Lett. **B329**, 361 (1994), hep-ph/9405211.

[83] Z. Nagy and Z. Trócsányi, Nucl. Phys. Proc. Suppl. **74**, 44 (1999), hep-ph/9808364.

[84] SM MC Working Group, SM and NLO MULTILEG Working Group, J. Alcaraz Maestre *et al.*, The SM and NLO Multileg and SM MC Working Groups: Summary Report, in *Proceedings, 7th Les Houches Workshop on Physics at TeV Colliders: Les Houches, France, May 30-June 17, 2011*, pp. 1–220, 2012, 1203.6803.

[85] J. Carter and G. Heinrich, Comput. Phys. Commun. **182**, 1566 (2011), 1011.5493.

[86] S. Borowka, J. Carter, and G. Heinrich, Comput. Phys. Commun. **184**, 396 (2013), 1204.4152.

[87] S. Borowka and G. Heinrich, Comput. Phys. Commun. **184**, 2552 (2013), 1303.1157.

[88] S. Borowka *et al.*, Comput. Phys. Commun. **196**, 470 (2015), 1502.06595.

[89] S. Borowka *et al.*, (2017), 1703.09692.

[90] A. V. Smirnov and M. N. Tentyukov, Comput. Phys. Commun. **180**, 735 (2009), 0807.4129.

[91] A. V. Smirnov, V. A. Smirnov, and M. Tentyukov, Comput. Phys. Commun. **182**, 790 (2011), 0912.0158.

[92] A. V. Smirnov, Comput. Phys. Commun. **185**, 2090 (2014), 1312.3186.

[93] A. V. Smirnov, Comput. Phys. Commun. **204**, 189 (2016), 1511.03614.

[94] C. Bogner and S. Weinzierl, Comput. Phys. Commun. **178**, 596 (2008), 0709.4092.

[95] T. Hahn, Comput. Phys. Commun. **168**, 78 (2005), hep-ph/0404043.

[96] M. Czakon, Comput. Phys. Commun. **175**, 559 (2006), hep-ph/0511200.

[97] A. V. Smirnov and V. A. Smirnov, Eur. Phys. J. **C62**, 445 (2009), 0901.0386.

[98] S. G. Gorishnii, A. L. Kataev, and S. A. Larin, Phys. Lett. **B259**, 144 (1991).

[99] L. R. Surguladze and M. A. Samuel, Phys. Rev. Lett. **66**, 560 (1991), [Erratum: Phys. Rev. Lett.66,2416(1991)].

[100] O. V. Tarasov, A. A. Vladimirov, and A. Yu. Zharkov, Phys. Lett. **B93**, 429 (1980).

[101] R. K. Ellis, D. A. Ross, and A. E. Terrano, Nucl. Phys. **B178**, 421 (1981).

[102] Z. Kunszt, P. Nason, G. Marchesini, and B. R. Webber, QCD AT LEP, in *LEP Physics Workshop Geneva, Switzerland, February 20, 1989*, pp. 373–453, 1989.

[103] JADE, OPAL, P. Pfeifenschneider *et al.*, Eur. Phys. J. **C17**, 19 (2000), hep-ex/0001055.

[104] S. Bethke, Z. Kunszt, D. E. Soper, and W. J. Stirling, Nucl. Phys. **B370**, 310 (1992), [Erratum: Nucl. Phys.B523,681(1998)].

[105] M. Cacciari, G. P. Salam, and G. Soyez, Eur. Phys. J. **C72**, 1896 (2012), 1111.6097.

[106] S. Bentvelsen and I. Meyer, Eur. Phys. J. **C4**, 623 (1998), hep-ph/9803322.

[107] Z. Bern, V. Del Duca, W. B. Kilgore, and C. R. Schmidt, Phys. Rev. **D60**, 116001 (1999), hep-ph/9903516.

[108] S. Catani, D. de Florian, and G. Rodrigo, JHEP **07**, 026 (2012), 1112.4405.

[109] S. Catani and M. Grazzini, Nucl. Phys. **B591**, 435 (2000), hep-ph/0007142.

[110] Z. Nagy and D. E. Soper, JHEP **09**, 114 (2007), 0706.0017.

[111] Z. Bern, L. J. Dixon, and D. A. Kosower, Nucl. Phys. **B513**, 3 (1998), hep-ph/9708239.